Entropy driven phase transition in hard core lattice gas models in three dimensions

By

N Vigneshwar

PHYS10201404002

The Institute of Mathematical Sciences, Chennai

A thesis submitted to the

Board of Studies in Physical Sciences

In partial fulfillment of requirements

For the Degree of

DOCTOR OF PHILOSOPHY

of

HOMI BHABHA NATIONAL INSTITUTE

June, 2019

Homi Bhabha National Institute

Recommendations of the Viva Voce Committee

As members of the Viva Voce Committee, we certify that we have read the dissertation prepared by N Vigneshwar entitled “Entropy driven phase transition in hard core lattice gas models in three dimensions" and recommend that it maybe accepted as fulfilling the thesis requirement for the award of Degree of Doctor of Philosophy.

Date: **3/7/2020**

Chairman: Purusattam Ray

Date: **3/7/2020**

Guide/Convener: Rajesh Ravindran

Date: **3/7/2020**

Member 1: Gautam I Menon

Date: **3/7/2020**

Member 2: Pinaki Chaudari

Date: **3/7/2020**

Member 3: Sanatan Digal

Date: **3/7/2020**

External Examiner: Kabir Ramola

Final approval and acceptance of this dissertation is contingent upon the candidate’s submission of the final copies of the dissertation to HBNI.

I hereby certify that I have read this dissertation prepared under my direction and recommend that it may be accepted as fulfilling the dissertation requirement.

Date: **3/7/2020**

Place: **Chennai**

Guide

STATEMENT BY AUTHOR

This dissertation has been submitted in partial fulfilllment of requirements for an advanced degree at Homi Bhabha National Institute (HBNI) and is deposited in the Library to be made available to borrowers under rules of the HBNI.

Brief quotations from this dissertation are allowable without special permission, provided that accurate acknowledgement of source is made. Requests for permission for extended quotation from or reproduction of this manuscript in whole or in part may be granted by the Competent Authority of HBNI when in his or her judgement the proposed use of the material is in the interests of scholarship. In all other instances, however, permission must be obtained from the author.

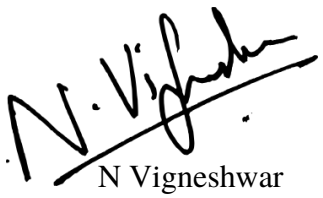

N Vigneshwar

DECLARATION

I, hereby declare that the investigation presented in the thesis has been carried out by me. The work is original and has not been submitted earlier as a whole or in part for a degree / diploma at this or any other Institution / University.

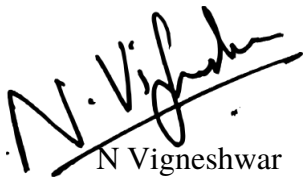

N Vigneshwar

List of Publications arising from the thesis

- **Journal**

1. **Different phases of a system of hard rods on three dimensional cubic lattice**

   N Vigneshwar, D Dhar and R Rajesh

   Journal of Statistical Mechanics: Theory and Experiment, 113304 (2017)

2. **Phase diagram of a system of hard cubes on the cubic lattice**

   N Vigneshwar, D Mandal, K Damle, D Dhar and R.Rajesh

   Physical Review E 99, 052129 (2019)

N Vigneshwar

List of presentations and participations at conferences

- **Contributed presentations**

1. Presented poster on *Phase diagram of a system of hard cubes on the cubic lattice* in the *5th Indian Statistical Physics Communuty Meeting 2018* in ICTS, Bangalore
2. Presented poster on *Phase diagram of a system of hard rods on the cubic lattice* in the *4th Indian Statistical Physics Community Meeting 2017*, in ICTS, Bangalore

- **Conferences attended**

1. *One Day Soft Matter Symposium* held at Indian Institute of Technology, Madras (25th January, 2019)
2. *Indian Statistical Physics Community Meeting 2018* (ISPCM 2018) held at International Centre for Theoretical Sciences, Bangalore (16-18 February, 2018)
3. *Indian Statistical Physics Community Meeting 2017* (ISPCM 2017) held at International Centre for Theoretical Sciences, Bangalore (17-19 February, 2017)
4. *Bangalore School on Statistical Physics - VII* held at International Centre for Theoretical Sciences, Bangalore (01-15 July, 2016)

To

My Parents

ACKNOWLEDGEMENTS

I would like to express my sincere gratitude and my thanks to my supervisor Prof. R. Rajesh for his constant support and encouragement during my PhD life for the last five years. His ability to guide me by making me comfortable and to answer all my queries and his approachable nature at all times has been a godsend to me. It was a privilege to work with him during my PhD years.

I am thankful to my collaborators Prof. Deepak Dhar, Prof. Kedar Damle and Dipanjan Mandal for sharing their knowledge and expertise with me and I am helpful for their advice during the course of their collaboration.

I am thankful to my Doctoral Committee members, Prof. Gautam I Menon, Prof. Purusattam Ray, Prof. Pinaki Chaudari and Prof. Sanatan Digal for their valuable advice and suggestions about my thesis work.

I would like to thank IMSc for the High-Performance computing facilities and library, especially System administrators Mangal Pandi and G Srinivasan for their expertise and their patience whenever I encountered any problem. Most of the numerical simulations in this thesis have been carried out on the supercomputing machines Nandadevi cluster

I would like to thank my friends Prashant R, Jilmy Joy, Madhusudhan Raman, Chandrasekhar K, Devanand N S, Ria Sain and others. Finally, I would like to express my love and gratitude to my parents for their continuous support and their faith in me without whom, it would not have been possible to reach this far.

Contents

List of Figures

List of Tables

Chapter 5

Conclusion

In this thesis we have studied, in detail, the phase diagram of system of particles in three-dimensions by Monte Carlo simulations using a grand canonical cluster algorithm. These models are: (1) hard rods of length k on a cubic lattice and (2) hard $2 \times 2 \times 2$ cubes on a cubic lattice.

In **Chapter 1**, we have described a historical overview of entropy-driven phase transitions and introduced hard-core exclusion models both in the continuum and on lattices to study such transitions.

In **Chapter 2**, we have described a cluster grand canonical algorithm and have explained its implementation on a system of hard rods of length k on a square lattice. It has been also shown that this algorithm can equilibrate densities close to full-packing and its generalization to three-dimensional systems has also been explained.

In **Chapter 3**, we have obtained the phase diagram of a system of hard rods of length k on a cubic lattice using the cluster grand canonical algorithm. We showed that for $k \leq 4$, the system is in a disordered isotropic phase at all densities ρ, and there are no phase transitions. For $k = 5, 6$, the system undergoes a single transition into a high density layered-disordered phase, where the system breaks up into two dimensional layers, but

disordered within a layer. For $k = 7$, we find that as density is increased, the system makes a transition into a nematic phase. Further increase of density results in a layered-disordered phase. We also observe a layered-nematic phase between the nematic and layered-disordered phases, which we argued is a finite-size effect. For $k > 7$, we expect that the phase diagram to remain qualitatively similar and we have shown the onset of nematic phase for $k = 8, 9, 10$. The generalization of the hard rods in three-dimensions would be hard cuboids, presumably of the type $m \times m \times mk$. This system would exhibit a rich phase diagram and obtaining it as a function of both m and k would be a challenging task.

In **Chapter 4**, we find that this system of cubes goes through four distinct phases as the density of cubes is increased: disordered, layered, sublattice ordered, and columnar ordered. By studying systems of different sizes, we argue that the disordered-layered phase transition is continuous, while the layered-sublattice and sublattice-columnar transitions are discontinuous. We construct a Landau theory written in terms of the layering order parameter $\mathbf{L}$ and columnar order parameter $\mathbf{C}$ which is able to describe the different phases that are observed in the simulations and the order of the transitions. Additionally, our results near the disordered-layered transition are consistent with the Landau theory prediction of scaling behaviour in the $O(3)$ universality class perturbed by cubic anisotropy. The generalization of this model could be $k \times k \times k$ cubes on a cubic lattice. Preliminary simulations for $3 \times 3 \times 3$ cubes suggest that the sublattice phase does not exist, but the layered and columnar phases exist. One could also revisit the continuum problem by extrapolating the lattice problem by taking $k \to \infty$ to check what the high-density phase of the continuum model could be.

Synopsis

A phase transition or a transformation is a sudden change from one phase to another when some thermodynamic parameter is varied. Typically, as temperature is increased, systems undergo a phase transition from an energetically favoured low-temperature ordered state to an entropically favoured high temperature disordered state. This typically involves a gain in entropy which competes with the rise in internal energy. This competition between the internal energy and entropy drives the phase transition. Examples of such energy-driven transitions are ferromagnetic transitions in spin systems, liquid-gas transition of water, etc. However there exists systems for which the ordered phase has more entropy than the disordered phase with no appreciable difference in internal energy. These transitions are primarily driven by entropy and thus called entropy driven transitions. Example systems in which entropy-driven phase transitions occur include freezing transition of hard spheres [1], phase separation in binary hard-core mixtures [2], gas adsorption on metallic surfaces [3], transitions between nematic, smectic and cholesteric phases in liquid crystals [4], nanotube gels [5], transitions to a nematic phase in aqueous solutions of tobacco mosaic viruses [6], emergence of cholesteric phases in *fd* viruses [7], isotropic-nematic transitions in rod-like boehmite particles [8], nematic phases in rodlike silica particles with varying aspect ratio [9], emergence of biaxial nematic and smectic phases in banana shaped liquid crystals under pressure [10] and emergence of geometrical frustration in triangular cells under biaxial compression [11].

Minimal models for studying entropy driven phase transitions are models with only ex-

cluded volume interactions. In such systems, all allowed configurations have equal energy, and therefore any phase transitions are driven purely by gain in entropy. Hard-core lattice gas (HCLG) models are discrete versions of the hard-core exclusion models in the continuum where the particles are placed on the underlying lattice sites. Well studied models include two dimensional systems of dimers, trimers, squares, rods, tetrominos, rectangles, discretized discs, Y-shaped molecules, mixtures of hard objects. The only exactly solvable model is the hard hexagon model (nearest neighbour exclusion model on the triangular lattice). The other models have been studied using approximate methods such as density functional theories, high and low density expansions, mean field theories, etc., or through extensive Monte Carlo simulations. Being able to predict the macroscopic material behaviour from knowing its constituent building blocks would help to engineer the synthesis of materials with prescribed properties. However, despite a long history of study, a general understanding of the dependence of the nature of the emergent phases on the shapes of the particles, as well as the order of appearance of the phases with increasing density, is lacking. Thus, it is important to determine the detailed phase diagram of differently shaped particles, as the first step to a more general understanding.

In three dimensions, the understanding is much less. Detailed phase diagrams are known for very few systems. This is primarily due the fact that Monte Carlo simulations with local moves are often inefficient in equilibrating the system, when either the excluded volume per particle is large or when the density is close to the full packing.

In this thesis we study two problems on a cubic lattice: (1) hard rods of length k and (2) hard cubes of size $2 \times 2 \times 2$. We obtain the detailed phase diagram and characterize the nature of the phase transitions for both these models. The results that we have obtained are summarized below.

Hard rods of length k on a cubic lattice

Consider a cubic lattice of size $L \times L \times L$ with periodic boundary conditions. The lattice sites may be occupied by rods that occupy k consecutive lattices sites in any one of the three mutually orthogonal directions. The rods interact only through excluded volume interactions, i.e., a lattice site may be occupied by at most one rod. We associate a weight e^{μ} with each rod, where μ is the chemical potential rescaled by temperature. We will call a rod oriented in the x-, y- and z-directions as x-mer, y-mer, and z-mer respectively. The site of a rod with the smallest x-, y-, and z-coordinates will be called its head.

Early work based on virial expansion [12], high density expansions [13] and the Guggenheim approximation [14], predicted a transition from the low-density disordered phase to a nematic-ordered phase, as the density is increased. Exact solution for the problem for any k on the random layered tree like lattice shows the presence of a single isotropic-nematic transition for $k \geq 4$ when the coordination number is $q = 6$ [15]. It is however clear that at densities near full packing, nematic order will not survive, as there are exponentially many disordered configurations. But, the nature of the high-density disordered phase is not well-understood [4, 16]. In two dimensions, it is known that the system of rods for $k \geq 7$ undergoes two transitions as density is increased: first from a isotropic phase to a nematic phase and the second from the nematic phase to a high density disordered phase [16]. For $k < 7$, there are no phase transitions.

We use grand canonical Monte Carlo simulations to determine the different phases in the hard rod model as a function of the density, for different rod-lengths k. Conventional algorithms with local evaporation and deposition moves fail to equilibrate the system (within available computer time) at large densities because the system gets stuck in long-lived metastable states. Instead, we implement a Monte Carlo algorithm with cluster moves [17, 18] that has recently proved useful in equilibrating systems of hard particles with large excluded volume interactions at densities close to one [17, 18] and even at full packing [19].

The main results in this thesis are:

- There are no phase transitions when $k \leq 4$.
- For $k = 5, 6$, the system undergoes a single transition from a disordered phase to a layered-disordered phase. In the layered-disordered phase, the fractional number of rods of two orientations are roughly equal, whereas the number of rods in the third orientation is suppressed.
- A nematic phase is observed for $k \geq 7$.
- There exists four phases for $k \geq 7$ as a function of density: disordered, nematic, layered-nematic and layered-disordered.
- In the layered-nematic phase, each plane has two dimensional nematic order, but there is no overall bulk nematic order.
- We argue that the layered-nematic phase is a finite-size artefact which is observed in simulations and will be unstable in the thermodynamic limit. This can be explained using a perturbative expansion about a pure bulk nematic phase at small defect densities.
- The disordered to layered-disordered transition in rods of size $k = 5, 6$ is shown to be first order.
- The critical values for the disordered-layered transition are: $\mu_c(5) \approx 3.82$ and $\rho_c(5) \approx 0.874$ and $\mu_c(6) \approx 1.0$ and $\rho_c(6) \approx 0.68$.
- The disordered-nematic transition for $k = 7$ is expected to be very weakly first order from symmetry considerations, but no signature of first-order nature was seen as it requires simulations of large system sizes.
- The critical values for the disordered-nematic transition for $k = 7$ is $\mu_c \approx -0.23$, corresponding to $\rho_c \approx 0.556$.

Hard $2 \times 2 \times 2$ cubes on a cubic lattice

Consider a $L \times L \times L$ cubic lattice with periodic boundary conditions and even L. The lattice may be occupied by cubes of size $2 \times 2 \times 2$ (i.e having side-length of 2 lattice spacings). We associate a weight $z = e^{\mu}$ with each cube, where z is the activity and μ is the chemical potential. The cubes interact through only excluded volume interaction, *i.e.* no two cubes can overlap in volume. For a cube, we identify the vertex with minimum x-, y-, and z-coordinates as its head. The configuration of the system can thus be fully specified by the spatial coordinates of the heads of all the cubes in the system.

We study the model using grand canonical Monte Carlo simulations by implementing a generalization of the algorithm as described in Refs. [17, 18].

Earlier Monte Carlo studies of the discrete problem [20] found no phase transitions for densities up to full packing. On the other hand, for cubes with sides of length two, the approximate density functional theory predicts that there should be a transition from a disordered phase to a layered phase at low densities and from a layered phase to a columnar phase at higher densities. When the length of a side is six, the theory predicts a transition from a disordered phase to a solid, and then to two types of columnar phases [21]. Simulations of a mixture of cubes of sizes two, and four or six, show a demixing transition [22] in contradiction to predictions from density functional theory [23]. However, the prediction for a pure system of cubes have not, to our knowledge, been tested in large scale simulations.

The main results in this thesis are:

- The system of cubes shows four distinct phases as the density of cubes is increased: disordered, layered, sublattice ordered, and columnar ordered.

- Disordered Phase: All sublattices are equally occupied i.e., $\rho_i \approx \rho/8$ for $i = 1, \cdots, 8$. The sublattices are shown in Fig. 1.

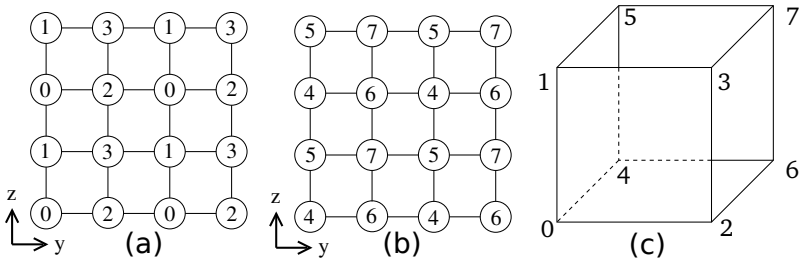

Figure 1: The lattice is divided into eight sublattices $0, 1, \ldots, 7$ depending on whether the x-, y- and z- coordinates are even or odd. Labelling of sublattices corresponding to yz-planes whose x-coordinate is (a) even, or (b) odd. (c) A $2 \times 2 \times 2$ cube with all of its vertices labelled with appropriate sublattices to show the relative positions of the planes shown in (a) and (b).

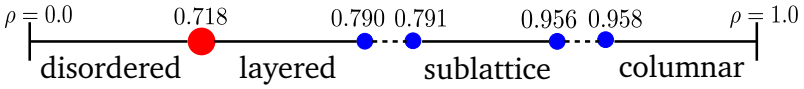

Figure 2: Numerically obtained phase diagram for $2 \times 2 \times 2$ hard cubes. The red dot represents a continuous transition and the dotted lines represent regions of coexistence.

- Layered Phase: The system spontaneously breaks up into parallel slabs of size $2 \times L \times L$ which are preferentially occupied by cubes. Four sublattices are preferentially occupied and translation symmetry is thus broken along exactly one principal axis. The layered phase is six-fold degenerate.

- Sublattice Phase: One sublattice is preferentially occupied, breaking translational symmetry along all three principal directions. The sublattice phase is eight-fold degenerate.

- Columnar Phase: Two sublattices are preferentially occupied and the system spontaneously breaks up into weakly interacting parallel columns of size $2 \times 2 \times L$ which are preferentially occupied by cubes, breaking translational symmetry along two principal directions. The columnar phase is twelve-fold degenerate.

- The disordered-layered phase transition is continuous in nature and finite size scaling is consistent with the universality class of the $O(3)$ model with cubic anisotropy.

- Both the layered-sublattice and sublattice-columnar transitions are discontinuous. A schematic of the phase diagram in the density ρ line is shown in Fig. 4.16.

- A Landau theory written in terms of the layering order parameter and columnar order parameter is constructed, which is able to describe the different phases that are observed in the simulations and the order of the transitions.

Chapter 1

Introduction

Matter exists in macroscopic states, called *phases*, which have qualitatively and quantitatively different mechanical and chemical properties. A phase transition or a transformation is a sudden change from one phase to another when some thermodynamic parameter is varied. This manifests itself as *singularities* in the thermodynamic functions. These singularities can occur only in an infinite system. Examples of phase transitions include boiling of liquids, magnetic transitions in spin systems, structural transitions in crystals etc.

Phase transitions can be classified into two types: discontinuous or first order transitions and continuous transitions. In discontinuous transitions, the first derivative of free energy with respect to some thermodynamic parameter has a discontinuity. In case of the liquid-gas transition in three-dimensions, the internal energy, which is the first derivative of free energy with temperature is discontinuous across the phase-boundary. The size of the discontinuity is the latent heat. In continuous transitions, the first derivatives of free energy are continuous, but the second or higher order derivatives of free energy diverge at the critical point.

In these transitions, near the critical point, huge fluctuations in thermodynamic parameters occur. The typical length scale of the fluctuations in space is called the correlation length

ξ. In discontinuous transitions, ξ remains finite, whereas in continuous transitions, ξ diverges. This divergence of ξ has huge implications in the study of phase transitions.

A quite elegant way of looking at phases of matter is to associate them as manifestations of some *broken symmetries*. In this approach, a phase transition involves a breaking of some symmetry of the Hamiltonian. A phase transition can be usually characterized by a local order parameter $m(\mathbf{x})$, which is not invariant under some symmetry group $\mathcal{G}$ of the Hamiltonian. The expectation value of the order parameter is zero in the fully symmetric phase i.e., $\langle m(\mathbf{x})\rangle = 0$ and non-zero in the broken symmetric phase i.e., $\langle m(\mathbf{x})\rangle \neq 0$. A phase transition involves a spontaneous breaking of the symmetry group $\mathcal{G}$ of the Hamiltonian into $\mathcal{N}$, which is a subgroup of $\mathcal{G}$.

Ginzburg and Landau proposed a theory in which the free energy, $F[m(\mathbf{x})]$ is a integral in space over smooth polynomial functions of the order parameter $m(\mathbf{x})$, whose coefficients are analytic functions of temperature and other external fields [24].

$$F[m(\mathbf{x})] = \int \mathrm{d}^d\mathbf{x} \left[a_0(T)|\nabla m(\mathbf{x})|^2 + a_1(T)m(\mathbf{x}) + a_2(T)m(\mathbf{x})^2 + a_4(T)m(\mathbf{x})^4 + \cdots\right]. \tag{1.1}$$

The functional $F[m(\mathbf{x})]$ should be invariant under the operations of the symmetry group $\mathcal{G}$. The equilibrium states of the system are found by minimizing the free energy and the equilibrium value for the order parameter is simply the value which minimizes the free energy. This formulation of phase transitions was very elegant as it introduced ideas of universality, in which the free energy can be written depending only on the symmetry of the system regardless of other system-specific parameters and use of a single parameter i.e., order parameter to characterize the system near the critical point.

The divergence of ξ and the singular nature of many thermodynamic quantities, mainly second derivatives of free energy near the critical points are power law functions of temperature and the exponents are called critical exponents. These exponents only depend on the symmetry and dimensionality of the system under consideration, and not on the

microscopic details of the system. Thus, near the critical point because of this *universal* behaviour, any model however contrived in construction becomes *real* near the critical point and can be used as analogues to study actual real-life systems.

It is also possible to have a line of critical points along which exponents vary continuously. A realisation of this is the well-studied Ashkin-Teller model. The model consists of two Ising spins S_i and σ_i sitting on a site i on a bipartite lattice, interacting via this Hamiltonian $\mathcal{H}$,

$$\mathcal{H} = J_1 \sum_{\langle i,j \rangle} S_i S_j + J_2 \sum_{\langle i,j \rangle} \sigma_i \sigma_j + \mu \sum_{\langle i,j \rangle} S_i S_j \sigma_i \sigma_j, \tag{1.2}$$

where the $\langle \cdots \rangle$ implies summation over the nearest neighbours. If $\mu = 0$, the system behaves like two independent Ising systems with two different critical temperatures if $J_1 \neq J_2$ and the model reduces to a 4-state Potts model if $J_1 = J_2 = \mu$ [25]. More details about the Ashkin-Teller model can be found in Refs. [26, 27, 28]. Within the context of study of hard-core lattice gas models, Ashkin-Teller behaviour is observed in many models, of which a few examples are given in the sections below.

1.1 Entropy-driven phase transitions

The free energy F of a system is:

$$F = U - TS, \tag{1.3}$$

where U is the internal energy of the system, S is the entropy and T is the temperature. In the low temperature regime, the free energy is lowered by those states which have lower internal energy, typically the ordered phases. Whereas, in the high temperature regime, the free energy is lowered by increasing the entropy in which case, typically the disordered phase is favoured. These transitions are primarily driven by temperature and are called energy-driven phase transitions. Typical examples of such transitions are ferromagnetic

transitions in spin systems, liquid-gas transition of water, etc.

However there exists systems for which the ordered phase has more entropy than the disordered phase with no appreciable difference in internal energy. These transitions are primarily driven by entropy and thus called entropy-driven transitions. Example systems in which entropy-driven phase transitions occur include freezing transition of hard spheres [1], phase separation in binary hard-core mixtures [2], phase transitions on adsorbed surfaces [3], transitions between nematic, smectic and cholesteric phases in liquid crystals [4], nanotube gels [5], transitions to a nematic phase in aqueous solutions of tobacco mosaic viruses [6], emergence of cholesteric phases in *fd* viruses [7], isotropic-nematic transitions in rod-like boehmite particles [8], nematic phases in rodlike silica particles with varying aspect ratio [9], emergence of biaxial nematic and smectic phases in banana shaped liquid crystals under pressure [10] and emergence of geometrical frustration in triangular cells under biaxial compression [11].

1.1.1 Hard-Core models

The minimal models for studying entropy driven phase transitions are models with only excluded volume interactions, in which the energy of overlap is set to infinity and thus temperature plays no role as there is no relevant energy scale. Therefore, all phase transitions are driven purely by gain in entropy.

The first demonstration of the entropy-driven transition in a model system was shown in a system of long hard rods in three dimensional continuum by L Onsager in 1948 [29]. It undergoes a phase transition from a disordered isotropic phase to an orientationally ordered nematic phase with increasing density. In this case, it was shown that loss of orientational entropy in the nematic phase is more than compensated by the gain in the translational entropy due to the alignment of the rods and the ordered state gains overall entropy to become the most preferred state. The phases of this system of hard ellipsoidal

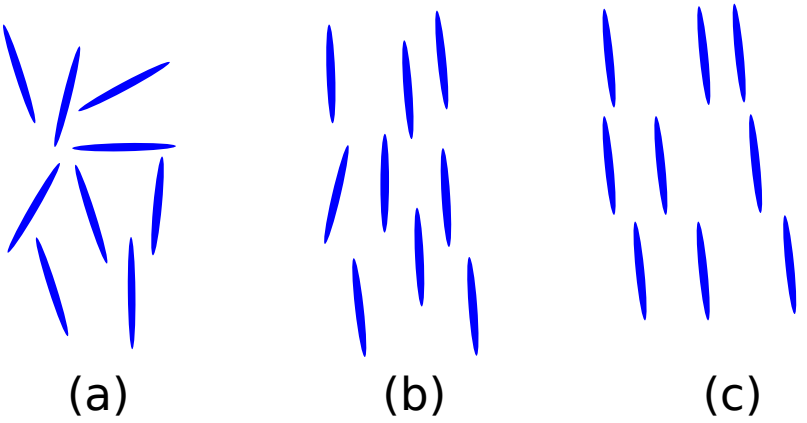

Figure 1.1: Schematic diagram of ellipsoidal rods as a function of increasing density. (a) Disordered phase where there is no translational and orientational order (b) Nematic phase where there is orientational order, but no translational order (c) Smectic phase where there is orientational and partial translational order. The density increases from left to right. The translational invariance is broken parallel to the nematic director.

rods is shown in Fig. 1.1 as a function of increasing density, in which the system goes from a low density disordered fluid phase, where there is no orientational or translational order to an intermediate density nematic phase, which exhibits orientational ordering, but no translational order [29] and a higher density smectic phase which exhibits orientational order and partial breaking of translational invariance [30, 31].

Another earlier example of entropy-driven phase transition is a freezing transition in a system of hard spheres in the three-dimensional continuum, which was theoretically predicted in 1950 [32]. This seemed fairly counter-intuitive as it was commonly thought that a freezing transition would require an attractive potential and in this case, only hard-core repulsion potential was enough to be able to form a solid phase. This was subsequently confirmed by numerical studies in which the system of hard spheres in the three-dimensional continuum showed a first order freezing transition from a fluid phase to a solid phase [33, 34].

These hard-core models are able to explain phases seen in physical systems with more complicated interactions. The nematic transitions in liquid crystals can be analysed by modelling them as hard rods in the continuum [4]. A freezing transition is seen in hard

spheres of polymethyl methacrylate (PMMA) colloids suspended in poly-12-hydroxystearic acid [1]. The adsorption of gas molecules on metallic surfaces can be mapped on hard-core lattice gas models and these can be used to study the phase behaviour of monolayer adsorption. Chlorine gas adsorbed on Ag(100) planes forms a $c(2 \times 2)$ structure at 650K which can be mapped to a hard square model [35]. Disordered phases, $c(2\times2)$ and $p(2\times2)$ phases can be seen on system of selenium adsorption on Ni(100) planes and it has been found that these transitions are of Ashkin-Teller universality class [36]. Other systems include adsorption of oxygen on Mo(110) [37] or Pd(100) [38] and order-disorder transitions of bromide adsorption on Ag(100) surfaces [39]. These models can be mapped to lattice models if the gas-gas interaction is negligible when compared to lowest mode of the surface corrugation potential [3]. Crystal-crystal transition in Brownian particles can be mapped to hard rectangle models [40, 41].

Various shapes of hard particles have been used as templates to study entropy-driven phase transitions by use of numerical simulations and approximate methods. Isotropic-Nematic phase transition has been studied in hard helices by Monte-Carlo simulations [42] and pentagonal particle in two-dimensional continuum undergo a transition from a disordered fluid phase to an intermediate rotator solid phase to a *striped* crystalline phase as a function of density [43]. Simulations of various particles like ellipsoids, truncated cylinders, platelets etc. have been studied and their phase diagrams are described in Ref. [44]. Other exotic shapes include banana-shaped particles [10], hard dumbbells [45, 46], bent-shaped hard needles [47], hard oblate mesogens [48], non-convex platelets [49] and so on.

1.1.2 Hard-core lattice gas models

Hard-core lattice gas (HCLG) models are discrete versions of the hard-core exclusion models in the continuum where the particles are placed on the underlying lattice sites. These models have a rich history in the study of phase transitions and anisotropic particles of various shapes and sizes have been studied on different lattices. In addition to their

interest of being the simplest models to show phase transitions, they are also of interest in many other systems such as enumeration of directed animals in three dimensions [50, 51], Yang-Lee singularities [52], frustrated quantum spin systems [53, 54], thermodynamics and transport of linear adsorbates [55], jamming in granular media [56] etc. HCLG models also provide interesting examples of entropy-driven phase transitions, and like in the continuum, have rich phase diagrams.

One of the earliest HCLG models was used to study melting in discretized lattice discs in 1958 [57]. The study of hard rods on lattices have had a lot of historical significance and earlier work were concerned with calculating entropy in limiting cases of full-packing, especially dimers. A dimer is a rod which occupies two consecutive lattice sites either in the horizontal or vertical direction. In two dimensions, for dimers, it may be shown rigorously that the system is disordered at all densities [58], while at full packing, there exists an exact solution [59, 60] and the system is power-law correlated [61, 62]. One of the few solved models is the hard hexagon gas on a triangular lattice which undergoes a continuous transition from a disordered fluid phase to a solid phase [63]. Other rigorous results are known for hard triangles at full packing [64], long rods of length k on a square lattice [65] and hard plates in three dimensions of size $1 \times k^{\alpha} \times k$, where $\alpha \in [0, 1]$ [66]. Other well studied models include trimers [67], squares [68, 69, 70, 71, 72, 73], rods [16, 74, 18], pentamers [75], tetrominos [76], rectangles [77, 78, 79, 72, 80], discretized discs [81, 82], Y-shaped molecules [83], mixtures [19, 84, 85, 86] of hard objects.

In three dimensions, the results are much fewer and the complete phase diagram is not known for any system. Monte Carlo studies of discretized lattice spheres on a cubic lattice were carried out for different radii and the phase diagrams were obtained for different sizes of the spheres [20]. Simulations of a mixture of cubes of sizes two, and four or six, show a demixing transition [22] in contradiction to predictions from density functional theory [23].

Despite the long history of study of such systems, there is no general framework which

relates the dependence of shape of the particles to its emergent phases. Being able to predict the macroscopic material behaviour from knowing its constituent building blocks would help to engineer the synthesis of materials with prescribed properties [87, 88]. This leaves us with approximate theories and numerical simulations. It is generally hoped that numerical simulations would help to build the phenomenology of these systems. But, Monte Carlo simulations with local moves are often inefficient in equilibrating the system when the excluded volume is large or packing fraction is high. This puts a restriction on the kind of systems one can study. So, the development of efficient algorithms which can simulate particles at high densities or high exclusion volumes in higher dimensions serves as the prime motivation of this thesis.

In this thesis, we analyse two HCLG models on lattices. Secs 1.2 – 1.3 analyse the hard rods of length k in two and three dimensional lattices and also address the questions raised. In Sec. 1.4, we study about hard cubes in a cubic lattice.

1.2 Hard rods in two dimensions

In two dimensional continuum, a system of hard rods of infinitesimal thickness with restricted orientations in two directions undergoes a continuous transition from a disordered phase to a nematic phase in the Ising universality class as a function of density [89]. If one were to relax the restriction on the orientations and allow the rods to freely rotate in the plane, there is no nematic phase as the rotational symmetry cannot be broken in two dimensions [90], but the system undergoes a Kosterlitz-Thouless type transition into a high density phase with power law correlations [91, 92, 93, 94].

On lattices, we take hard rods of length k, which occupies k adjacent lattice sites, either in the horizontal or vertical directions. These rods interact purely via hard-core repulsion or in other words, each lattice site is either empty or occupied by a single rod. For dimers ($k = 2$), the system has no transition for any non-zero vacancy density [58, 95, 96].

A dimer model with additional nearest neighbour exclusion undergoes a discontinuous transition [97] and with other attractive interactions may also lead ordered phases [98, 99, 100]. The fully packed limit admits an analytic solution using Pfaffians [59, 60] and the correlations between two vacancies have a power lay decay on square lattice [101]. A height representation exists in the fully-packed limit [102] that breaks down for a non-zero vacancy density. A vector-field height representation is available for a fully-packed system of rods of length k [67, 103]. The fully-packed limit for rods of $k \geq 2$ was argued to be disordered in Refs. [16, 4]. For some time, it was unclear whether a pure lattice model can exhibit a nematic phase even for a large k [4].

Recently it was rigorously proven that a nematic phase exists for $k \gg 1$ [65]. This approach relies on coarse-graining the lattice on the length-scale comparable to the rod length k. The lattice is divided into square plaquettes of length $\ell \sim k/2$ to ensure that rods of the same orientations have their centres fully inside this square plaquette. The plaquettes which enclose the horizontal rods are given value $+1$ and vertical rods -1. The plaquettes that enclose no rods (exceedingly rare) are given value 0. Therefore, the problem now reduces to that a three-state spin system with short-ranged interaction and spin-blocks of horizontal rods (those with values $+1$), that have a repulsive interaction with those of spin-blocks of vertical rods (those with values -1). Typical spin configurations involve large clusters of $+1(-1)$ typically separated by a boundary of 0s or those of opposite spins. These contours are studied by Pirogov-Sinai theory (details can be found in Ref. [104]). With this, an orientationally ordered state that does not break translational symmetry is most preferred at intermediate densities has been be shown in Ref. [65].

The isotropic-nematic transition can be studied on a Bethe-like lattice. In a traditional Bethe lattice of coordination number $q \geq 6$, nematic order is destroyed by interchange of the bonds with respect to a tree-node as it is similar to interchange of the rod-label, which is an invariant operation [15]. So, a new lattice is constructed in Ref. [15], called random locally treelike layered (RLTL) lattice, in which exact equations for entropy can

be derived . A nematic phase is present for $k \geq 4$ in a RLTL of $q = 4$.

The exact entropy $\mathcal{S}(\eta_x, \eta_y)$ of two types of rods, where η_x is the number density of rods of type x of length k and η_y is the number density of rods of type y of length k on a RLTL lattice for $q = 4$ case [15] is:

$$\begin{aligned}\mathcal{S}(\eta_x, \eta_y) &= [1-(k-1)\eta_x]\ln[1-(k-1)\eta_x] + [1-(k-1)\eta_y]\ln[1-(k-1)\eta_y] \\ &\quad -(1-k\eta)\ln(1-k\eta) - \eta_x \ln\eta_x - \eta_y \ln\eta_y, \end{aligned} \tag{1.4}$$

where $\eta = \eta_x + \eta_y$. To study the isotropic-nematic transition at constant η, define the order parameter ϵ to be

$$\epsilon = \frac{\eta_x - \eta_y}{\eta}, \tag{1.5}$$

and for small ϵ-expansion, we obtain

$$\mathcal{S}(\epsilon, \eta) = A(\eta) + B(\eta)\epsilon^2 + C(\eta)\epsilon^4 + \cdots, \tag{1.6}$$

where $C(\eta) < 0$ to ensure stability of the entropy functional and it can be shown that $B(\eta)$ changes sign only for $k \geq 4$ and $\eta_c \sim k^{-2}$ for large k.

In two-dimensional lattices, Monte Carlo simulations show that the system is disordered at all densities for $k \leq 6$ [16] and for $k \geq 7$, the system undergoes a transition from a low-density disordered phase to an intermediate density nematic phase [16, 18, 105]. This transition belongs to the Ising and 3-state Potts universality classes on square [74, 106, 89] and triangular lattices [106, 107] respectively.

As argued previously, the high-density phase is unlikely to be nematic due to the fact that the nematic phase has a lower entropy than the disordered phase. A lower bound on the entropy can be found by arguing that the fully packed phase is populated with plaquettes of size $k \times k$ which can be filled completely with k horizontal or vertical rods. These plaquettes are independent. So, the number of configurations Ω_{FP} of the plaquettes is

given by:

$$\Omega_{FP}(L,k) \geq 2^{L^2/k^2}, \tag{1.7}$$

and the entropy per site S_{FP} is:

$$S_{FP} \geq \frac{1}{L^2} \ln \Omega_{FP}(L,k) = \frac{1}{k^2} \ln 2. \tag{1.8}$$

A better estimate of entropy for the fully packed phase can be arrived by dividing the $L \times L$ into strips of size $L \times k$ [16]. Let F_L be the number of ways to fill up strip with rods of length k. A recursion relation for F_L can be written as:

$$F_L = F_{L-1} + F_{L-k}. \tag{1.9}$$

For $F_L \approx \lambda^L$ for large L, we obtain

$$\lambda^k - \lambda^{k-1} - 1 = 0. \tag{1.10}$$

Now, we want to know the asymptotic form of λ as $k \to \infty$. We define $f(\lambda) = \lambda^k - \lambda^{k-1} - 1$.

- If $\lambda < 1$ and $k \gg 1$ $\quad \Rightarrow \lambda^k \to 0$ and $f(\lambda) = -1$,

- If $\lambda \geq 1$ and $k \gg 1$ $\quad \Rightarrow \lambda^k \approx \lambda^{k-1} \Rightarrow \lambda = 1$ and $f(\lambda) = -1$.

This implies $\lambda = \lambda(k)$ and $\lambda \to 1$ as $k \to \infty$.

Ansatz: $\lambda(k) = \exp(c\, k^{-\alpha})$.

$$f(\lambda) = \exp(c\, k^{1-\alpha}) - \exp(c\, k^{1-\alpha}) \exp(c\, k^{-\alpha}) - 1. \tag{1.11}$$

It is obvious from the above equation that $\alpha = 1$ and $c = c(k)$. Therefore,

$$f(\lambda) = \exp(c) - \exp(c)\,\exp(-ck^{-1}) - 1 = 0. \tag{1.12}$$

Rearranging the terms and taking log on both sides to yield,

$$c(k) = \ln k - \ln c(k). \tag{1.13}$$

This is a transcendental equation. But from the previous ansatz, we demand that $c(k)/k \to 0$ as $k \to \infty$. This means that $\ln c(k) < c(k)$ in this limit and $c(k) = \ln k\,[1 + \epsilon_1(k)]$ where $\epsilon_1(k)$ is a small parameter. Putting it in Eq. (1.13) and we obtain the following:

$$\begin{aligned} \epsilon_1 \ln k &= -\ln(\ln k) - \epsilon_1, \\ \Rightarrow \epsilon_1 &= -\frac{\ln(\ln k)}{\ln k}. \end{aligned}$$

Evaluating up to second order we obtain,

$$c(k) = \ln k \left[1 - \frac{\ln(\ln k)}{\ln k} + \frac{\ln(\ln k)}{(\ln k)^2} + \cdots\right]. \tag{1.14}$$

Therefore,

$$\lambda = 1 + \frac{1}{k}\ln\left(\frac{k}{\ln k}\right) + \frac{\ln(\ln k)}{k \ln k} + \cdots. \tag{1.15}$$

Therefore, the total number of ways to fill up the entire lattice is $F_L^{L/k}$. The entropy per site of this fully packed state, for $k \gg 1$ is

$$S_D(\rho = 1) = \frac{1}{k}\ln\lambda = \frac{1}{k^2}\ln k. \tag{1.16}$$

For densities away from the packed state, the state is obtained by evaporating a fraction of the rods from the fully packed state. Let ϵ be the fraction of rods evaporated and assuming that the entropy arising from the delocalised vacancies contribute to lower order

corrections, the entropy of a high density state is

$$S_D(\rho = 1 - \epsilon) \approx S_D(\rho = 1) + \frac{1}{k}[-\epsilon \ln \epsilon - (1 - \epsilon)\ln(1 - \epsilon)]. \tag{1.17}$$

An estimate of the entropy of the nematic phase in a square lattice of size $L \times L$ can also be made [16]. In this case, it was assumed the system was comprised of only one type of rods (say in the horizontal direction) and vacancies. The act of filling up each row is independent of other rows, so the problem is effectively one dimensional. A particular row is comprised of $\rho L/k$ rods and $L(1 - \rho)$ vacancies where ρ is the packing fraction. Therefore, the number of configurations of the rods and vacancies in a row is given by:

$$\Omega_N(\rho) = \frac{[L(1 - \rho) + \frac{\rho L}{k}]!}{[\frac{\rho L}{k}]![L(1 - \rho)]!}, \tag{1.18}$$

and for the entire system, the number of configurations would be Ω_N^L. From this, it is easily seen that entropy per site S_N in the thermodynamic limit $L \to \infty$ in this reference nematic state is given by:

$$S_N(\rho) = \frac{1}{L} \ln \Omega_N(\rho) = \left(1 - \rho + \frac{\rho}{k}\right)\ln\left(1 - \rho + \frac{\rho}{k}\right) - (1 - \rho)\ln(1 - \rho) - \frac{\rho}{k}\ln\left(\frac{\rho}{k}\right). \tag{1.19}$$

For high densities, $\rho = 1 - \epsilon$ where ϵ is very small. Therefore, the entropy is

$$S_N(\epsilon) = \epsilon \ln\left(\frac{1}{k\epsilon}\right) + \epsilon + O(\epsilon^2). \tag{1.20}$$

From Fig. 1.2, at high densities, the nematic phase has lower entropy than the disordered phase and both the curves meet at $\epsilon \sim A/k^2$ [16].

The simple evaporation-deposition algorithm used in Ref. [16] fails to equilibrate the system at densities beyond $\rho \leq 0.85$ due to the presence of long-lived metastable states. In addition to single update move, diffusion and rotational moves were also added to decrease the equilibration times. In a diffusion move, a horizontal or vertical rod is shifted

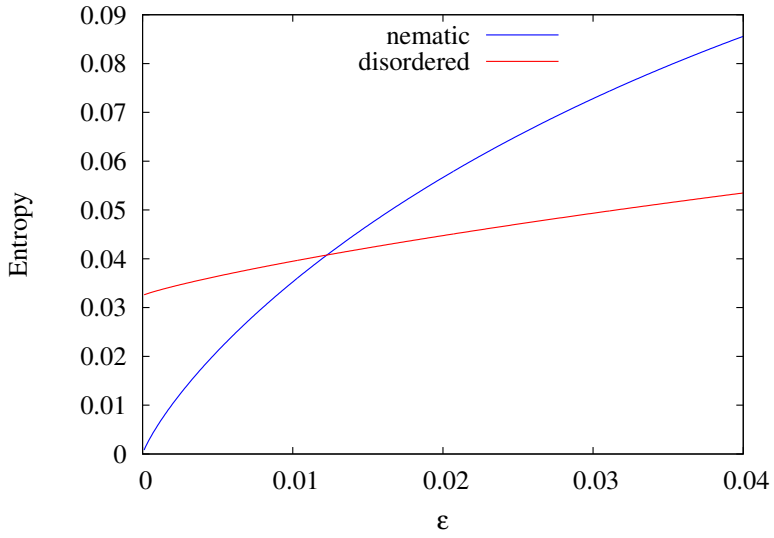

Figure 1.2: Entropy as a function of ϵ from Eq. (1.20) and Eq. (1.17) for $k = 8$.

one lattice site in a random direction, subject to the hard-core constraint. In a rotational move, a randomly chosen horizontal (vertical) rod is flipped to a vertical (horizontal) direction, also subject to the hard-core constraint. These moves helped to show that the nematic order parameter decreases with increasing density beyond 0.86 [108]. These optimizations were still not enough to show the existence of the high density disordered phase as it could not destabilize the metastable phases.

Newer results using Monte Carlo simulations with an improved cluster algorithm [17] in systems of hard rods shows a second transition from a intermediate nematic phase to a high-density disordered phase for $k \geq 7$ on two-dimensional lattices [18]. The universality class of the second transition has been difficult to resolve due to the presence of large correlations in square lattices, though it has been claimed that crossover to Ising exponents can happen for larger system sizes [18]. Addition of repulsive interactions to hard rods on a RLTL lattice also shows the existence of a high-density re-entrant disordered phase for $k \geq 4$ [105].

The generalization of rods on lattice are hard rectangles of size $m \times mk$. The phase diagram is difficult to study for $m > 1$ for arbitrary k due to the inefficiency of Monte Carlo

algorithms at high densities and large exclusion volumes. Putting $k = 1$ gives rise to the hard square model. The $m = 2$ hard square model has been extensively simulated and found to undergo a continuous transition from a disordered phase to a columnar phase under the Ashkin-Teller universality class [68, 69, 70, 71, 72, 73, 109] and squares of $m = 3$ undergo a first-order transition from a disordered phase to a columnar phase [81, 109].

With an efficient Monte Carlo algorithm, it has been possible to obtain the phase diagram of hard rectangles for $m = 2, 3$ [77]. For $m = 2$ and $k = 2, 3$, the system undergoes a continuous transition from a disordered phase to a solid phase within the Ashkin-Teller universality class. For $k = 4, 5, 6$, the system undergoes two continuous transition from a disordered to a columnar phase to a solid phase. Both transitions belong to Ashkin-Teller universality class. For $k \geq 7$, there are four phases: disordered, nematic, columnar and solid phase. The disordered-nematic transition is continuous, but the universality class in unclear [77]. The nematic-columnar transition is continuous and falls under the Ising universality class.

For $m = 3$ and for $2 \leq k \leq 6$, the system undergoes two discontinuous transitions from a disordered phase to a columnar phase and from a columnar phase to a solid phase as a function of density. Nematic order is present for $k \geq 7$ and there is a discontinuous transition from a disordered phase to a nematic phase for $m = 3$. The nematic transition occurs at density $\rho_c \sim 4.80k^{-1}$ for large k, independent of m [79]. Studies have also been conducted where k is not an integer [78].

1.3 Hard rods in three dimensions

A system of long hard rods in three dimensional continuum is known to undergo a phase transition from a disordered isotropic phase to an orientationally ordered nematic phase with increasing density, was shown by L Onsager [29]. At even higher densities, a system of spherocylinders will show a smectic/columnar phases with partial translational order

along with orientational order [30, 31] and solid-like phases [110].

The Onsager approach relies on the fact that free energy of a system, F_{tot} of spherocylinders with length l and diameter d can be split like

$$F_{\text{tot}} = F_{\text{ideal}} + F_{\text{exc}}, \tag{1.21}$$

where F_{ideal} is the ideal gas component and F_{exc} is the excess free energy due to the exclusion effects, which is treated by virial expansions. The simplicity of this approach is that, under the limit $l/d \to \infty$, only the second virial coefficient B_2 contributes and other coefficients become zero and the free energy functional can be written exactly [29].

$$F_{\text{tot}} = \ln \eta + \int \mathrm{d}\mathbf{\Omega}\, f(\mathbf{\Omega}) \ln f(\mathbf{\Omega}) + \eta l^2 d \int \mathrm{d}\mathbf{\Omega}_1 \int \mathrm{d}\mathbf{\Omega}_2\, f(\mathbf{\Omega}_1) f(\mathbf{\Omega}_2) |\sin \gamma|, \tag{1.22}$$

where $\eta = N/V$ is the concentration, $f(\mathbf{\Omega})$ is the orientational distribution function and γ is the angle subtended by two intersecting spherocylinders. The minimization of the free energy functional with respect to the orientational distribution function cannot be analytically solved. The first term in the integral of Eq. (1.22) represents the entropy of *demixing* or orientational entropy component, which comes from the ideal gas component. The second term in the integral represents the exclusion effects.

Onsager used a counter-intuitive ansatz $f(\theta)$, where θ is the azimuthal angle in spherical coordinates.

$$f(\theta, \alpha) = \frac{\alpha \cosh(\alpha \cos\theta)}{4\pi \sinh \alpha}, \tag{1.23}$$

and numerically minimized Eq. (1.22) with respect to α [111]. Other ansatz for $f(\mathbf{\Omega})$ have been used to obtain essentially the same results. An overview on different methods used to minimize Eq. (1.22) can be found in Ref. [111]

The three-dimensional Zwanzig gas in the continuum contains long rods in the form of cuboids of dimensions $l \times d \times d$, which can orient itself in the three mutually orthogonal

directions. In a system of N rods which can point in either in the x-, y- or z- in a region of volume in a three-dimensional space V. The configuration integral Q_N is given by:

$$Q_N = \frac{1}{N!}\frac{1}{3^N}\sum_{u=1}^{3}\int \mathrm{d}^3\mathbf{R}\, \exp\left[-\beta U(\mathbf{R})\right], \tag{1.24}$$

where $U(\mathbf{R})$ is the potential between the rods. The excess free-energy can be written as:

$$\exp\left[-\beta\Phi_N(u)\right] = \frac{1}{V^N}\int \mathrm{d}^3\mathbf{R}\, \exp\left[-\beta U(\mathbf{R})\right], \tag{1.25}$$

where $\Phi_N(u)$ depends upon the number of rods in each of the orientations where N_i is the number of rods in the ith direction, such that $\Phi_N(u) = \Phi_N(N_1, N_2, N_3)$ with a combinatorial factor $\dfrac{N!}{N_1!\,N_2!\,N_3!}$. Therefore, we obtain

$$Q_N = \frac{V^N}{3^N}\sum_{N_1,N_2,N_3=0}^{N}\frac{1}{N_1!\,N_2!\,N_3!}\exp\left[-\beta\Phi_N(N_1,N_2,N_3)\right]\delta_{N_1+N_2+N_3,N}. \tag{1.26}$$

Under the thermodynamic limit, the summation in Eq. (1.26) can be replaced by the maximum summand, called $\Phi_N^{\max}$. We define $N_i = x_i N$ and $N/V = \eta$. Therefore, the free energy $\mathcal{F}(\eta, x_i)$ can be written down as [12]

$$\mathcal{F}(\eta, x_i) = \ln\eta + \sum_{i=1}^{3} x_i \ln x_i + \frac{\beta\,\Phi_N^{\max}}{N}, \tag{1.27}$$

and the excess free energy is given by:

$$-\frac{\beta\,\Phi_N^{\max}}{N} = \sum_{m,n,p=1}^{\infty} B(m,n,p)\, F_{mnp}(x_1,x_2,x_3)\,\eta^{m+n+p-1}, \tag{1.28}$$

where $F_{mnp}(x_1, x_2, x_3) = x_1^m x_2^n x_3^p$. The integrals can be decomposed into 3 directions and

can be solved separately. As an example, for parallel rods

$$\begin{aligned} B(2,0,0) &= \frac{1}{2!0!0!}\int \mathrm{d}r_{12}\, f_{12}, \\ &= -4ld^2, \end{aligned} \tag{1.29}$$

and for perpendicular rods

$$B(1,1,0) = -2(l+d)^2 d. \tag{1.30}$$

Taking the limit $l \to \infty$ and $d \to 0$ such that $l^2 d$ is finite, we obtain $B(1,1,0) = -2l^2 d[1 + O(d/l)]$ and $B(2,0,0) = 0$. The above limit ensures that only planar graphs contribute as it can be seen as a set of intersecting rods and two intersecting rods always lie in a plane and $B(m,n,0) = B(n,m,0) = B(m,0,n) = B(n,0,m) = B(0,n,m) = B(0,m,n)$ and Eq. (1.28) can be simplified by settting $x_1 = x_2 = x$ and $x_3 = 1-2x$ to estimate the isotropic-nematic transition:

$$-\frac{\beta\,\Phi_N^{\max}}{N} = \sum_{m,n} B(m,n,0)\theta^{m+n-1} F_{mn}(x), \tag{1.31}$$

where $F_{mn}(x) = x^{m+n} + x^m(1-2x)^n + x^n(1-2x)^m$ and Eq. (1.27) simplifies as:

$$\mathcal{F}(\eta, x) = \ln\eta + 2x\ln x + (1-2x)\ln(1-2x) + 2l^2 d\,\eta\,[x^2 + 2x(1-2x)]. \tag{1.32}$$

Setting $x = 1/3 - \epsilon$ and $l = k$ and $d = 1$, Eq. (1.32) simplifies to

$$\mathcal{F}(\eta, x) = (9 - 6k^2\,\eta)\epsilon^2 - 9\epsilon^3 + \frac{81}{2}\epsilon^4 + O(\epsilon^5). \tag{1.33}$$

The isotropic-nematic transition is a first order transition and the critical density $\rho_c = k\eta_c \sim k^{-1}$, which has been verified in cubic lattices [112].

The corresponding problem on lattices where the orientation of rods are restricted to the lattice directions has also been studied in parallel. Consider a system of monodispersed rods of length k that occupy k consecutive lattice sites along any one of the lattice directions. Monodispersed refers to the fact that all the rods have the same length k. Two rods

cannot overlap. Early work based on virial expansion [12], high density expansions [13] and the Guggenheim approximation [14], predicted a transition from the low-density disordered phase to a nematic-ordered phase, as the density is increased.

In three dimensions, dimer models at full packing on bipartite lattices are known to show a Coulomb phase, with algebraic decay of orientational correlations [62], while for non-bipartite lattices, the correlations decay faster, and in some exactly solved cases, correlations are strictly zero beyond a finite range [113]. Not much is known for larger values of k. It would be expected that, like in the continuum, there will be an isotropic-nematic transition as the density is increased above zero. Theories based on Bethe approximation [14], density functional theory [114], and exact solutions on tree-like lattices [15] predict a first order isotropic-nematic transition for $k \geq 4$. However, the topological structure of Bethe or tree-like lattices does not allow for the possibility of having flippable squares of size $k \times k$. This is unlike the case of hypercubic lattices where the possibility of flippable squares of size $k \times k$ leads to a finite entropy per rod at full packing, and leads to a high-density disordered phase, which does not occur on tree-like lattices. Also, the minimum value of k for such a transition to occur in three dimensions is not known.

Questions addressed

Unlike in two dimensions, the phase diagram of monodispersed rods on a three dimensional cubic lattice is not known. It is not clear what the high density phase will be. Also, are there phases different from a nematic phases. The questions addressed in the thesis are:

What is the minimum value of k for which nematic order is present in three-dimensions?

In two-dimensions, it was found that nematic order is present for $k \geq 7$. Is it the same in three-dimensions or different. Are there phase transitions possible for k less than this minimum value?

What is the high density phase for hard rods in three-dimensions?

Would the high density phase be qualitatively similar to the low density phase, as in two-dimensions or would it be different.

Is it possible to obtain the entire phase diagram of hard rods as a function of k and ρ where k is the length of the rod and ρ is the density? What is the nature of the phase transitions?

1.4 Hard cubes in three dimensions

Of the non-spherical shapes, the simplest is a cube, which has the additional feature that cubes can be packed to fill all space. Studies in complicated shapes such as rhombohedra [115] or in general three dimensional regular polyhedra or corner-rounded polyhedra [116, 117, 118] have been studied as more realistic models for experimental self-assembling systems [119, 120, 121], applications to drug delivery where shape of the carrier may decide its effectiveness [122], biological material like immunoglobulin [123], molecular logic gates [124, 125, 126], etc.

Theoretical studies in the continuum have focused on two cases: unoriented cubes whose faces are free to orient in any direction, and parallel hard cubes whose faces are parallel to the coordinate axes. The system of unoriented cubes was shown, using Monte Carlo and event driven molecular dynamics simulations, to undergo a first order freezing transition from a fluid to a solid phase at a critical packing fraction $\eta \approx 0.51$ [127]. Other simulations, however, found a cubatic phase that is sandwiched between the fluid and solid phases for packing fractions in the range $0.52 < \eta < 0.57$ [87]. It has been claimed in Ref. [127] that the cubatic phase is a finite-size artefact. The solid phase in this case is stabilized by an anomalously large concentration of vacancies [127].

In the case of parallel hard cubes, early work focused on finding the equation of state using

high-density expansions [128], and low-density virial expansion up to the seventh virial coefficient [129, 130]. Monte Carlo simulations show that the system of parallel hard cubes undergoes a continuous freezing transition from a disordered fluid phase to a solid phase at density $\rho \approx 0.48$ [131, 132]. The data near the critical point are consistent with the three-dimensional Heisenberg universality class [132]. These results are consistent with theoretical predictions using density functional theory [133]. Within this theory, the columnar phase is found to be not a stable phase at high densities [132, 133]. Thus, it would appear that parallel hard cubes in the continuum show only one phase transition and the high density phase is crystalline.

Earlier Monte Carlo studies of the discrete problem [20] found no phase transitions for densities up to full packing (in Ref. [20], the problem of cubes correspond to $\sigma = 2$). On the other hand, for cubes with sides of length two, the approximate density functional theory predicts that there should be a transition from a disordered phase to a layered phase at low densities and from a layered phase to a columnar phase at higher densities. When the length of a side is six, the theory predicts a transition from a disordered phase to a solid, and then to two types of columnar phases [21]. Simulations of a mixture of cubes of sizes two, and four or six, show a demixing transition [22] in contradiction to predictions from density functional theory [23]. However, the prediction for a pure system of cubes have not, to our knowledge, been tested in large scale simulations.

Questions Addressed

Lattice density functional theory predicts that hard cubes of edge-length two has three phases-disordered, layered and columnar [21], whereas Monte Carlo simulations of hard cubes of edge-length two in a cubic lattice, albeit for small system sizes find no signature of any phase transition [20].

What is the phase diagram of $2 \times 2 \times 2$ *cubes on a cubic lattice? What are the nature of the phase transitions.*

1.5 Overview of the thesis

The remainder of the thesis is organized as follows

In **Chapter 2**, a Monte Carlo algorithm with cluster moves is described and the implementation on a reference system of hard rods of length k in a square lattice of size $L \times L$ is discussed. Additional moves have been added to reduce the equilibration times at high densities are described. This algorithm does not suffer from jamming, like the single rod update algorithms and densities close to full packing can be probed. The generalization of this algorithm to three-dimensional systems is also discussed.

In **Chapter 3**, hard rods of size k is studied on a cubic lattice. For rods of length $k = 5, 6$, we find a transition from a low density disordered phase to a layered-disordered phase in which the fractional number of one orientation becomes very small, and system develops a layer-like structure, where each layer is a plane with most of the rods being of two orientations lying within the plane, and very weak correlations between different layers. When $k \geq 7$, at intermediate densities, we numerically observe two other phases: a nematic phase, and a new phase that we call the layered-nematic phase. In the layered-nematic phase, each plane has two dimensional nematic order, but there is no overall bulk nematic order. We also show that the layered-nematic phase is an finite size effect and give an estimate for the cross-over length scale to destabilize the layered-nematic phase. At even higher densities, the nematic order within a layer is also lost.

In **Chapter 4**, a system of $2 \times 2 \times 2$ hard cubes is studied on the cubic lattice. We find that this system of cubes goes through four distinct phases as the density of cubes is increased: disordered, layered, sublattice ordered, and columnar ordered. The disordered-layered phase transition is continuous, while the layered-sublattice and sublattice-columnar tran-

sitions are discontinuous. A Landau theory is written in terms of the layering order parameter **L** and columnar order parameter **C** which is able to describe the different phases that are observed in the simulations and the order of the transitions. Additionally, our results near the disordered-layered transition are consistent with the Landau theory prediction of scaling behaviour in the $O(3)$ universality class perturbed by cubic anisotropy.

In **Chapter 5**, we summarize our results and list some interesting open problems.

Chapter 2

Computational Methods

2.1 Introduction

In this chapter, we discuss a Monte Carlo algorithm with cluster moves which we have used in this thesis. The necessity of this algorithm is due to the fact that conventional Monte Carlo algorithm involving only evaporation and deposition of single particles have large relaxation times at high densities. In Sec. 2.2, we describe a system of hard rods in a square lattice. In Sec. 2.3, we discuss the need for a cluster algorithm. In Sec. 2.4, we describe the implementation of the algorithm for a system of hard rods in a square lattice. We extend this algorithm for hard rods in three-dimensions in Sec. 2.5 and hard cubes in three dimensions in Sec. 2.6

2.2 Model

In this section, we describe a monodispersed system of hard rods of length k in a square lattice of size $L \times L$. The rods primarily interact only via hard core exclusion and they are not allowed to intersect. Each rod occupies k consecutive sites either in the horizontal

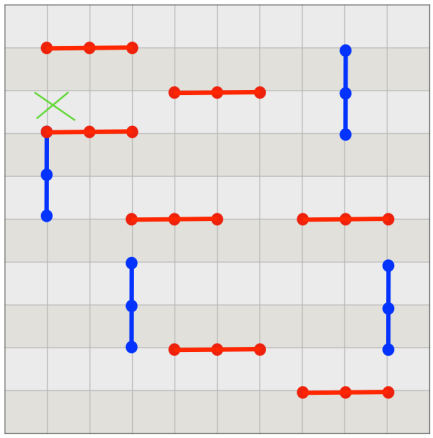

Figure 2.1: A snapshot of hard rods of length k in a square lattice.

or vertical direction, as shown in Fig. 2.1. We associate a weight $z = e^{\mu}$ with each rod, where z is the fugacity and μ is the chemical potential rescaled by temperature. The grand canonical partition function $\mathcal{L}(z)$ is given by:

$$\mathcal{L}(z) = \sum_{n_h, n_v} C(n_h, n_v)\, z^{n_h+n_v}, \tag{2.1}$$

where n_h and n_v are the number of the horizontal and vertical rods respectively and $C(n_h, n_v)$ is the number of configurations for n_h horizontal rods and n_v vertical rods. The horizontal rods are called x-mers and vertical ones are called y-mers. Earlier work done in the system of hard rods in two dimensions used a Monte Carlo algorithm involving only evaporation and deposition of single rods and found that the nematic phase exists for rods of length $k \geq 7$ [16]. For $k = 7$, this algorithm is able to equilibrate the system only when density was less than 0.85. At these densities, the phase is nematic.

2.3 Need for a cluster algorithm

The failure of algorithms with single-rod moves at high densities necessitates us to look for other approaches for simulating hard core lattice gas systems. The natural generaliza-

tion are cluster algorithms, which might solve the equilibration problem at high densities. Cluster algorithms have been used in spin systems for a long time, like the Swendsen-Wang algorithm for Ising spin systems [134] which uses the Fortuin-Kastelyn representation to map the Ising model to a random cluster model [135]. In this algorithm, a bond is formed between nearest neighbour spins that have the same sign with a probability $p = 1 - \exp(-2\beta J)$ where J is the coupling constant. This assignment is used to identify spins that are connected by bonds as clusters. Within a cluster, the spins are flipped with probability $1/2$. This happens for all the clusters and bond assignment starts again. The algorithm works because it is rejection-free as each cluster can be flipped independent of each other. This reduces the critical slowing down at the critical point that local update algorithm suffers from. A single cluster variant of the Swendsen-Wang algorithm, called the Wolff cluster algorithm was developed, which has a lower dynamical exponent than the former [136]. These have been generalized to other spin systems also.

In case of systems of hard particles, a cluster algorithm, called pivot cluster algorithm was developed for a hard sphere system in the continuum, which can be implemented in any dimension by C Dress and W Krauth [137]. In this, an arbitrary configuration $\mathcal{T}$ is rotated by π around an arbitrary point p, called a pivot which leads to a transformed configuration $\bar{\mathcal{T}}$. Both $\mathcal{T}$ and $\bar{\mathcal{T}}$ are superimposed to identify the clusters of overlapping spheres. The particles in each cluster is interchanged, independent of other clusters. The algorithm satisfies detailed balance trivially, as the probability of choosing a new configuration is proportional to its Boltzmann weight, and is independent of the current configuration.

In case of hard core lattice gas models, a cluster algorithm called a pocket algorithm was developed for a system of hard dimers on a square lattice [138] which is equivalent to the above mentioned pivot cluster algorithm. In this, for a given configuration of dimers and vacancies, a random symmetry axis is chosen and a dimer is reflected about the axis. If it overlaps with other dimers, they are also reflected and the move continues until there are no remaining overlapping dimers. This method is fairly fast and has minimal overhead,

but extension to other rods with higher lengths has proven to be difficult.

2.4 Description of the algorithm

We describe below a grand canonical Monte Carlo algorithm with cluster moves [17, 18, 19, 81] that help in equilibrating systems of hard particles with large excluded volume at densities close to full packing [17, 18] or at full packing [19]. A row is chosen at random and all the x-mers in that row are removed. The row consists of empty intervals, separated from one another by untouched y-mers. The row is now re-occupied by x-mers with the correct equilibrium probabilities. The calculation of these probabilities reduces to a one dimensional problem which may be solved exactly, and is described below. The evaporation and deposition move satisfies detailed balance as the transition rates depend only on the equilibrium probabilities of the new configuration.

The relevant probabilities are calculated as follows. Let $\Omega_o(z;\ell)$ be the grand partition function for an open chain of length ℓ. It follows a simple recursion

$$\Omega_o(z;\ell) = \underbrace{\Omega_o(z;\ell-1)}_{\text{1st site is unoccupied}} + \underbrace{z\Omega_o(z;\ell-k)}_{\text{1st site is occupied by head of } k\text{-mer}}, \tag{2.2}$$

subject to initial conditions $\Omega_o(z;\ell) = 1$ for $\ell = 0 \cdots k-1$.

Eq. (2.2) is a linear homogeneous recursion relation. So, the solutions will be of the form $\Omega_o(z;\ell) = \lambda^\ell$. Substituting this in Eq. (2.2) would yield

$$\lambda^k - \lambda^{k-1} - z = 0, \tag{2.3}$$

which is called the characteristic equation. The roots $\{\lambda_i\}$ can be obtained numerically and the most general form for $\Omega_o(z;\ell)$ is $\Omega_o(z;\ell) = \sum_{i=1}^{k} a_i \lambda_i^\ell$.

To solve for $\{a_i\}$, we set up the equations from the initial conditions

$$\underbrace{\begin{pmatrix} 1 & 1 & \cdots & 1 \\ \lambda_1 & \lambda_2 & \cdots & \lambda_k \\ \vdots & \ddots & \ddots & \vdots \\ \lambda_1^{k-1} & \lambda_2^{k-1} & \cdots & \lambda_k^{k-1} \end{pmatrix}}_{\text{Vandermonde Matrix}} \times \begin{pmatrix} a_1 \\ a_2 \\ \vdots \\ a_k \end{pmatrix} = \begin{pmatrix} 1 \\ 1 \\ \vdots \\ 1 \end{pmatrix}. \tag{2.4}$$

We then obtain $a_n = \prod_{\substack{m=1 \\ m \neq n}}^{k} \frac{1}{(\lambda_n - \lambda_m)}$.

The probability p_ℓ of the first site of an open chain of size ℓ to be occupied by a x-mer is:

$$p_\ell = z \frac{\Omega_o(z; \ell - k)}{\Omega_o(z; \ell)}. \tag{2.5}$$

If the occupation is successful, we repeat the same with the interval length reduced to $\ell - k$ and if it is not successful, it is repeated with interval length $\ell - 1$.

For periodic boundary conditions, the partition function $\Omega_p(z; \ell)$ of a periodic ring of size of ℓ is given by:

$$\Omega_p(z; \ell) = \Omega_o(z; \ell - 1) + kz\, \Omega_o(z; \ell - k). \tag{2.6}$$

This recursion relation may be explained as follows. Choose a first site. This site may either be empty (first term in Eq. (2.6)) or occupied by any monomer of a rod of length k (second term in Eq. (2.6)). The factor k in the second term in Eq. (2.6) is due to the fact that the k-mer can be placed in k different ways. The probability of an empty periodic ring of size L is

$$p_L = kz \frac{\Omega_o(z; \ell - k)}{\Omega_p(z; \ell)}. \tag{2.7}$$

The probabilities $\{p_\ell\}$ for $\ell = 0, \cdots, L-1$ can be stored to reduce computational overhead. Each row can be independently updated and therefore the algorithm is easily parallelized. After all the rows are updated, the same is done for columns.

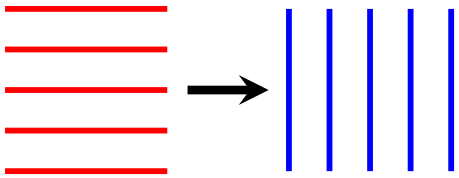

Figure 2.2: A schematic diagram illustrating the flip move in the Monte Carlo algorithm. If there is a $k \times k$ square, that is fully covered by k parallel k-mers as shown in (a), then the orientations of the k-mers within the square are flipped to the configuration shown in (b).

One of the ways to reduce the equilibration times at higher densities is to add additional local moves, which we call flip moves. If there is a $k \times k$ square, that is fully covered by k parallel k-mers, then we can flip the orientation of k-mers, within this square, without affecting any other rods, as shown in the schematic diagram in Fig. 2.2. Clearly, the flip move does not violate the hard-core constraint and satisfies detailed balance. A single Monte Carlo move involves $2L$ rows and column updates and L^2 flips for small system sizes or L^2/k^2 flips for a larger system size.

To get an estimate of the efficiency of the flip move, we plot the temporal evolution of the packing fraction ρ for high density in Fig. 2.3. Clearly, the addition of the flip move reduces the equilibration time by almost two orders of magnitude in the high density regime.

2.5 Extension to hard rods in three dimensions

Consider a cubic lattice of size $L \times L \times L$ with periodic boundary conditions. The lattice sites may be occupied by rods that occupy k consecutive lattices sites in any one of the three mutually orthogonal directions. We will call a rod oriented in the x-, y- and z-directions as x-mer, y-mer, and z-mer respectively. The site of a rod with the smallest x-, y-, and z-coordinates will be called its head.

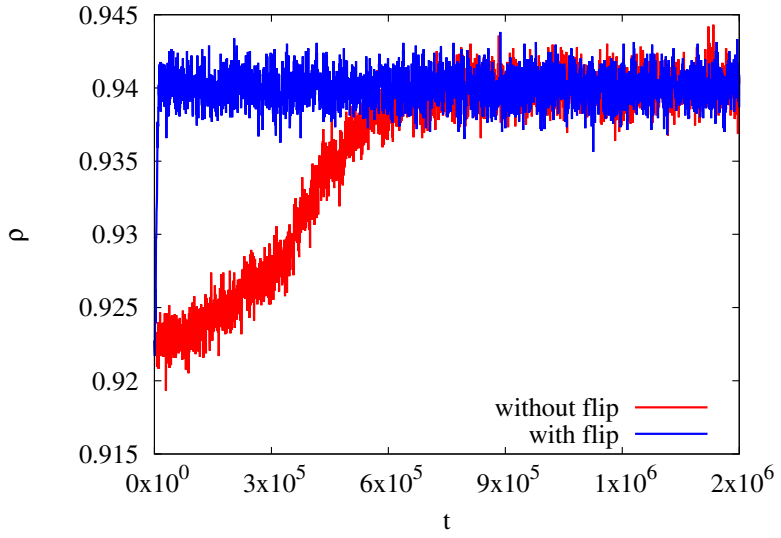

Figure 2.3: Temporal evolution of the packing fraction ρ for a hard rod system in a square lattice of size $L = 336$ with $\mu = 6.5$ and $\rho \approx 0.94$. The addition of flip move reduces the equilibration time by almost two orders of magnitude.

The Monte Carlo algorithm that we use is the following: remove all the x-mers, leaving all y-mers and z-mers undisturbed. The empty intervals in each row in the x-direction, separated from each other by y-mers or z-mers, is now re-occupied by x-mers with the correct equilibrium probabilities. The calculation of these probabilities are given in Sec. 2.4. Following evaporation and deposition of x-mers, we repeat the set of steps with y-mers, and then with z-mers.

To reduce equilibration and auto-correlation times at high densities, we also implement a flip move. We define one Monte Carlo time step as updating every row in the x-, y- and z- directions (total of $3L^2$ rows), and L^3(in case of small system sizes) or L^3/k^2(in case of large system sizes) flip moves.

The flip move is crucial for equilibrating the system at densities close to full packing. Figure 2.4 shows the time evolution of density ρ for a system with $k = 7$, starting from nematic initial conditions in which most of the rods lie in the x-direction, using the evaporation-deposition algorithm with and without the flip move. The value of μ is such that the equilibrium configuration does not have nematic order (see Sec. 3.5 for de-

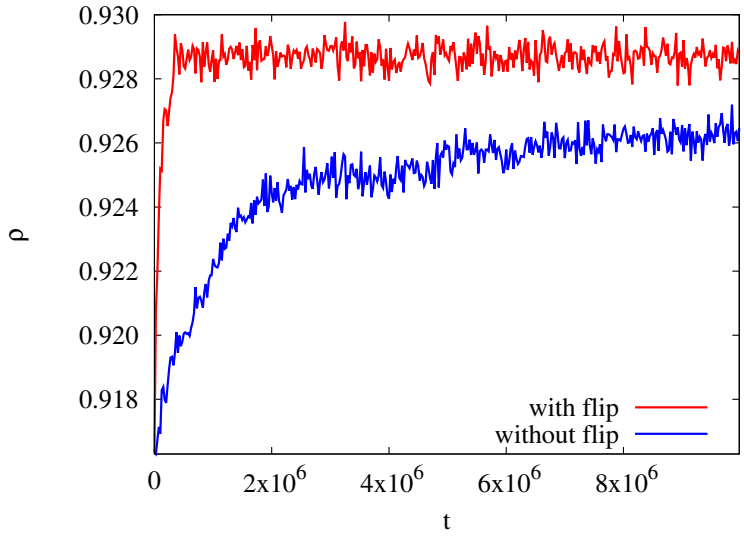

Figure 2.4: The temporal evolution of the density ρ in a system with $k = 7$, when the system is evolved using the evaporation-deposition algorithm with and without the flip move. The initial configuration has nematic order while the equilibrium configuration has layered order. The data are for system size $L = 112$ and $\mu = 6.0$.

tails). When the flip move is present, ρ reaches its equilibrium value in about 3×10^5 Monte Carlo steps. On the other hand, when the flip move is absent, the system does not reach equilibrium even after 10^7 Monte Carlo steps.

The algorithm is easily parallelized as all the rows can be updated simultaneously. The flip move may also be parallelized by choosing a plane and then choosing one of the k^2 sublattices randomly. All $k \times k$ squares with their left bottom corner lying in this sublattice may be updated simultaneously. The left bottom corner here signifies to the point with the minimum horizontal coordinate in either the $xy-$, $yz-$ and $zx-$plane. All the data presented in **Chapter 3** is obtained through a parallelized implementation of the algorithm.

2.6 Extension to hard cubes in three dimensions

Consider a $L \times L \times L$ cubic lattice with periodic boundary conditions and even L. The lattice may be occupied by cubes of size $2 \times 2 \times 2$ (i.e having side-length of 2 lattice

spacings) whose positions are in registry with the lattice sites. For a cube, we identify the vertex with minimum x-, y-, and z-coordinates as its head. The configuration of the system can thus be fully specified by the spatial coordinates of the heads of all the cubes in the system.

Choose at random one of the $3L^2$ rows, where each row consists of L consecutive sites in any one direction. Evaporate all the cubes whose "heads" that lie on this row. The row now consists of empty intervals separated from each other by sites that cannot be occupied by the head of a cube due to the hard constraints arising from cubes in neighbouring rows. The empty intervals are reoccupied by new configurations of cubes with the correct equilibrium probabilities. The calculation of these probabilities reduces to a one dimensional problem which may be solved in Sec. 2.4. This evaporation and deposition move satisfies detailed balance as the transition rates depend only on the equilibrium probabilities of the new configuration. We use a parallelized version of the algorithm described above, which exploits the fact that the rows separated from each other by a distance two can be updated independently and concurrently. We check for equilibration by taking different initial configurations of the system that correspond to different phases and confirming that the results are independent of the initial configuration. We find that the algorithm is able to equilibrate systems with density upto ≈ 0.95 for $L \gtrsim 100$, though slightly larger densities may be attained for smaller systems.

Chapter 3

Different phases of a system of hard rods on three dimensional cubic lattice

3.1 Introduction

In this chapter, we study the problem of a monodispersed system of rods of length k using grand canonical Monte Carlo simulations that is implemented through an algorithm with cluster moves. For $k \leq 4$, we find that the system remains disordered and is in the isotropic phase at all densities. When $k = 5, 6$, we observe a single transition from a low density disordered phase in which the the fractional number with different orientations is nearly equal, to a layered-disordered phase in which the fractional number of one orientation becomes very small, and system develops a layer-like structure, where each layer is a plane with most of the rods being of two orientations lying within the plane, and very weak correlations between different layers. When $k \geq 7$, at intermediate densities, we numerically observe two other phases: a nematic phase, and a new phase that we call the layered-nematic phase. In the layered-nematic phase, each plane has two dimensional nematic order, but there is no overall bulk nematic order. At even higher densities, the nematic order within a layer is also lost. This transition is essentially a 2-d transition,

as different layers are nearly independent. We argue that the observation of the layered-nematic phase in our simulations is a finite size effect, and in the thermodynamic limit, when there is nematic order within a layer, aligning the orientation of different layers is entropically favoured, and the nematically-ordered phase will have higher entropy than the layered-nematic phase.

The rest of the chapter is organized as follows. In Sec. 3.2, we define the model precisely and describe the grand canonical Monte Carlo scheme that is used to simulate the system. Section 3.3 describes the different phases – isotropic, nematic, layered-nematic and layered-disordered – that we observe in our simulations. In Sec. 3.4, we use perturbation theory to argue that the layered-nematic phase observed in simulations is an artefact of finite system sizes, and the observed behaviour should cross over to nematic order for length-scales greater that some crossover scale $L^*(\rho)$, where ρ is the density of covered sites. Section 3.5 contains results of detailed simulations for systems with $k = 2, 3, \ldots, 7$. The minimum length of rods that is needed for each of the phases to exist is determined. The critical densities and chemical potentials, and other critical parameters are determined for $k = 5, 6, 7$. We end with a summary and discussion of results in Sec. 3.6.

The contents of this chapter has been published in Ref. [139].

3.2 Model Description and Monte-Carlo Algorithm

Consider a cubic lattice of size $L \times L \times L$ with periodic boundary conditions. The lattice sites may be occupied by rods that occupy k consecutive lattices sites in any one of the three mutually orthogonal directions. The rods interact only through excluded volume interactions, i.e., a lattice site may be occupied by at most one rod. We associate a weight $z = e^{\mu}$ with each rod, where z is the fugacity and μ is the chemical potential rescaled by temperature. We will call a rod oriented in the x-, y- and z-directions as x-mer, y-mer, and z-mer respectively. The site of a rod with the smallest x-, y-, and z-coordinates will be

called its head.

We use grand canonical Monte Carlo simulations to determine the different phases in the hard rod model as a function of the density, for different rod-lengths k, as described in Sec. 2.5.

3.3 Different phases

In this section, we describe and define the different phases that we observe in our Monte Carlo simulations. Let ρ_x, ρ_y and ρ_z be the density of sites occupied by x-mers, y-mers and z-mers respectively, and $\rho = \rho_x + \rho_y + \rho_z$ is the total fraction of sites occupied by k-mers. We define the vectorial order parameter

$$\mathbf{Q} = |\mathbf{Q}|e^{i\theta} = \rho_x + \rho_y\, e^{\frac{2\pi i}{3}} + \rho_z\, e^{\frac{4\pi i}{3}}. \tag{3.1}$$

We define the bulk nematic order parameters as

$$Q_N = \langle |\mathbf{Q}| \rangle, \tag{3.2}$$

$$P_2 = \langle \cos(3\theta) \rangle, \tag{3.3}$$

where $\langle \cdots \rangle$ denotes average over the equilibrium probabilities. θ is the polar angle subtended by the vector order parameter $\mathbf{Q}$. θ takes values 0, $2\pi/3$, $4\pi/3$ in the nematic phase, and values $\pi/3$, π, $5\pi/3$ in both the layered-nematic and layered-disoeredered phases.

Isotropic phase: In the isotropic phase, the system is disordered with $\rho_x \approx \rho_y \approx \rho_z$. The probability distribution of $\mathbf{Q}$ is centred about the origin and the order parameters take the value $Q_N \approx 0$ and $P_2 \approx 0$.

Nematic phase: In the nematic phase, a majority of the rods are of one orientation, while

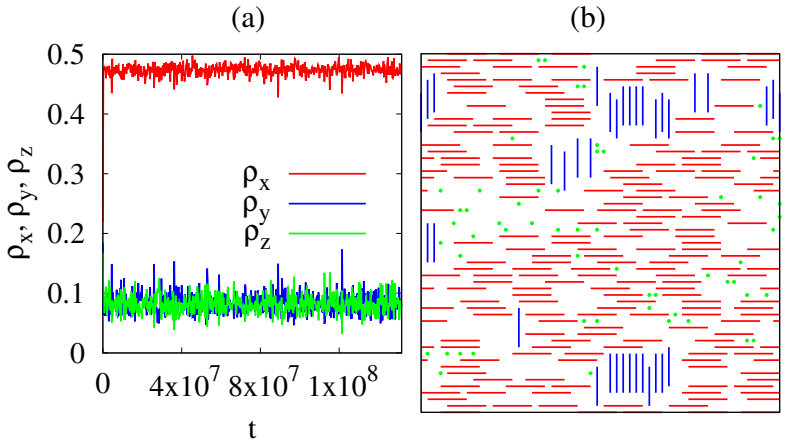

Figure 3.1: (a) Time evolution of the densities of rods along the three orientations in the nematic phase when $\mu = 0.3$ and $\rho \approx 0.63$ for $k = 7$ and $L = 56$. The initial configuration is disordered. (b) Snapshot of a randomly chosen xy plane after equilibration. The majority of rods are x-mers. The green solid circles represent z-mers passing through the given xy-plane.

the rods of the other two orientations have smaller, roughly equal densities. If x- is the preferred direction, then $\rho_x \gg \rho_y \approx \rho_z$, as can be seen in the temporal evolution of three densities shown in Fig. 3.1(a). A snapshot of a randomly chosen xy plane, as shown in Fig. 3.1(b), clearly shows that most rods are x-mers. In the nematic phase, $Q_N \approx \rho$ and $P_2 \approx 1$.

Layered-Nematic phase: In the layered-nematic phase, there is spontaneous symmetry breaking, and one of the xy, yz or zx planes is selected, and the density of rods that are oriented perpendicular to this plane is suppressed [see Fig. 3.2(a)], making the system layered. If the chosen plane is the xy plane, then $\rho_x \approx \rho_y \gg \rho_z$. In the layered-nematic phase, within a xy-plane, the rods have two-dimensional nematic order. This may seen in the snapshots, shown in Fig. 3.2(b)–(d), of three randomly chosen xy planes. Each of the planes has two-dimensional nematic order, but could be majority x-mers or y-mers. Also, the majority orientation within a plane changes frequently with time in our simulations. This is demonstrated in Fig. 3.2(e), where the time evolution of the local nematic order parameter $n_x(z) - n_y(z)$ is shown for four xy planes, where $n_x(z)$ and $n_y(z)$ are the densities of sites occupied by x-mers and y-mers in layer z. There are roughly equal number of

planes with majority x-mers and majority y-mers, as may be seen from the double-peaked probability distribution function $P(n_x - n_y)$, shown in Fig. 3.2(f), which is obtained by averaging over the different xy planes and over time. If the system has layered-nematic phase, $Q_N \approx \rho/2$ and $P_2 \approx -1$.

Layered-Disordered phase: In the layered-disordered phase, like in the layered-nematic phase, majority of the rods lie in one of the xy, yz or zx planes [see Fig. 3.3(a)]. Let the chosen plane be the xy plane, i.e., $\rho_x \approx \rho_y \gg \rho_z$. In the layered-disordered phase, unlike the layered-nematic phase, the rods within a xy plane do not have nematic order, i.e., $n_x(z) \approx n_y(z)$ for each layer z. This may seen in the snapshots, shown in Fig. 3.3(b)–(d), of three randomly chosen xy planes, where in each of the planes, there are roughly equal number of x-mers and y-mers present. The nematic order in each plane fluctuates about zero, as may be seen from the time evolution of the nematic order of four planes as shown in Fig. 3.3(e)] as well as probability distribution [see Fig. 3.3(f)] of the local nematic order parameter $n_x(z) - n_y(z)$. In the layered-disordered phase, $Q_N \approx \rho/2$ and $P_2 \approx -1$.

We find that onset of the layered disordered phase in 3-d for $k = 7$ occurs at approximately $\rho_{2,3d} \approx 0.914 \pm 0.01$ [Fig. 4(d)], which is not very different from the corresponding value in two dimensions ($\rho_{2,2d} \approx 0.917 \pm .005$) [18]. This is consistent with the picture that at high densities, the layers are only very weakly coupled, the transition from nematic (or layered nematic) to the layered disordered phase is essentially driven by the 2-dimensional transition within a layer.

The bulk order parameters Q_N and P_2 do not distinguish between the layered-nematic and layered-disordered phases and take the values $Q_N \approx \rho/2$ and $P_2 \approx -1$ for both phases. Though we observe both these phases in our simulations, we argue in the next section that the layered-nematic phase has lower entropy per site than the nematic phase, and is thus a metastable phase.

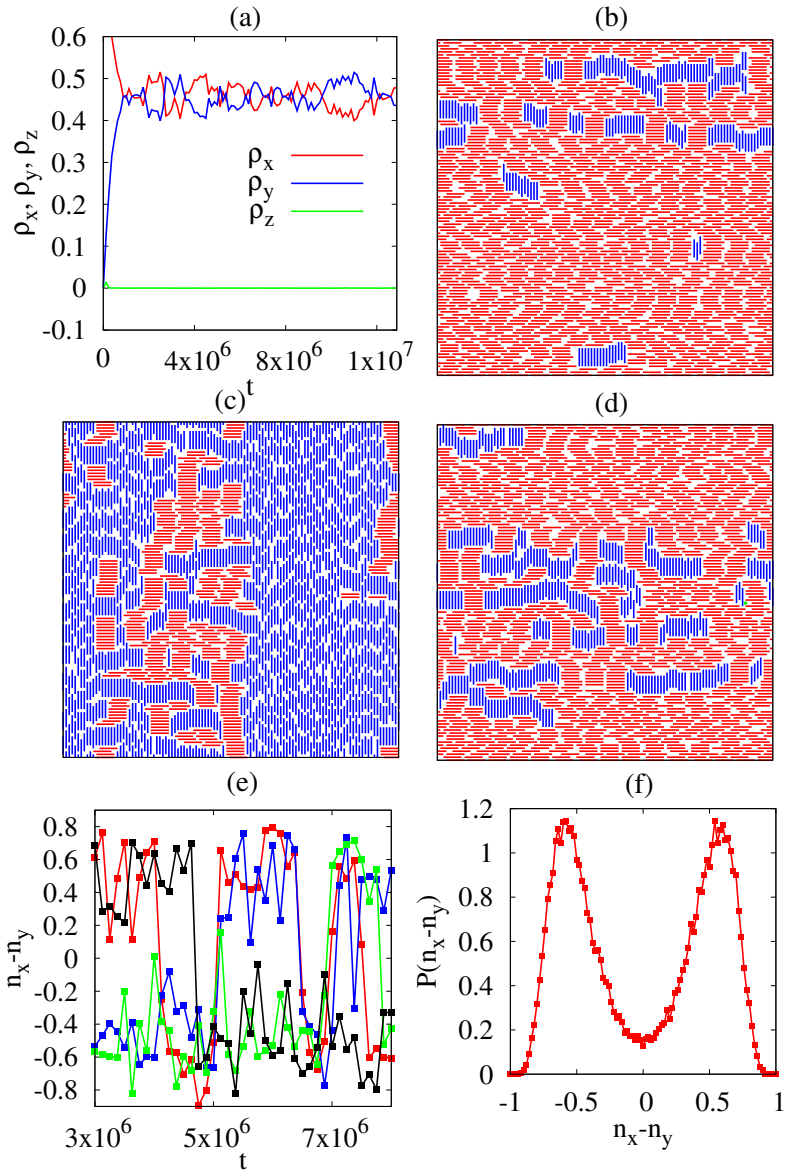

Figure 3.2: (a) Time evolution of the densities of rods along the three orientations in the layered-nematic phase when $\mu = 5.55$ and $\rho \approx 0.914$ for $k = 7$ and $L = 112$. The initial configuration has nematic order, where most of the rods are in x-direction. (b)–(d) Snapshots of three randomly chosen xy planes after equilibration. In each of the planes, either horizontal or vertical rods are in majority. (e) Time evolution of $n_x(z) - n_y(z)$, where $n_x(z)$ and $n_y(z)$ are the densities of x-mers and y-mers in layer z, for $z = 0, 24, 49, 74$. The nematic order in each plane keeps switching between majority x-mers and majority y-mers. (d) The probability distribution $P(n_x(z) - n_y(z))$, averaged over time and all planes, exhibits two symmetric peaks.

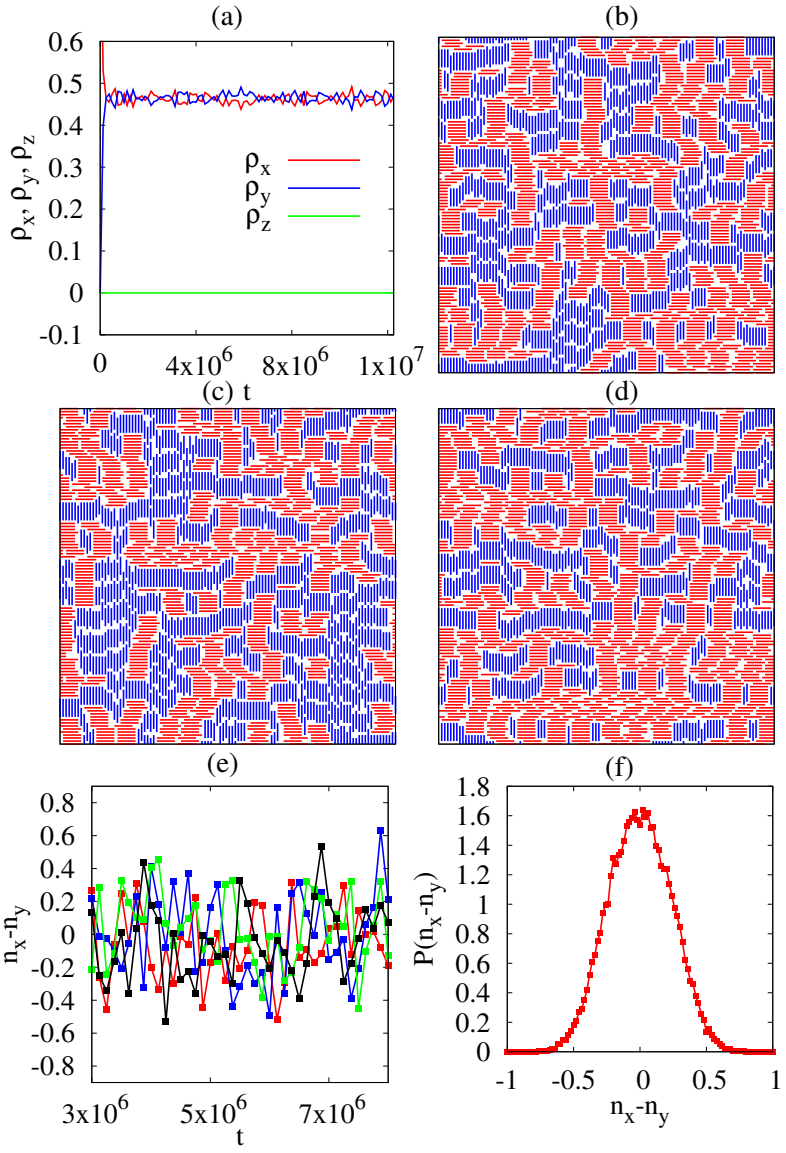

Figure 3.3: (a) Time evolution of the densities of rods along the three orientations in the layered-disordered phase when $\mu = 6.0$ and $\rho \approx 0.928$ for $k = 7$ and $L = 112$. The initial configuration has nematic order, where most of the rods are in x-direction. (b)–(d) Snapshots of three randomly chosen xy planes after equilibration. In each of the planes, there are roughly equal number of x-mers and y-mers. (e) Time evolution of $n_x(z) - n_y(z)$, where $n_x(z)$ and $n_y(z)$ are the densities of x-mers and y-mers in layer z, for $z = 0, 24, 49, 74$. It fluctuates about zero for all z. d) The probability distribution $P(n_x(z) - n_y(z))$, averaged over time and all planes, is peaked about 0.

3.4 The instability of the layered-nematic phase

In this section, we discuss the instability of the layered-nematic phase. We argue that the layered-nematic phase seen in our simulations is the result of finite size of our samples, and different layers would be expected to develop alignment and hence the usual nematic order if we could study samples of much larger sizes. This is done using a perturbative expansion similar to the high density expansion developed for hard squares and rectangles [69, 70, 80, 81, 72].

We start by considering a system in which the activities of rods in different directions are different: in the x- and y-directions, it is z, but in the z-direction it is z'. When $z' = 0$, the different z-layers decouple, and the problem reduces to the problem of k-mers on a two dimensional square lattice. We assume that z is such that in each layer there is nematic ordering, but in different layers, it may be in different directions. We consider the spontaneous-symmetry broken state $\{\sigma\}$, where the ordering direction in the layer $z = i$ is σ_i, taking values ± 1, depending on the mean orientation being in the x- or y-directions. There are 2^L such states, for the $L \times L \times L$ lattice, say with fixed boundary conditions that enforce the specified layered order.

When $z' = 0$, the states with different $\{\sigma\}$ are degenerate. We now develop a perturbation theory for the partition function $\mathcal{L}_{\{\sigma\}}(z, z')$ in powers of $z' = \exp(\mu')$ [70, 80]:

$$\mathcal{L}_{\{\sigma\}}(z, z') = \mathcal{L}_{\{\sigma\}}(z, 0)\left[1 + A_{\{\sigma\}}(z)z' + B_{\{\sigma\}}(z)z'^2 + \ldots\right]. \tag{3.4}$$

Define $\eta(\vec{R})$ as the indicator variable that takes a value 1 in a configuration, iff one can place the head of a z-mer at $\vec{R}$, and zero otherwise. Then it is easy to see that

$$A_{\{\sigma\}} = \sum_{\vec{R}} \langle \eta(\vec{R}) \rangle_{\{\sigma\}} \tag{3.5}$$

and

$$B_{\{\sigma\}} = \sum_{\vec{R}_1,\vec{R}_2} \langle \eta(\vec{R}_1)\eta(\vec{R}_2)\rangle_{\{\sigma\}}, \tag{3.6}$$

where the sum over $\vec{R}_1$ and $\vec{R}_2$ is over all position of 2 non-overlapping z-mers. The expectation values of products of $\eta(\vec{R})$'s factorize into terms that depend on correlations of unoccupied sites within a layer. Clearly, we get $A = L^3\epsilon^k$, independent of $\{\sigma\}$, where $\epsilon = 1 - \rho$ is the density of holes in the problem. Hence any difference between different layer-orderings only shows up in the B.

Let us denote the probability that in a 2-d layer, both sites (x, y) and $(x+\Delta_1, y+\Delta_2)$ are unoccupied as $\alpha(\vec{\Delta})$ or $\beta(\vec{\Delta})$, when the nematic ordering in the plane in x- or y- respectively, with $\vec{\Delta} = (\Delta_1, \Delta_2)$. Then, $B_{\{\sigma\}}(z)$ is a sum of terms of the form $\alpha(\vec{\Delta})^r\beta(\vec{\Delta})^s$, where r is the number of planes with x-ordering that intersect both rods, and s is the corresponding number of planes with y-ordering. By symmetry in the x and y directions, there will also be a term $\alpha^s\beta^r$ for the same $\{\sigma\}$ corresponding to separation $\vec{r}' = (\Delta_2, \Delta_1)$ between the rods. But we notice that, for all $\alpha, \beta \geq 0$, and integers $r, s \geq 0$,

$$\alpha^r\beta^s + \alpha^s\beta^r \leq \alpha^{r+s} + \beta^{r+s}. \tag{3.7}$$

This can be shown as following. Let us assume with no loss of generality that $\alpha \geq \beta$. Then for any $r, s \geq 0$, $(\alpha^r - \beta^r)(\alpha^s - \beta^s) \geq 0$. Equation (3.7) follows from this observation.

This implies that the second correction term, when all in-plane nematic orientations are parallel is greater than the term when they are not. Thus, the concentration of z-rods induces an effective aligning interaction between nearby layers. Note that this interaction term is proportional to the volume of the system, and would dominate over the degeneracy 2^L term coming from the number of different states $\{\sigma\}$. This is an order-by-disorder mechanism, where the degeneracy between different equal-weight states $\{\sigma\}$ is lifted, once the perturbation z' is introduced.

However, the excess free energy in the ordered nematic state per unit volume is only of

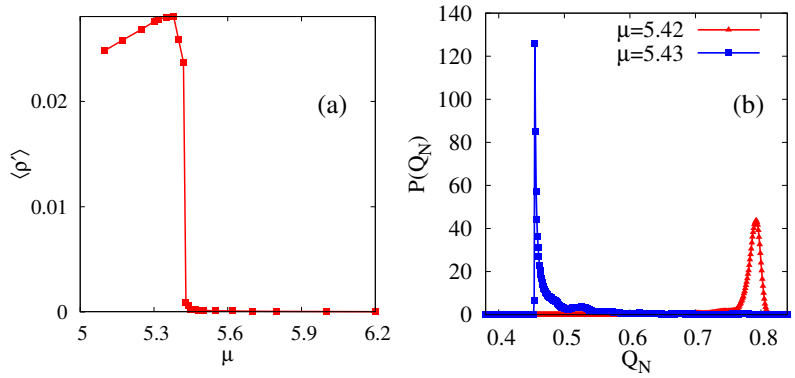

Figure 3.4: (a) The variation of $\langle\rho'\rangle$, the minimum of the densities of the rods of different orientations, with μ for $L = 112$ and $k = 7$ in the vicinity of transition from nematic phase to a layered-nematic phase. ρ' has a discontinuity as μ changes from $\mu = 5.42$ to $\mu = 5.43$, representing the onset of a layered phase. The lower values of $\langle\rho'\rangle$ stabilizes the layered-nematic phase for finite system sizes. (b) Corresponding probability distribution $P(Q_N)$ near the vicinity of nematic-layered transition. The peak of $P(Q_N)$ jumps as μ changes from $\mu = 5.42$ to $\mu = 5.43$.

$O([\rho'/k]^2)$, where ρ'/k is the number density of z-mers. In our simulations, for larger values of μ, ρ' becomes very small, for instance in $L = 112$ and $k = 7$, from Fig. 3.4, we see that $\rho'(\mu = 5.42) = 0.023$ and $\rho'(\mu = 5.43) = 0.0009$, just beyond onset of the layered nematic phase, representing an order of magnitude decrease in ρ' as μ is increased, so that one expects to see configurations with non-parallel nematic order between layers with significant weight if the disordering term $L \ln 2$ is of same order as the the ordering term $L^3(\rho'/k)^2$. Hence, we expect that for $L > L^* \sim k/\rho'$, the ordering term will win, and nematic ordered state will dominate. However, in our simulations, for $\mu = 5.42, k = 7$, $\rho' \approx 0.023$, and so, L^* is of order 300. For lower values of μ, ρ' is larger, and we do see the nematic order. In the other case of $\mu = 5.43$, $L^*(\rho' = 0.0009) \sim 7000$. This is much higher than the system size $L = 112$, implying that the layered-nematic phase is favoured for $\mu = 5.43$.

We now estimate L^* for large k by estimating the the free-energy cost of changing the orientation of one z-layer (say, the layer $z = 0$), to be along y-axis, while the remaining layers are all aligned in the x-direction. Let S_a be the state of fixed chemical potential z, where all the k-mers are aligned in the x-direction. We denote by S_b the state where

the $z = 0$ layer has orientation along the y-direction, and all other rods are oriented in the x-direction. Let $\mathcal{L}^{(a)}(z, z')$ and $\mathcal{L}^{(b)}(z, z')$ denote the grand partition function of these two cases, where z and z' are the activities of the rods in the xy plane and those perpendicular to it respectively. Then $\Delta F_{b,a} = -\ln \mathcal{L}^{(b)}(z, z') + \ln \mathcal{L}^{(a)}(z, z')$ is the free energy cost of creating a mis-aligned layer in the nematically ordered state S_a. These partition functions have a perturbation expansion in powers of z' as defined in Eq. (3.4). As explained above, we get $A_a = A_b$. Then, it is easy to see that to second order in z'^2, we obtain

$$\Delta F_{b,a} = [B_b(z) - B_a(z)]\, z'^2. \tag{3.8}$$

As noted above, this calculation requires the knowledge of the vacancy-vacancy correlations within a layer as a function of density. This is non-trivial, but we note that typically, the nematic order is near 1, and to a good approximation, the qualitative behaviour of vacancy-vacancy correlations is the same as that in the problem where the *all* the rods are constrained to lie in the same direction within a plane. Then the problem reduces to a one dimensional problem, for which the behaviour of correlations is known. Let $g(R, \epsilon)$ be the vacancy-vacancy pair correlation function of a gas of hard k-mers in one dimension:

$$g(R, \epsilon) = \epsilon^{-2} \left[\text{ Prob (site } x \text{ and } x + R \text{ are both unoccupied)} \right], \tag{3.9}$$

where $\epsilon = 1 - \rho$ is the density of empty sites.

The calculation of $g(R, \epsilon)$ is straightforward. Given a configuration of k-mers on a line, we construct another configuration, where the gaps between rods are the same as the first configuration, but the size of each rod is only 1. In this gas, different sites are *uncorrelated*, and the fractional density of unoccupied sites is $\epsilon' = \epsilon k/[1 + (k - 1)\epsilon]$.

This can be shown as follows. Let $C_o(L, N)$ and $C_p(L, N)$ be the number of ways to put N rods in a segment of length L with open and periodic boundary conditions respectively. It

is clear that

$$C_o(L,N) = \binom{L-Nk+N}{L-Nk}, \tag{3.10}$$

$$C_p(L,N) = C_o(L-1,N) + kC_o(L-k,N-1),$$
$$= L\,\frac{(L-1-Nk+N)!}{(N)!(L-Nk)!} \tag{3.11}$$

We put m rods in segment of $R-1$ and $N-m$ rods in segment $L-R-1$.

$$\text{Prob (site } x \text{ and } x+R \text{ are both unoccupied)} = \sum_{m=0}^{\lfloor (R-1)/k \rfloor} \frac{C_o(R-1,m)C_o(L-R-1,N-m)}{C_p(L,N)}. \tag{3.12}$$

Under the limit $R \ll L$, this yields,

$$\frac{C_o(L-R-1,N-m)}{C_p(L,N)} = \epsilon(L-Nk)^{R-mk}\,N^m\frac{1}{(L-Nk+N)^{R-mk+m}},$$
$$= \epsilon\epsilon'^{R-mk}(1-\epsilon')^m. \tag{3.13}$$

Therefore,

$$\text{Prob (site } x \text{ and } x+R \text{ are both unoccupied)} = \sum_{m=0}^{\lfloor (R-1)/k \rfloor} C_o(R-1,m)\epsilon\epsilon'^{R-mk}(1-\epsilon')^m \tag{3.14}$$

Then, it is easy to obtain

$$g(R,\epsilon) = \epsilon^{-1}\sum_{m=0}^{\lfloor (R-1)/k \rfloor}\binom{R-1-mk+m}{R-1-mk}\epsilon'^{R-mk}(1-\epsilon')^m. \tag{3.15}$$

In particular, for $r \le k$, we have $g(r,\epsilon) = \epsilon^{-1}\epsilon'^r$. Also, it is straightforward to obtain $g(mk+1,\epsilon) \approx \epsilon^{-1}\epsilon' \exp(-m\epsilon')$, where m is an integer smaller than ϵ'^{-1}, and fixed $\epsilon' \ll 1$, corresponding to the limit $\epsilon k \ll 1$. We note that $g(mk+2,\epsilon)$ is smaller than $g(mk+1,\epsilon)$ by a factor ϵ' for small m. Thus, $g(R,\epsilon)$ will show prominent oscillations of period k for $R \ll k\epsilon'^{-1}$. These oscillations may be seen in Fig. 3.5, where $g(R,\epsilon)$ has been numerically

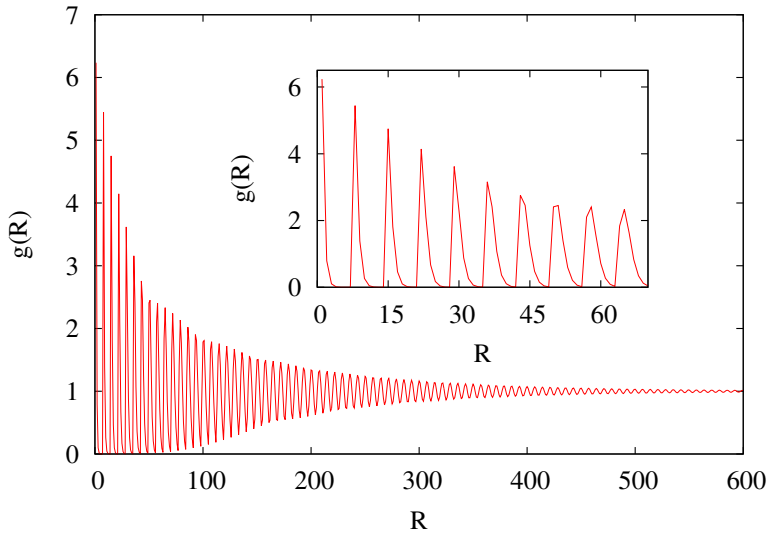

Figure 3.5: The variation of $g(R, \epsilon)$ [see Eq. (3.15)] with R for $k = 7$ and $\epsilon = 0.02$. Inset: The behaviour for small R, where the period of the oscillations are seen more clearly.

evaluated for $k = 7$ and $\epsilon = 0.02$. It shows oscillations of period 7 before converging to 1 for large R.

To compute $\Delta F_{b,a}$, it is easily seen that the most dominant contribution, when two rods are present in the z-direction, arises when both rods have heads in the same plane with same y-coordinates, and intersect the plane $z = 0$. The calculation is straightforward and gives

$$\Delta F_{b,a} = kL^2 z'^2 \epsilon^{2k} \sum_{R=1}^{\infty} [g(R, \epsilon) - 1][g(R, \epsilon)]^{k-1}, \tag{3.16}$$

$$= kL^2 z'^2 \epsilon^{2k} S(k, \epsilon). \tag{3.17}$$

In the sum in Eq. (3.16), the main contribution is from terms with $R = mk + 1$, where $m = 0, 1, \ldots (\epsilon' k)^{-1}$. All these terms have roughly the same contribution $(\epsilon'/\epsilon)^k$. Thus, we expect that the sum $S(k, \epsilon) \sim (\epsilon'/\epsilon)^k (\epsilon' k)^{-1}$. However, $\epsilon'/\epsilon \sim k \exp(-\epsilon k)$. Hence, we conclude that within second order perturbation theory

$$\Delta F_{b,a} \sim L^2 \epsilon'^{-1} k^k e^{-k^2 \epsilon} (z' \epsilon^k)^2. \tag{3.18}$$

The transition from the nematic to layered-disordered phase occurs at vacancy density $\epsilon \sim k^{-2}$ [18], corresponding to $\epsilon' \sim k^{-1}$. If we put $z' = z \sim k^k$, and $\Delta F_{b,a} = \ln 2$ due to the fact that there are 2^L possible states, we obtain $L^* \sim k^{\frac{k-1}{2}}$ for large k. For $k = 7$, $L^* \sim 340$, in fair agreement with our earlier estimate. However, L^* increases rapidly with k. For example, it is $L^* \sim 2 \times 10^{12}$ for $k = 20$. Thus, in simulations, while the layered nematic phase is thermodynamically unfavoured, it will always be observed in simulations due to the limitations in system sizes that can be simulated within available computer time.

3.5 Phase diagram and critical behavior

We numerically determined the order parameters Q_N [see Eq. (3.2)] and P_2 [see Eq. (3.3)] as function of ρ for different k as shown in Fig. 3.6. We first determine k_{min}, the minimum value of k required for each of the phases to appear.

3.5.1 k_{min}

From Fig. 3.6, it is evident that for $k \leq 4$, both Q_N and P_2 are zero for all values of ρ. There are no phase transitions and the system is in the disordered isotropic phase for all densities.

For $k = 5$ and $k = 6$, Q_N increases from 0 to 0.5 at high densities, while P_2 simultaneously decreases from 0 to -1. These values are indicative of the layered phase, and show that the system undergoes a single transition from an isotropic phase to a layered phase. Thus, for observing a layered phase, $k \geq k_{min}^{layered} = 5$. We note that there is no nematic phase when $k = 5, 6$. The critical values for the isotropic-layered transition are: $\mu_c(5) \approx 3.82$ and $\rho_c(5) \approx 0.874$ and $\mu_c(6) \approx 1.0$ and $\rho_c(6) \approx 0.68$.

When $k = 7$, it may be seen from Fig. 3.6 that Q_N increases from zero to $\approx \rho$ and then decreases to $Q_N \approx \rho/2$. Simultaneously, P_2 increases to 1 and then drops sharply to -1.

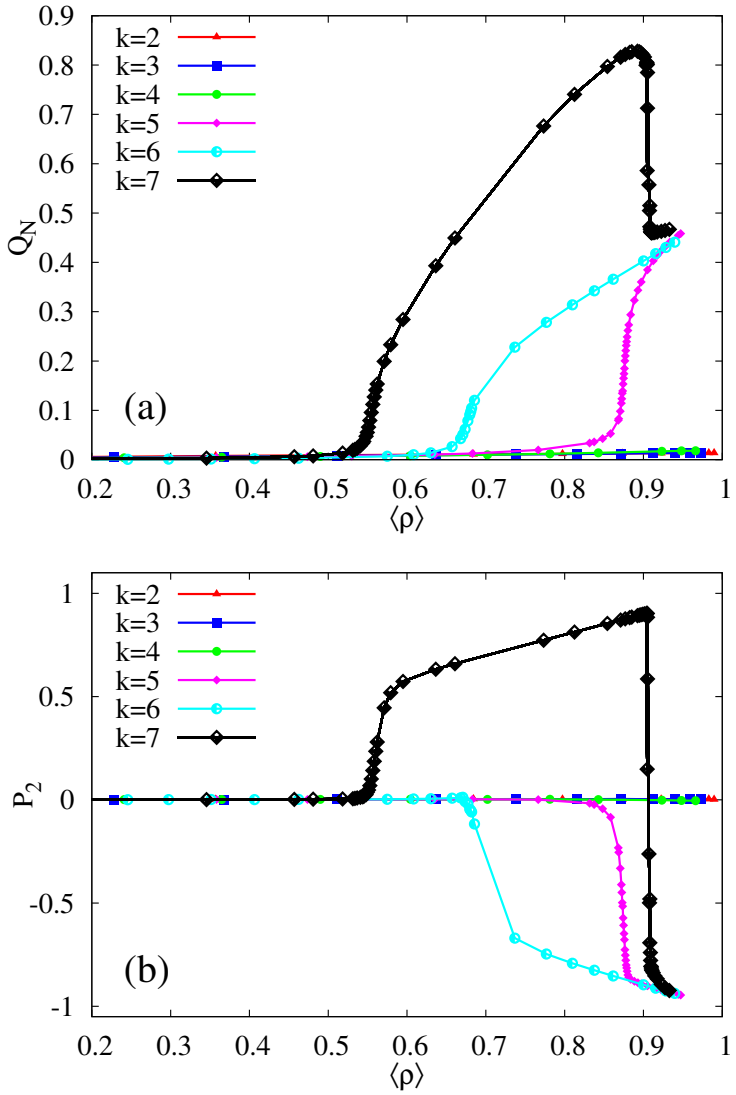

Figure 3.6: The order parameters (a) Q_N [see Eq. (3.2)] and (b) P_2 [see Eq. (3.3)] as a function of mean density $\langle\rho\rangle$ for $k = 2, \ldots, 7$. The data are for systems with $L = 10k$.

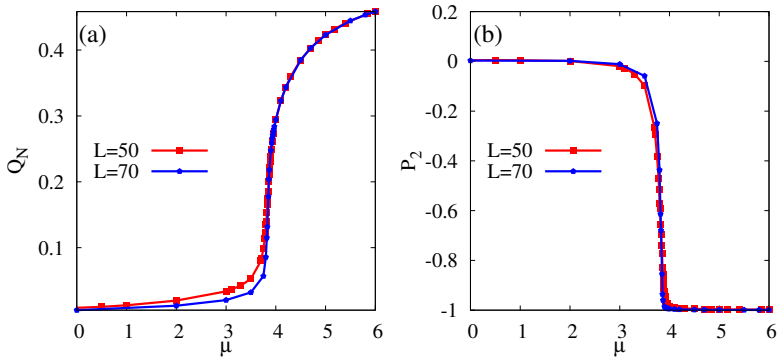

Figure 3.7: The order parameters (a) Q_N and (b) P_2 for $k = 5$ as a function of μ for two different system sizes. The data is very weakly dependent on the system size.

These values are indicative of nematic and layered phases. We conclude that a nematic phase exists for $k \geq k_{min}^{nematic} = 7$. In our simulations, we find that the layered phase may be further divided into layered-nematic and layered-disordered phases, but is presumably an artefact of the small sizes of our system, as discussed in Sec. 4.8.

3.5.2 $k = 5, 6$

Rods of length $k = 5$ are the smallest to show the layered-disordered phase at high densities. We first show that this phase is stable and that the Monte Carlo algorithm equilibrates the system at these densities. To show the stability, we compare the order parameters Q_N and P_2 for two different system size in Fig. 3.7. The data has only a very weak dependence on the system size, showing that the finite size effects are not important and that the layered phase is stable in the thermodynamic limit. The critical values for the transition is $\mu_c(5) \approx 3.82$ and $\rho_c(5) \approx 0.874$, estimated by determining the value of μ for which the probability distribution for Q_N shows a double-peaked structure.

To check that at the high values of μ and densities ρ, our simulations do not suffer from slow down due to jamming problems, we observed the evolution with two different initial conditions: one corresponding to a nematic phase and the other corresponding to an isotropic phase and check that the final state is independent of the initial conditions. The time evolution of $|\mathbf{Q}|$ is shown in Fig. 3.8 for both of these initial conditions. Clearly,

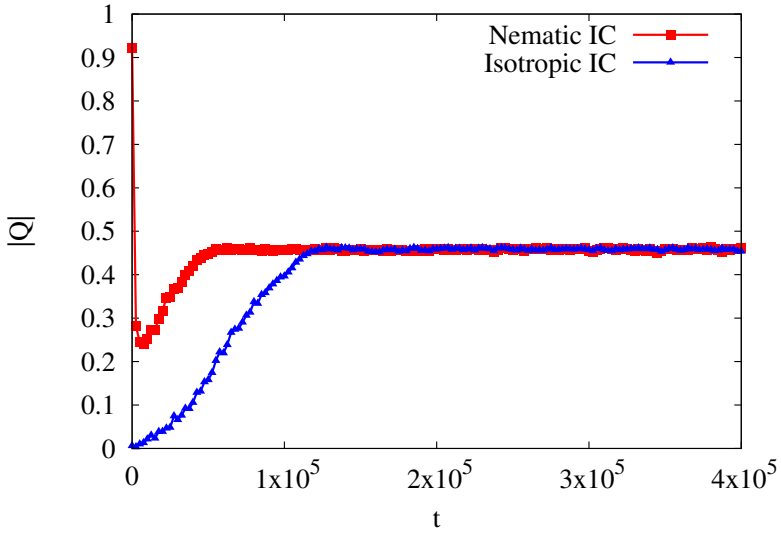

Figure 3.8: The time evolution of $|\mathbf{Q}|$ when the phase at time $t = 0$ is nematic or isotropic. IC in the legends is an acronym for initial conditions. The data are for $L = 70$, $k = 5$, and $\mu = 6.0$ and $\rho \approx 0.944$. The system loses memory of its initial state within 10^5 Monte Carlo steps, and equilibrates into a layered phase characterized by $\langle|\mathbf{Q}|\rangle \approx \rho/2$.

the system loses memory of the initial conditions quite rapidly, and the order parameter reaches a value close to 0.5, indicative of the layered phase.

We now study of the isotropic to layered-disordered transition. In the symmetry-broken state, there are three possible choices of the layering orientation. By analogy to the three state Potts model, we expect that this transition should be first order. The numerical data is consistent with a first order transition. First, we show in Fig. 3.9(a) the probability distribution of the order parameter Q_N near the transition point. The distribution has two peaks for values of μ close to the transition point, one near $Q_N \approx 0$, corresponding to the isotropic phase and the other close to $Q_N \approx 0.25$, corresponding to the layered phase. Double peaked distribution are a signature of first order transitions and co-existence. This can be further confirmed by looking at two-dimensional density plots of $P(\mathbf{Q})$, as shown in Fig 3.9(b)–(e), where as μ is increased, the simultaneous presence of peaks at the origin and and at $\pi/3$, π and $5\pi/3$ can be seen in Fig 3.9(c) and (d).

Further evidence of the first order nature may be obtained by studying the Binder cumu-

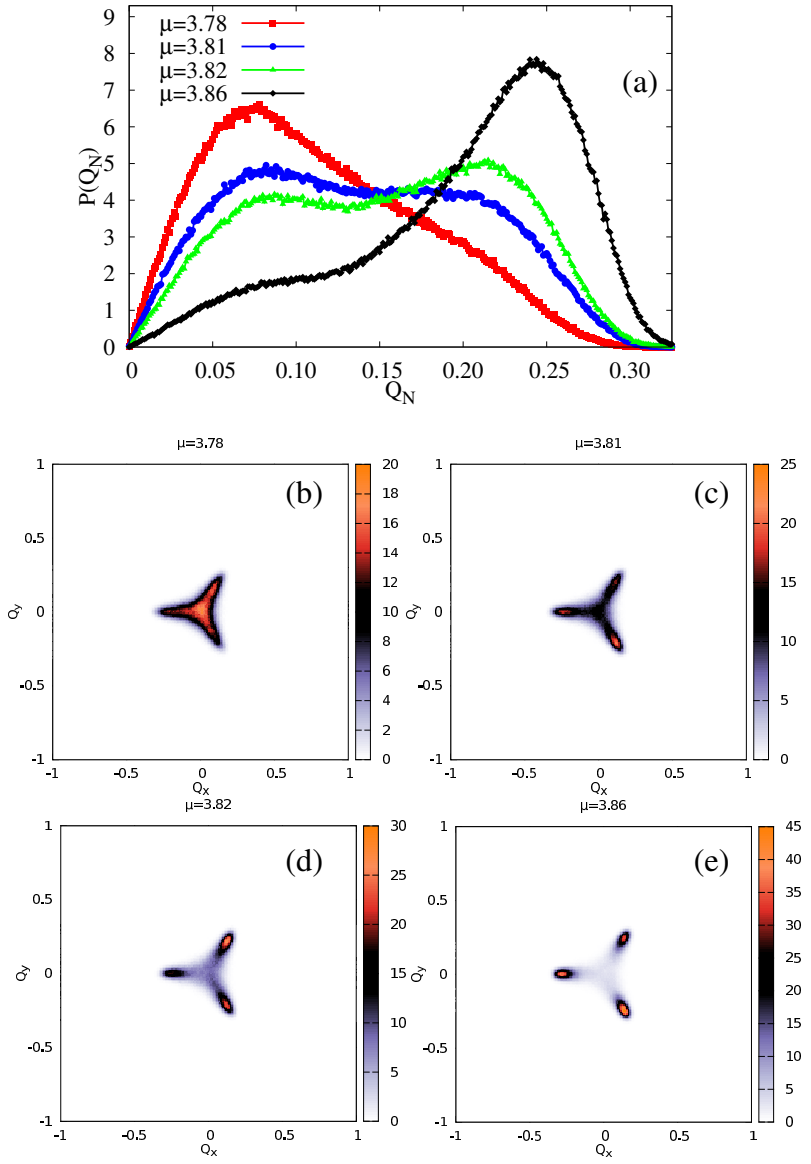

Figure 3.9: (a) The probability distribution $P(|\mathbf{Q}|)$ near the isotropic-layered transition for $L = 50$ and $k = 5$. (b)–(e) The two dimensional color plots for $P(\mathbf{Q})$ for different values of μ near the isotropic layered transition for $L = 50$ and $k = 5$.

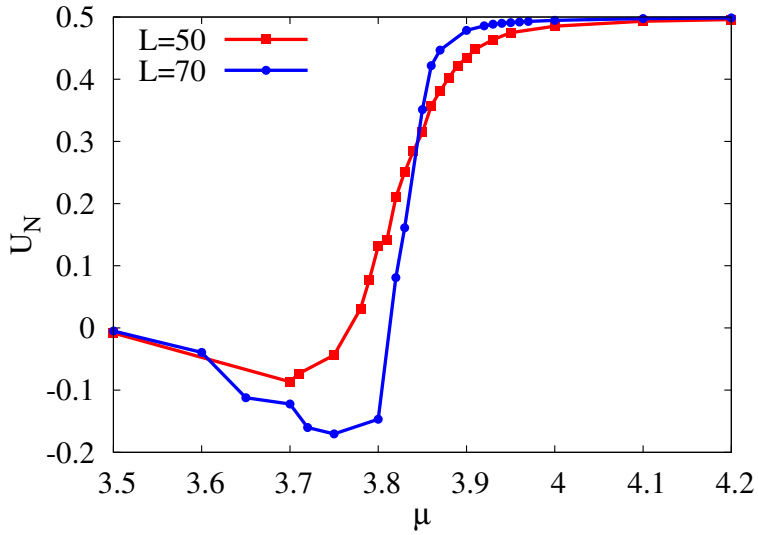

Figure 3.10: The variation of the Binder cumulant U_N [see Eq. (3.19)] with μ for two different system sizes. The data are for $k = 5$ near the isotropic-layered transition. U_N becoming negative is suggestive of a first order transition.

lant for a vector order parameter.

$$U_N = 1 - \frac{\langle |\mathbf{Q}|^4 \rangle}{2 \langle |\mathbf{Q}|^2 \rangle^2}. \tag{3.19}$$

In a continuous transition, the value of the Binder cumulant at the critical point is independent of the system size, providing a convenient tool to obtain the critical point [140]. U_N is zero in the isotropic phase and 1/2 in the completely ordered phase. The variation of U_N with μ is shown in Fig. 3.10. The Binder cumulant becomes negative near the transition point, with its minimum decreasing with system size. Binder cumulant becoming negative is a strong signature of the transition being first order [141].

The results for $k = 6$ are very similar to those of $k = 5$. The system undergoes a single transition from isotropic to layered phase with critical parameters $\mu_c(6) \approx 1.0$ and $\rho_c(6) \approx 0.68$. We note that the critical values are smaller than that for $k = 5$.

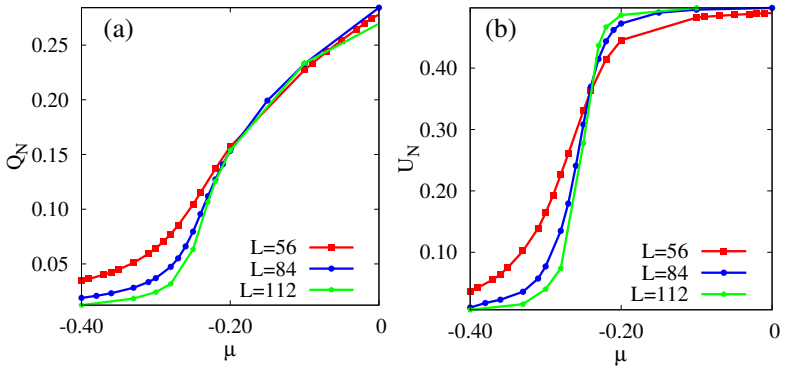

Figure 3.11: The variation of the (a) order parameter Q_N and (b) Binder cumulant U_N with μ for three different system sizes. The curves for the Binder cumulants cross at $\mu \approx -0.23$.

3.5.3 $k = 7$

When $k = 7$, the system undergoes a transition from an isotropic phase to a nematic phase at low densities and from nematic phase to a layered phase at high densities (see Fig. 3.6). Here, we analyse the nature of the transitions as well as the nature of the layered phase. We first discuss the isotropic-nematic transition. As in the case of $k = 5, 6$, there are three symmetric nematic phases corresponding to the three different orientations. By analogy with the three state Potts model, we expect that the transition will be first order in nature. The dependence of the order parameter Q_N and the Binder cumulant U_N on μ for different system sizes are shown in Fig. 3.11. Q_N does not show any sign of a discontinuity, nor does the Binder cumulant become negative, both being signatures of a first order transition. Likewise, the probability distribution for Q_N, shown in Fig. 3.12 does not show a bimodal distribution for any values of μ near the critical point. In the absence of signatures for a first order transition, we estimate the critical parameters to be $\mu_c \approx -0.23$ corresponding to $\rho_c \approx 0.556$, from the crossing of the Binder cumulants for different system sizes. The three state Potts model in 3-dimensions has a very weak first order transition that is difficult to detect in numerical simulations and we expect that the same difficulty holds for the problem of rods. Our simulations do not find a clear evidence of the nature of this phase transition.

We now examine the transition from nematic to layered phase. For $k = 7$ and $L = 112$,

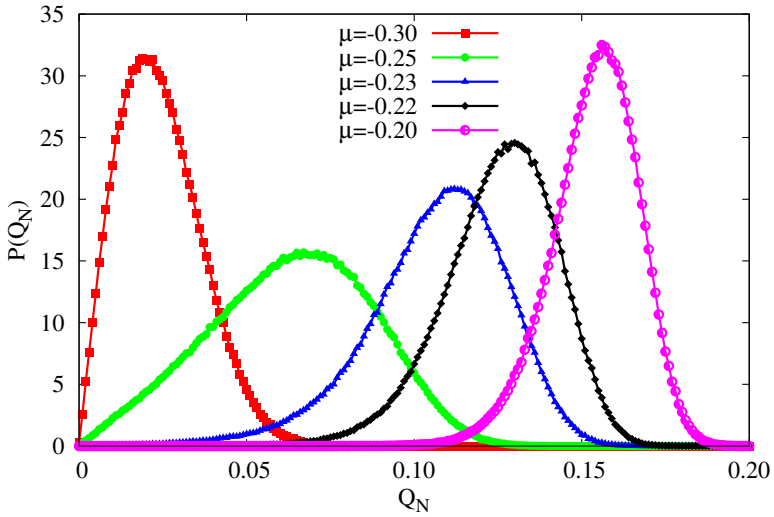

Figure 3.12: Probability distribution $P(Q_N)$ for $k = 7$ and $L = 112$ near the I-N transition. $P(Q_N)$ is unimodal and the peak position shifts continuously to the right with increasing μ.

we find a range of μ ($5.43 < \mu < 5.60$) for which the system finds itself in the layered-nematic phase. We check that this phase is stable for the finite systems we have studied, by simulating with initial condition that is isotropic, nematic and layered-disordered. Also, we notice that the transition from nematic to layered nematic is accompanied by a sharp decrease in ρ'. However, as we do not expect this to be a thermodynamic phase transition, we did not undertake a detailed study of the layered-nematic phase.

3.6 Summary and discussion

To summarize, we studied the problem of monodispersed hard rods on a three dimensional cubic lattice using grand canonical Monte Carlo simulations and theoretical methods to obtain the phases for rods of length k. We showed that for $k \leq 4$, the system is in a disordered isotropic phase at all densities ρ, and there are no phase transitions. For $k = 5, 6$, the system undergoes a single transition into a high density layered-disordered phase, where the system breaks up into two dimensional layers, but disordered within a layer. For $k = 7$, we find that as density is increased, the system makes a transition into a nematic

phase. Further increase of density results in a layered-disordered phase.

We also observe a layered-nematic phase between the nematic and layered-disordered phases, which we argued is a finite-size effect. By developing a perturbation expansion in terms of number of z-mers, we estimated the system size that is required for the layered-nematic phase to be destabilized into a nematic phase to be $L^* \sim k^{(k-1)/2}$. Thus, L^* increases rapidly with k with $L^* \sim 340$ for $k = 7$. Therefore, in simulations of systems with larger k, we expect that there will be a range of densities for which the layered nematic phase will be observed.

For values of $k > 7$, we expect that the phase diagram remains qualitatively the same as that for $k = 7$. We expect the critical density for the isotropic-nematic transition to decrease with increasing k, as is confirmed by Monte Carlo simulations of systems with $k = 8, 9, 10$. As seen from Fig. 3.13, ρ_c decreases from 0.556 for $k = 7$ to 0.364 for $k = 10$. Near the isotropic-nematic transition, the $O(\rho^2)$ term in the expansion of pressure as a function of density should be approximately of same magnitude as the first term of $O(\rho)$. Since the second virial coefficient for hard rods of length k varies as k^2 in all dimensions (for large k), the critical number density of rods scales as k^{-2} or equivalently the critical density $\rho_c^{I-N} \sim k^{-1}$, consistent with the estimate given in Ref. [112], where the numerical data for $k = 7, 8, 16, 25$ in three dimensions obey $\rho_c^{I-N} \sim k^{-1}$. The tabular form of the various cases studied and the phases and nature of transitions are mentioned in Table 3.1. On the other hand, the nematic-layered transition is essentially a two dimensional transition, as different layers are nearly independent. Thus, we expect that the critical density for this transition varies as $1 - a/k^2$ for large k, as in two dimensions [16].

These arguments are easily extended to higher dimensions. For large enough k, we will expect a isotropic-nematic transition at a critical density that scales as k^{-1}. A nematic phase may be thought of a union of parallel lines, with hard core constraint along a line, and the problem becomes essentially one dimensional, with weak correlations between

Cases Studied	Phases	Nature of transition
$k \leq 4$	Disordered	No transitions
$k = 5, 6$	Disordered → Layered-Disordered	First-order
$k \geq 7$	Disordered →Nematic→Layered-Nematic→Layered-Disordered	The disordered-nematic transition is expected to be weakly first order and the nematic-layered transition is first-order.

Table 3.1: A summary of the phases and nature of the phase transitions observed for the values of k that have been studied.

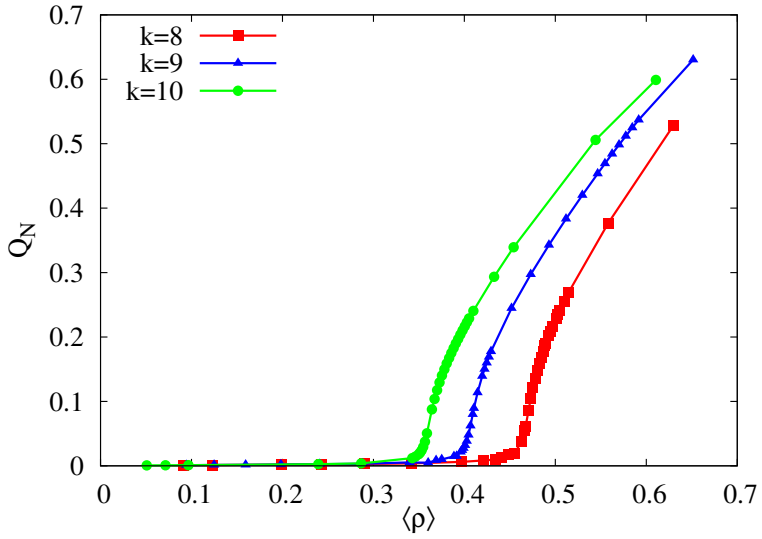

Figure 3.13: The behaviour of the order parameters Q_N near the isotropic-nematic transition for $k = 8, 9, 10$. The data are for $L = 10k$.

different lines. In the high-density phase, we expect that the system will break to *two-dimensional* layers, with only weak interaction between different layers. The critical density will be nearly independent of d for $d \ll k$. This critical density will vary as $1 - a/k^2$ for large k. Preliminary simulations in four dimensions are consistent with the above observations.

From the results of this chapter, it is clear that for $k \geq 5$, the fully packed phase shows spontaneous symmetry breaking by selecting the layering plane. It is thus qualitatively different from the $k \leq 4$. Extending the problem of rods to cuboids would result in a much richer phase diagram, as expected from the corresponding case of hard rectangles in two dimensions. However, simulations of such systems is a challenging task.

Note added

Recently, a study on the same system was published in Ref. [112]. There, the system is studied using grand canonical Monte Carlo simulations using local evaporation-deposition moves. Similar results are obtained. However, the algorithm is not able to efficiently equilibrate at high densities and thus could not access the isotropic-layered transition for $k = 5$ and the nematic-layered transition for $k = 7$. By studying larger system sizes, some numerical evidence for the first order nature of the isotropic-nematic transition could be found.

Chapter 4

Phase diagram of a system of hard cubes on the cubic lattice

4.1 Introduction

In this chapter, we study a system of $2 \times 2 \times 2$ hard cubes on the cubic lattice using grand canonical Monte Carlo simulations that implements an algorithm with cluster moves. The positions of cubes are discrete.

Here, we find that this system of cubes goes through four distinct phases as the density of cubes is increased: disordered, layered, sublattice ordered, and columnar ordered. In the layered phase, the system spontaneously breaks up into parallel slabs of size $2 \times L \times L$ which are preferentially occupied by cubes, in which the density oscillates along the direction perpendicular to the slabs with period two. Within each slab, the cubes are disordered; translation symmetry is thus broken along exactly one principal axis. In the solid-like sublattice ordered phase, the hard cubes preferentially occupy one of eight sublattices of the cubic lattice, breaking translational symmetry along all three principal directions. In the columnar phase, the system spontaneously breaks up into weakly interacting par-

allel columns of size $2 \times 2 \times L$ which are preferentially occupied by cubes, in which the density oscillates along the two directions perpendicular to the columns with period two. Within each column, the system is disordered, and the columns break translational symmetry along two principal directions. By studying systems of different sizes, we argue that the disordered-layered phase transition is continuous, while the layered-sublattice and sublattice-columnar transitions are discontinuous. We construct a Landau theory written in terms of the layering order parameter **L** and columnar order parameter **C** which is able to describe the different phases that are observed in the simulations and the order of the transitions. Additionally, our results near the disordered-layered transition are consistent with the Landau theory prediction of scaling behaviour in the $O(3)$ universality class perturbed by cubic anisotropy.

The remainder of this chapter is organized as follows. Section 4.2 defines the model precisely and describes the grand canonical Monte Carlo scheme that is used to simulate the system. Section 4.3 describes the different phases – disordered, layered, sublattice ordered and columnar ordered– that we observe in our simulations. In Sec. 4.4, we understand our simulation results in terms of a Landau theory approach. Sections 4.5 - 4.7 characterize the different phase transitions that occur in this system. Section 4.8 discusses the long lived metastable states that we observe at densities close to full packing. This section also presents a perturbation expansion that allows us to argue that the high density phase will be columnar. Finally, Sec. 4.9 contains a discussion of our results.

The contents of this chapter has been published in Ref. [142].

4.2 Model & Algorithm

Consider a $L \times L \times L$ cubic lattice with periodic boundary conditions and even L. The lattice may be occupied by cubes of size $2 \times 2 \times 2$ (i.e having side-length of 2 lattice spacings) whose positions are in registry with the lattice sites. We associate a weight

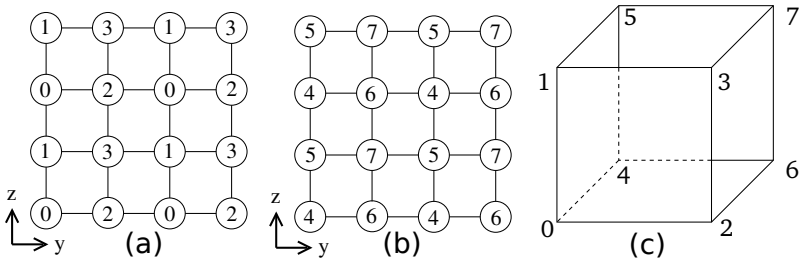

Figure 4.1: The lattice is divided into eight sublattices $0, 1, \ldots, 7$ depending on whether the x-, y- and z- coordinates are even or odd. Labelling of sublattices corresponding to yz-planes whose x-coordinate is (a) even, or (b) odd. (c) A $2 \times 2 \times 2$ cube with all of its vertices labelled with appropriate sublattices to show the relative positions of the planes shown in (a) and (b).

$z = e^{\mu}$ with each cube, where z is the fugacity and μ is the chemical potential. The cubes interact through only excluded volume interaction, *i.e.* no two cubes can overlap in volume. For a cube, we identify the vertex with minimum x-, y-, and z-coordinates as its head. The configuration of the system can thus be fully specified by the spatial coordinates of the heads of all the cubes in the system.

We study the model using grand canonical Monte Carlo simulations implementing an algorithm as described in Sec. 2.6.

4.3 Different Phases

We first define and describe the phases that we observe in our simulations. To do so, it is convenient to divide the lattice into 8 sublattices, depending on whether each x-, y-, and z-coordinates are odd or even. A site with coordinates (x, y, z) belongs to sublattice whose binary representation is (x mod 2) (y mod 2) (z mod 2), as shown in Fig. 4.1. We define ρ_i to be the fraction of lattice sites occupied by the cubes whose heads lie on the sublattice i. The total density of the system ρ is then

$$\rho = \sum_{i=0}^{7} \rho_i. \tag{4.1}$$

Further, let $\eta(x, y, z)$ be equal to 1 if (x, y, z) is occupied by a head of the cube, and be equal to 0 otherwise. Here, $\eta(x, y, z)$ acts as an indicator function. Consider the Fourier transform

$$\tilde{\eta}(k_x, k_y, k_z) = \frac{8}{L^3} \sum_{x,y,z} \eta(x, y, z)\, \mathrm{e}^{i(k_x x + k_y y + k_z z)}. \tag{4.2}$$

We define the order parameter $\mathbf{L}$ as

$$\mathbf{L} = (L_x, L_y, L_z), \tag{4.3}$$

where $L_x = \tilde{\eta}(\pi, 0, 0)$, $L_y = \tilde{\eta}(0, \pi, 0)$ and $L_z = \tilde{\eta}(0, 0, \pi)$. A non-zero value in L_x will imply that there is translational order of period two in x direction. Similar interpretations hold for L_y and L_z. The $\mathbf{L}$ vector is thus a measure of the layering tendency of the system in each Cartesian direction, and we shall refer to it as the layering vector. In a layered phase, only one Cartesian component of $\mathbf{L}$ is expected to be non-zero in the thermodynamic limit. In contrast, a columnar-ordered phase is characterized by a layering vector with two non-zero Cartesian components. Finally, a solid-like sublattice-ordered phase is characterized by a layering vector with all three components non-zero.

Note that $\mathbf{L}$ serves as a "faithful" order parameter for each of these three phases: In the layered case, it correctly distinguishes between the six symmetry-related states of the system (corresponding to the two possible layered states for layering along each of the three Cartesian directions) by taking on the six symmetry related values $(\pm|L|, 0, 0)$, $(0, \pm|L|, 0)$, and $(0, 0, \pm|L|)$. In the columnar-ordered case, it correctly distinguishes between the twelve symmetry-related columnar states by taking on the twelve symmetry-related values $(\pm|L|, \pm|L|, 0)$, $(0, \pm|L|, \pm|L|)$, and $(\pm|L|, 0, \pm|L|)$. Finally, the eight symmetry-related sublattice ordered states are correctly described by the eight symmetry-related values $(\pm|L|, \pm|L|, \pm|L|)$.

To characterize these phases, it is also useful to define two other measures of spontaneously broken symmetry: the columnar vector $\mathbf{C}$ whose components are given by

$C_x = \tilde{\eta}(0, \pi, \pi)$, $C_y = \tilde{\eta}(\pi, 0, \pi)$ and $C_z = \tilde{\eta}(\pi, \pi, 0)$, and the sublattice scalar $\phi = \tilde{\eta}(\pi, \pi, \pi)$. In contrast to **L**, neither **C** nor ϕ fully distinguish between the broken symmetry states in which they are non-zero in the thermodynamic limit. This is clear since **C** is expected to be non-zero in the columnar ordered phase and the sublattice ordered phase, but does not fully distinguish between the twelve symmetry-related columnar states or the eight symmetry-related sublattice ordered states of the system. Similarly, ϕ is expected to be non-zero in the sublattice ordered phase, but does not fully distinguish between the eight symmetry-related sublattice ordered states.

The underlying reason for this distinction between **L** on the one hand, and **C** and ϕ on the other, is clarified considerably if we pass from the globally defined quantities **L**, **C** and ϕ, to the corresponding local fields $\mathbf{L}(\vec{\mathrm{r}})$, $\mathbf{C}(\vec{\mathrm{r}})$ and $\phi(\vec{\mathrm{r}})$. These local fields should be thought of as being the coarse-grained variables (coarse-grained over a linear scale of a few lattice spacings) whose sum over the entire volume gives the corresponding global variables. Thinking in terms of these local fields, we see that $C_x(\vec{\mathrm{r}}) \sim L_y(\vec{\mathrm{r}})L_z(\vec{\mathrm{r}})$ (and similarly for the other components). This is related to the fact that the composite variable L_yL_z acts as a field that couples linearly to C_x in a Landau-type description of spontaneous symmetry breaking. Likewise, $\phi(\vec{\mathrm{r}}) \sim L_x(\vec{\mathrm{r}})L_y(\vec{\mathrm{r}})L_z(\vec{\mathrm{r}})$. Thus, $\mathbf{C}(\vec{\mathrm{r}})$ and $\phi(\vec{\mathrm{r}})$ take on mean values set by *composite* variables formed from the components of the local layering vector, which emerges as the fundamental quantity for describing the broken symmetries of the system. It is therefore not surprising that the corresponding global variables **C** and ϕ do not fully distinguish between different symmetry-related states with spontaneous columnar or sublattice order. This also suggests that a Landau theory for all three broken symmetry phases should involve **L** as the key variable, although we shall see below that the symmetry-allowed couplings between **L** and **C** and ϕ can also play a crucial role in determining the structure of the phase diagram.

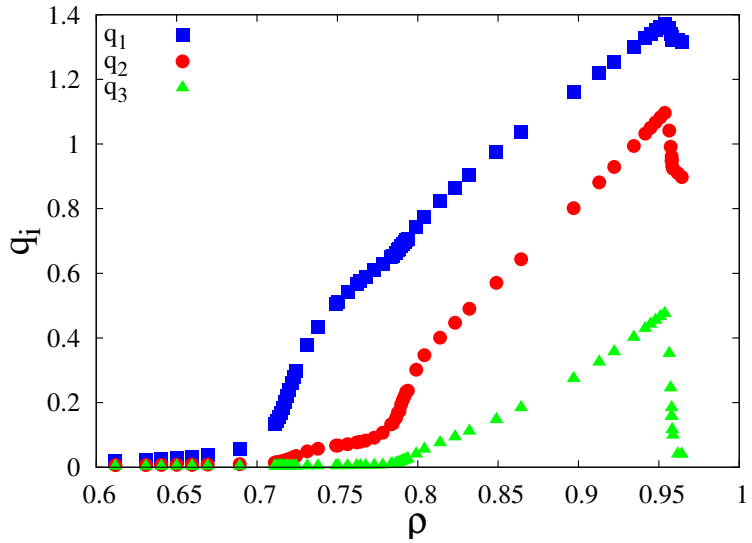

Figure 4.2: Variation of q_1, q_2, q_3, as defined in Eqs. (4.4)–(4.6), with density ρ. The data are for system size $L = 70$. Discontinuities in density are not visible at this resolution.

In our simulations, we measure the magnitudes of the global variables **L**, **C** and ϕ:

$$q_1 = \sqrt{L_x^2 + L_y^2 + L_z^2}, \tag{4.4}$$

$$q_2 = \sqrt{C_x^2 + C_y^2 + C_z^2}, \tag{4.5}$$

$$q_3 = |\phi|. \tag{4.6}$$

In addition, we monitor the joint probability distribution (histogram) of L_x, L_y and L_z in order to visualize the nature of the symmetry breaking present in various ordered states.

The variation of q_i with density ρ is shown in Fig. 4.2. For low densities $q_i \to 0$ in the thermodynamic limit for $i = 1, 2, 3$ and the system is in a disordered phase. As the density is increased, q_1 becomes non-zero in the thermodynamic limit when the density crosses $\rho \approx 0.718$, signalling the onset of spontaneous layering, while q_2 and q_3 continue to be zero in the thermodynamic limit. Upon further increasing the density, both q_2 and q_3 become non-zero in the thermodynamic limit when the density increases beyond $\rho \approx 0.79$. This corresponds to the onset of a crystalline phase with spontaneous sublattice ordering. Finally, when the density goes beyond $\rho \approx 0.957$, q_3 becomes zero, while q_2 and q_1 remain non-zero, corresponding to columnar order. Below, we describe the behaviour of

the system in each of these phases in some more detail.

Disordered Phase: At low densities, the cubes are in a disordered phase in which the cubes are far apart and there is no ordering. All the mean sublattice densities are equal, *i.e.*, $\rho_i \approx \rho/8$, for $i = 0, \ldots, 7$. In the disordered phase, all components of $\mathbf{L}$ tend to zero in the limit of large system sizes [see Eq. (4.3) for definition] and the system retains all the symmetries of the underlying cubic lattice.

Layered Phase: In the layered phase, translational symmetry is broken in only one direction. The cubes preferentially occupy either odd or even planes normal to this direction. This may be seen by examining snapshots of randomly chosen pairs of even and odd planes in the three directions as shown in Fig. 4.3, where the eight different colours represent cubes whose heads lie on a particular sublattice. Grey colour represents sites that are occupied by cubes whose heads are on neighbouring planes. In Fig. 4.3(a)-(d), showing the snapshots of randomly chosen even and odd yz and xz planes, there are approximately equal numbers of coloured cubes and grey cubes, showing both odd and even yz- and xz-planes are equally occupied. On the other hand, it can be seen that Fig. 4.3(e), showing a snapshot of a randomly chosen even xy plane, having much larger number of coloured squares than grey squares, while Fig. 4.3(f), shows snapshot of a randomly chosen odd xy plane, is mostly grey, showing that in this configuration, the heads of cubes preferentially occupy even xy-planes.

The breaking of translational invariance is also quantitatively reflected from the time evolution of the eight sublattice densities and L_x, L_y, L_z, as shown in Fig. 4.4(a) and (b) respectively. From Fig. 4.4(a), we see that four sublattices are preferentially occupied. From Fig. 4.4(b), we also see that one of the components of $\mathbf{L}$ is larger than the other two, i.e., $|L_z| \gg |L_x| \approx |L_y|$, confirming that the system is layered in the z-direction.

Sublattice Phase: In the sublattice phase, translational symmetry is broken in all three principal directions of the cubic lattice. In this phase, the cubes preferentially occupy one of the eight sublattices. This may be seen by examining the snapshots of randomly chosen

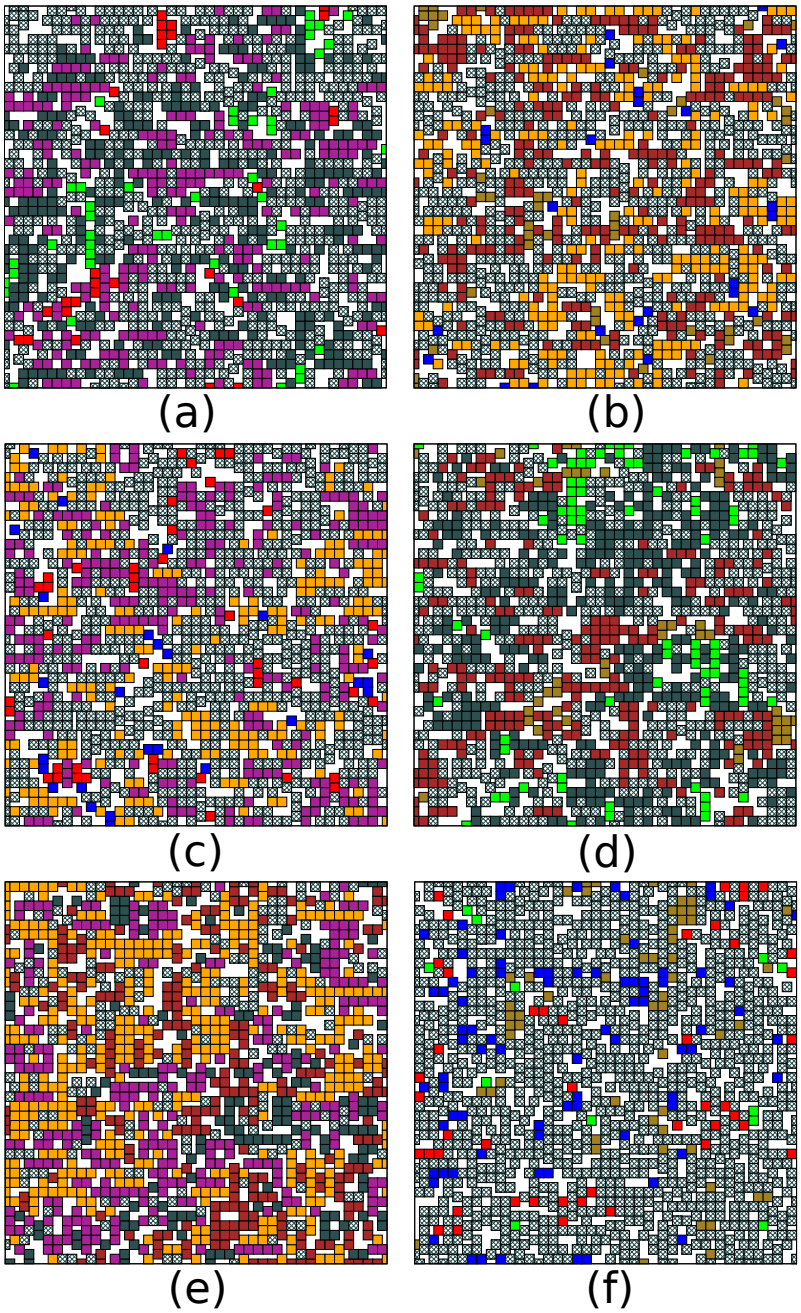

Figure 4.3: Snapshots of cross sections of equilibrated configurations in the layered phase, with layering vector pointing in the z-direction. The cross sections shown are of randomly chosen adjacent pairs of (a) even yz-, (b) odd yz-, (c) even xz-, (d) odd xz-, (e) even xy- and (f) odd xy-planes. The eight colours represent cubes with heads on different sublattices. The projections of cubes which protrude onto the plane from nearby planes are coloured in grey. (a)-(d) look statistically similar, while (e) is mostly coloured and (f) is mostly grey, showing a layering in the z-direction. The data are for system size $L = 150$, chemical potential $\mu = 2.4$, and density $\rho \approx 0.762$.

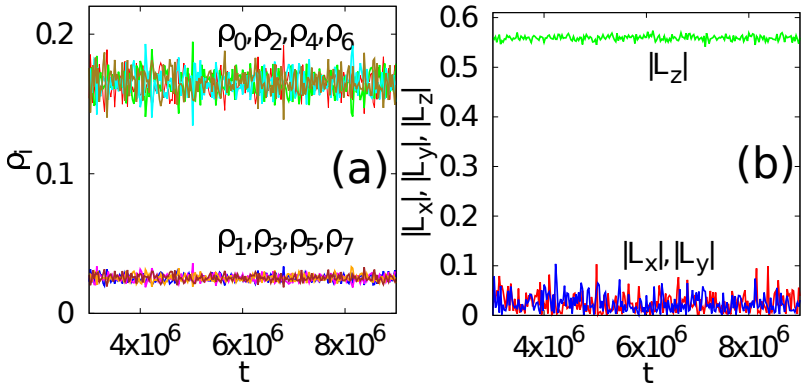

Figure 4.4: Temporal evolution of (a) eight sublattice densities $\rho_i, i = 0, \ldots, 7$ and (b) $|L_x|, |L_y|, |L_z|$ when the system is in a layered phase (layering in the z-direction). The data are for $\mu = 2.4$, $\rho \approx 0.762$, and system size $L = 150$.

pairs of even and odd planes in the three directions as shown in Fig. 4.5. It may be seen that in each of the directions, one of the planes has a larger number of cubes, compared to the grey squares. We see that in this case the cubes preferentially occupies simultaneously even yz, odd xz and even xy-planes, which implies most of the cubes occupy sublattice 2.

The breaking of translational symmetry is reflected in the time evolution of the eight sublattice densities and $|L_x|, |L_y|, |L_z|$ as shown in Fig. 4.6(a) and (b) respectively. In Fig. 4.6(a), sublattice 2 is preferentially occupied over the other seven sublattices. From Fig. 4.6(b), we also see that $|L_x|, |L_y|, |L_z|$ are non-zero and equal, i.e., $|L_x| \approx |L_y| \approx |L_z| \gg 0$, confirming that the system has sublattice order.

Columnar Phase: The system is in a columnar phase at large densities. In the columnar phase, the system breaks translational symmetry along two directions and the heads of the cubes preferentially occupy two sublattices. This may be seen by examining the snapshots of the planes in the three directions, as shown in Fig. 4.7. From Figs. 4.7(d) and (f), corresponding to snapshots of odd xz-plane and odd xy-plane respectively, it may be seen that these planes contain very few heads of cubes. Thus, most cubes have heads with even y-coordinate and even z-coordinate. If now the x-coordinate has no definite parity, then the phase will be columnar, else it will be a sublattice phase. From the snapshots of even and odd yz-planes, shown in Figs. 4.7(a) and (b), it can be seen that both planes have roughly

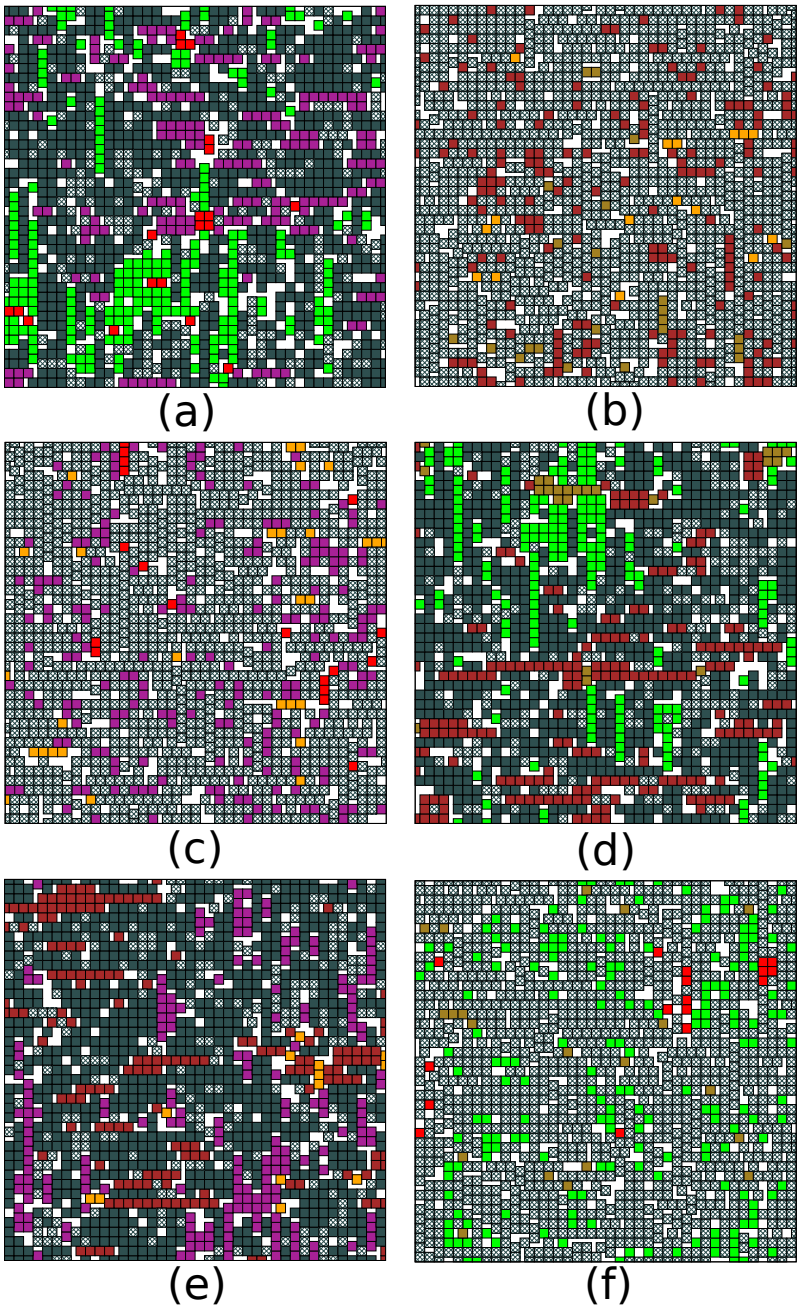

Figure 4.5: Snapshot of cross sections of equilibrated sublattice phase, where the cross sections are of randomly chosen adjacent pairs of (a) even *yz*-, (b) odd *yz*-, (c) even *xz*-, (d) odd *xz*-, (e) even *xy*- and (f) odd *xy*-plane. The eight colours represent cubes with heads on different sublattices. The projections of cubes which protrude onto the plane from nearby planes are coloured in grey. (a), (d) and (e) are mostly coloured by deep-green, while (b), (c) and (f) are mostly grey, showing the preferential occupancy of cubes in sublattice 2. The data are for system size $L = 150$ with chemical potential $\mu = 3.5$, and density $\rho \approx 0.864$.

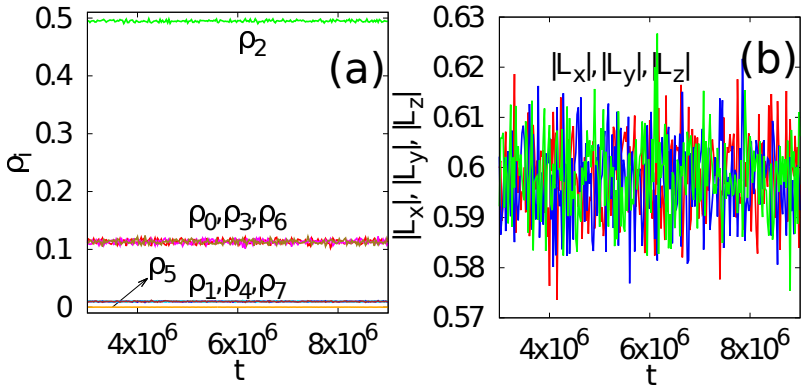

Figure 4.6: Temporal evolution of (a) eight sublattice densities $\rho_i, i = 0, \ldots, 7$ and (b) $|L_x|, |L_y|, |L_z|$ when the system is in a sublattice phase. The data are for $\mu = 3.5, \rho \approx 0.864$, and system size $L = 150$.

equal number of heads of cubes, showing that the x-coordinate has no definite parity. This feature may also be observed from the snapshots shown in Figs. 4.7(c) and (e) of even xz- and even xy- planes, where two colours are seen in each snapshot corresponding to even x and odd x.

From Fig. 4.8(a), we see that the sublattice 0 and 4 are preferentially occupied over the six sublattices corresponding to the heads of most of the cubes having odd y and z-coordinates. From Fig. 4.8(b), we see that two order parameters are large compared to one, i.e., $|L_y| \approx |L_z| \gg |L_x|$, this implies that translation symmetry is broken in both the y- and z-directions. The columnar phase can be visualized as a set of tubes extending along the x-direction, in which the cubes can slide along.

4.4 Landau theory for $2 \times 2 \times 2$ cubes

In this section, we formulate a Landau-type theoretical description of the phases found in Sec. 4.3. As noted earlier, spontaneous layering, sublattice ordering and columnar ordering are faithfully described by the layering vector $\mathbf{L}$, defined in Eq. (4.3), with the columnar vector $\mathbf{C}$ and the sublattice scalar ϕ more naturally thought of as composite objects constructed from the local layering order parameter field. It is therefore natural

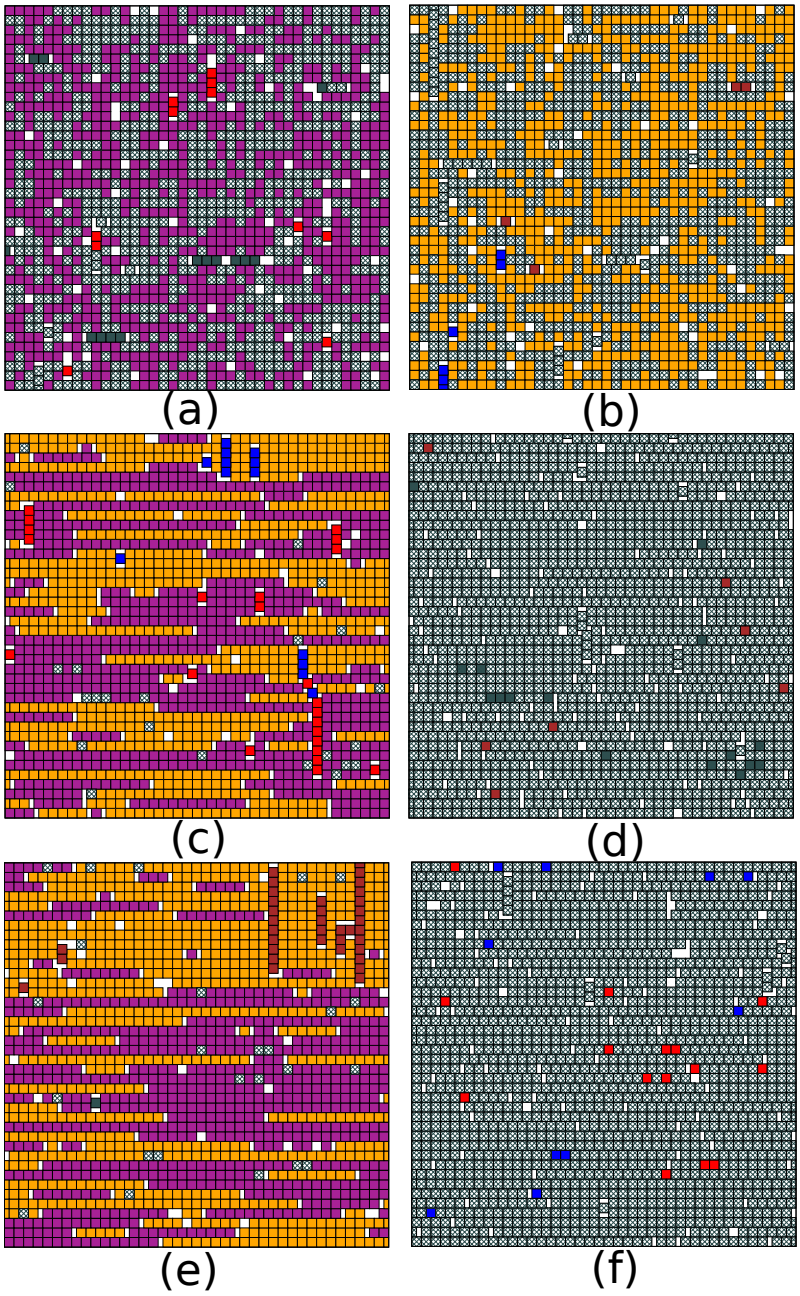

Figure 4.7: Snapshot of cross sections of an equilibrated columnar phase, where the columns are aligned in the x-direction and y- and z- coordinates are both mostly even. The cross sections are of randomly chosen adjacent pairs of (a) even yz-, (b) odd yz-, (c) even xz-, (d) odd xz-, (e) even xy-, and (f) odd xy-plane. The eight colours represent cubes with heads on different sublattices. The projections of cubes which protrude onto the plane from neighbouring planes are coloured in gray. Since (d) and (f) are mostly gray, the heads of most of the cubes have even y- and z- coordinates. Since (a) and (b) have roughly equal number of coloured squares, the heads of the cubes could have, with equal probability, either even or odd x-coordinates. The data are for system size $L = 150$, chemical potential $\mu = 5.5$, and density $\rho \approx 0.958$.

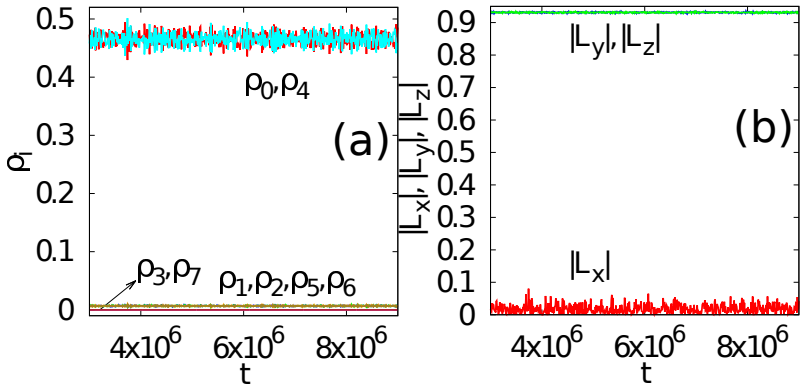

Figure 4.8: Temporal evolution of (a) the eight sublattice densities $\rho_i, i = 0, \ldots, 7$ and (b) $|L_x|, |L_y|, |L_z|$ when the system is in a columnar phase. The data are for $\mu = 5.5, \rho \approx 0.958$, and system size $L = 150$.

to try to construct the Landau theory in terms of the order parameter vector $\mathbf{L}$. Here, we demonstrate that while such a Landau theory correctly captures the low density disordered phase, the layered phase, and the sublattice phase, as well as phase transitions between them, it does not allow for the possibility of a columnar phase. To account for the columnar phase, we include the symmetry-allowed couplings to the columnar vector $\mathbf{C}$ and write down a coupled theory for $\mathbf{L}$ and $\mathbf{C}$. This augmented Landau theory correctly predicts the existence of a columnar phase, as well as the nature of the transition to the columnar phase.

We start by constructing the functional only in terms of $\mathbf{L}$. The symmetries of the Landau functional $\mathcal{F}(\{L_\alpha\})$ are that it is invariant under $\{L_\alpha \leftrightarrow -L_\alpha\}$ for $\alpha = (x, y, z)$ and cyclical permutations of the indices (x, y, z). With these constraints, the most general functional is

$$\mathcal{F} = a_L|\mathbf{L}|^2 + b_L|\mathbf{L}|^4 + 2\lambda_L(L_x^2L_y^2 + L_z^2L_y^2 + L_x^2L_z^2), \tag{4.7}$$

where we have truncated the expansion upto fourth order. To make sure that $\mathcal{F}$ goes to $+\infty$ when $|\mathbf{L}| \to \infty$, we require that $b_L > 0$ and $\lambda_L > -3b_L/2$. The Landau theory in Eq. (4.7) is that of $O(3)$ model with a cubic anisotropy.

The equilibrium phase is obtained from the global minimum of $\mathcal{F}$, and is obtained from

the solutions of $\nabla_L \mathcal{F} = 0$. In component form, these equations are

$$2a_L L_x + 4b_L L_x^3 + 4L_x(b_L + \lambda_L)(L_y^2 + L_z^2) = 0, \tag{4.8}$$

$$2a_L L_y + 4b_L L_y^3 + 4L_y(b_L + \lambda_L)(L_x^2 + L_z^2) = 0, \tag{4.9}$$

$$2a_L L_z + 4b_L L_z^3 + 4L_z(b_L + \lambda_L)(L_y^2 + L_x^2) = 0. \tag{4.10}$$

The solutions to Eqs. (4.8)–(4.10) may be found in closed form. We find that the solutions are of the form $(0,0,0)$, $(l,0,0)$, (s,s,s) and $(c,c,0)$ or its cyclic permutations. Substituting into Eqs. (4.8)–(4.10), the equations satisfied by l, s, c are

$$2b_L l^2 + a_L = 0, \tag{4.11}$$

$$(6b_L + 4\lambda_L)s^2 + a_L = 0, \tag{4.12}$$

$$(4b_L + 2\lambda_L)c^2 + a_L = 0. \tag{4.13}$$

The stability of the phases is determined by examining the Hessian $\mathcal{H}(\mathbf{L}_0)$ defined as

$$\mathcal{H}(\mathbf{L_0})_{\alpha\beta} = \left.\frac{\partial^2 \mathcal{F}}{\partial L_\alpha \partial L_\beta}\right|_{\mathbf{L}=\mathbf{L}_0}, \tag{4.14}$$

where α and β run over the indices (x, y, z). For $\mathbf{L}_0$ to be local minimum or locally stable, we require that the three eigenvalues of the Hessian, calculated at $\mathbf{L}_0$, are all positive.

For the disordered phase $(0,0,0)$, the Hessian is

$$\mathcal{H}(0,0,0) = \begin{bmatrix} 2a_L & 0 & 0 \\ 0 & 2a_L & 0 \\ 0 & 0 & 2a_L \end{bmatrix}, \tag{4.15}$$

whose three eigenvalues are all equal to $2a_L$. For the eigenvalues to be positive, we require that $a_L > 0$.

For the layered solution $(l, 0, 0)$, the Hessian is

$$\mathcal{H}(l,0,0) = \begin{bmatrix} -4a_L & 0 & 0 \\ 0 & -\frac{2a_L\lambda_L}{b_L} & 0 \\ 0 & 0 & -\frac{2a_L\lambda_L}{b_L} \end{bmatrix}, \tag{4.16}$$

whose eigenvalues are the diagonal entries in Eq. (4.16). For the eigenvalues to be positive, we require that $a_L < 0$ and $\lambda_L > 0$.

For the sublattice solution (s, s, s), the Hessian is

$$\mathcal{H}(s,s,s) = \begin{bmatrix} -\frac{4a_Lb_L}{3b_L+2\lambda_L} & -\frac{4a_L(b_L+\lambda_L)}{3b_L+2\lambda_L} & -\frac{4a_L(b_L+\lambda_L)}{3b_L+2\lambda_L} \\ -\frac{4a_L(b_L+\lambda_L)}{3b_L+2\lambda_L} & -\frac{4a_Lb_L}{3b_L+2\lambda_L} & -\frac{4a_L(b_L+\lambda_L)}{3b_L+2\lambda_L} \\ -\frac{4a_L(b_L+\lambda_L)}{3b_L+2\lambda_L} & -\frac{4a_L(b_L+\lambda_L)}{3b_L+2\lambda_L} & -\frac{4a_Lb_L}{3b_L+2\lambda_L} \end{bmatrix}, \tag{4.17}$$

whose eigenvalues are $-4a_L$, $4a_L\lambda_L/(3b_L + 2\lambda_L)$, and $4a_L\lambda_L/(3b_L + 2\lambda_L)$. For the eigenvalues to be positive, we require that $a_L < 0$ and $\lambda_L < 0$.

For columnar solution $(c, c, 0)$, the Hessian is

$$\mathcal{H}(c,c,0) = \begin{bmatrix} -\frac{4a_Lb_L}{2b_L+\lambda_L} & -\frac{4a_L(b_L+\lambda_L)}{2b_L+\lambda_L} & 0 \\ -\frac{4a_L(b_L+\lambda_L)}{2b_L+\lambda_L} & -\frac{4a_Lb_L}{2b_L+\lambda_L} & 0 \\ 0 & 0 & -\frac{2a_L\lambda_L}{2b_L+\lambda_L} \end{bmatrix}, \tag{4.18}$$

whose eigenvalues are $-4a_L$, $4a_L\lambda_L/(2b_L + \lambda_L)$, and $-2a_L\lambda_L/(2b_L + \lambda_L)$. The ratio of the second and third eigenvalues is -2. This implies that the three eigenvalues cannot be

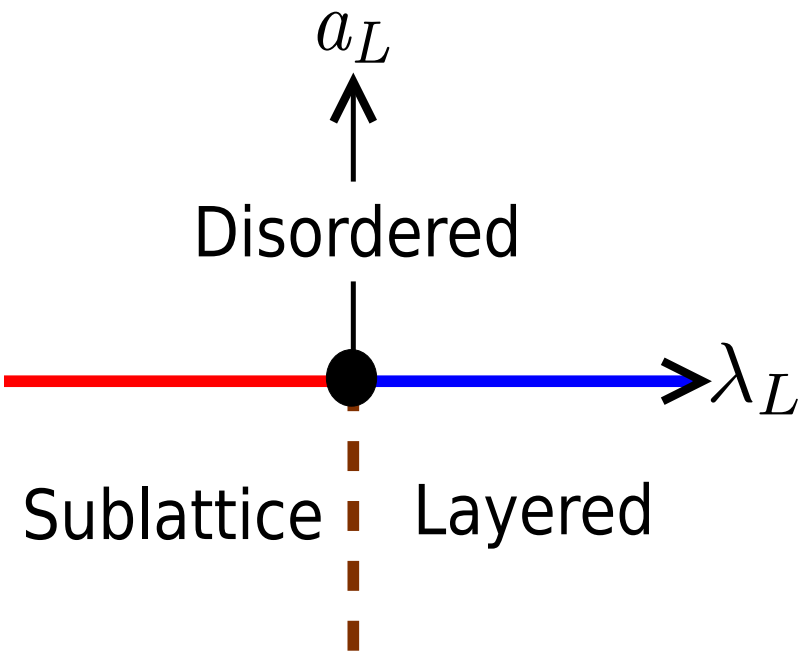

Figure 4.9: Phase diagram in the λ_L-a_L plane for the Landau theory of Eq. (4.7). The thick red and blue lines represent lines of continuous transition, whereas the dotted brown line is a first order transition line. The three phases meet at the multicritical point $(0, 0)$.

made simultaneously positive. Thus, the columnar solution is not a stable solution.

From the above analysis, we find that there exists a unique stable solution for each choice of a_L and λ_L. For $a_L > 0$ and any λ_L, the only stable phase is the disordered phase where $\mathbf{L} = 0$. For $a_L < 0$ and $\lambda_L > 0$, we find that stable solution is a layered phase, where $\mathbf{L}$ is a one-component vector of the form $(l, 0, 0)$. For the case where $a_L < 0$ and $\lambda_L < 0$, the stable solution is a sublattice phase, where $\mathbf{L}$ is vector of the form (s, s, s).

These observations are summarized in the phase diagram shown in Fig. 4.9. The disordered-layered transition and disordered-sublattice transitions are both continuous and, within Landau theory, belong to the universality class of the $O(3)$ model with cubic anisotropy. On the other hand, the sublattice-layered transition is discontinuous, as the orientation of the $\mathbf{L}$ vector changes abruptly from along one of the axes to $(1, 1, 1)$ or an equivalent direction.

The simplest Landau-type theory described in Eq. (4.7) predicts disordered, layered and sublattice phases, but disallows a columnar phase. To construct a minimal theory that pre-

dicts all the phases that are seen in the simulations, we extend the functional in Eq. (4.7) to explicitly depend on the columnar vector $\mathbf{C}(\vec{\mathrm{r}})$ defined earlier. Here, $\mathbf{C}(\vec{\mathrm{r}})$ should be thought of as an independent coarse-grained vector field since, $\langle C_x(\vec{\mathrm{r}})\rangle = \left\langle L_y(\vec{\mathrm{r}})L_z(\vec{\mathrm{r}})\right\rangle$, cannot be fully determined in terms of $\langle L_y(\vec{\mathrm{r}})\rangle$ and $\langle L_z(\vec{\mathrm{r}})\rangle$. The Landau functional $\mathcal{F}(\{L_\alpha, C_\alpha\})$ should be invariant under $L_\alpha \leftrightarrow -L_\alpha$, and $C_\alpha \leftrightarrow -C_\alpha$ for $\alpha = (x, y, z)$ and under cyclical permutations of the indices (x, y, z). The augmented functional, truncated upto fourth order is:

$$\begin{aligned}\mathcal{F} \;=\; & a_L|\mathbf{L}|^2 + b_L|\mathbf{L}|^4 + 2\lambda_L(L_x^2L_y^2 + L_z^2L_y^2 + L_x^2L_z^2) \\ & + a_c|\mathbf{C}|^2 + b_c|\mathbf{C}|^4 + 2\lambda_c(C_x^2C_y^2 + C_z^2C_y^2 + C_x^2C_z^2) \\ & - \mu(C_xL_yL_z + C_yL_xL_z + C_zL_xL_y),\end{aligned} \tag{4.19}$$

where μ couples the $\mathbf{L}$ and $\mathbf{C}$ vectors. This functional is similar to that proposed for studying spin-flop transitions in perovskites, where the anisotropic version was studied [143]. We restrict ourselves to $\mu > 0$ since this correctly describes the situation in a columnar ordered configuration of our system of cubes (with our definitions of these vectors, it is easy to see that C_x has the same sign as the product L_yL_z in a columnar ordered state with columnar vector pointing in the x direction, and similarly for columnar vectors pointing in the other Cartesian directions). As we demonstrate below, this augmented Landau theory now accounts for the presence of a stable columnar phase in addition to the other stable phases already obtained by thinking entirely in terms of $\mathbf{L}$

The extended functional in Eq. (4.19) has seven independent parameters and six variables. Deriving analytic equations of the phase boundary is not possible as that would require us to simultaneously solve six coupled equations. Rather, we focus on showing that there are parameter regimes for which the columnar phase, as well as the other phases exist and are stable. This is achieved by assigning numerical values to the parameters values and solving the coupled equations for equilibrium numerically. The stability is checked using

the Hessian $\mathcal{H}(\mathbf{L}, \mathbf{C})$:

$$\mathcal{H}(\mathbf{L}_0, \mathbf{C}_0)_{\alpha\beta} = \left.\frac{\partial^2 \mathcal{F}}{\partial\phi_\alpha \partial\phi_\beta}\right|_{\mathbf{L}=\mathbf{L}_0, \mathbf{C}=\mathbf{C}_0}, \tag{4.20}$$

where ϕ runs over the components of the vectors $\mathbf{L}$ and $\mathbf{C}$, is now a 6×6 matrix.

For analysing the functional in Eq. (4.19) to determine its global minima, we consider the four different cases discussed below. For each of these cases, we set $\mu = 2$ and fix the parameters b_L and b_c to be large and positive ($b_L = b_c = 8$).

Case 1. $a_L > 0$, $a_c > 0$: In this case, in the absence of the coupling ($\mu = 0$), both $\mathbf{L} = 0$, and $\mathbf{C} = 0$. For small positive μ, we expect the system to be still in the disordered phase. We confirm this by setting $a_L = a_c = 1.2$, and treating λ_L and λ_c as free parameters. For this case, whatever be the values and sign of λ_L and λ_c, we find that the disordered phase is the only stable phase.

Case 2. $a_L > 0$, $a_c < 0$: In this case, we expect that $\mathbf{L} = 0$, and $\mathbf{C} \neq 0$. Such solutions are unphysical, and we expect that the mapping from the microscopic variables of the model to the parameters of the Landau theory is such that, this regime is never reached.

Case 3. $a_L < 0$, $a_c > 0$: In this case, in the absence of coupling ($\mu = 0$), the $\mathbf{L}$ shows both layered and sublattice phases depending on the sign of λ_L. When $\mu \neq 0$, for these phases to be valid, $\mathbf{C}$ should be zero in the layered phase and have three non-zero components in the sublattice phase. We confirm that this is indeed the case by determining numerically the phase diagram for $a_L = -1.2$, $a_c = 1.2$. We find that the system is layered when $\lambda_L > 0$, and has sublattice order when $\lambda_L < 0$, irrespective of the sign of λ_c. The schematic λ_L-λ_c phase diagram for this case, obtained by minimizing the free energy at different sample phase points, is summarized in Fig. 4.10.

Case 4. $a_L < 0$, $a_c < 0$: In this case, we expect that when $\lambda_c > 0$, then the minimum of the free energy could occur for non-zero $\mathbf{C}$. We determine the phase diagram for $a_L = a_c = -1.2$. We find that for $\lambda_c > 0$ and $\lambda_L > 0$, there is a regime where the system is in a columnar phase. For large λ_c and λ_L, there are spurious unphysical solutions. For

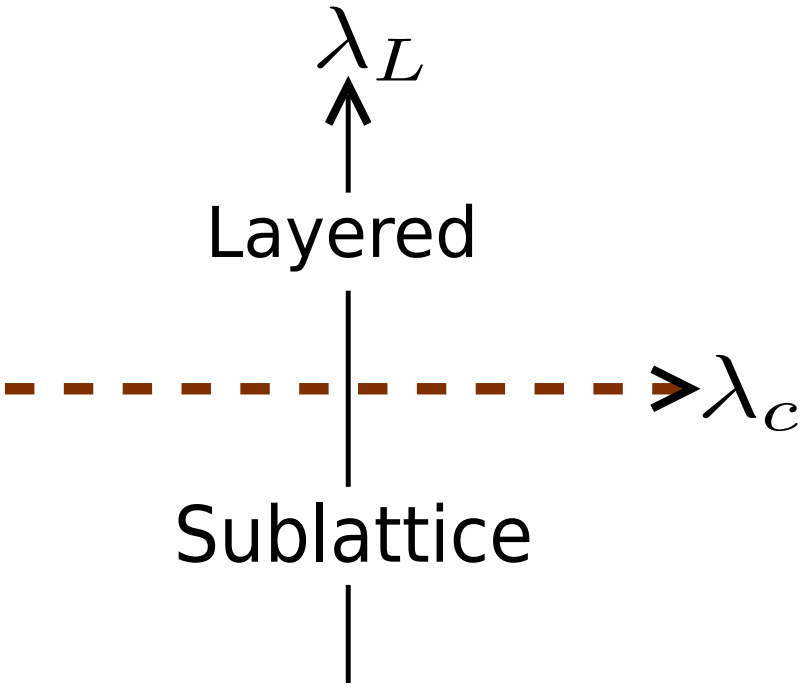

Figure 4.10: The schematic phase diagram in the λ_L-λ_c plane for the Landau free energy functional in Eq. (4.19) for the case $a_L < 0$, $a_c > 0$. The other parameters are $b_L = b_c = 8$, $\mu = 2$. The line $\lambda_L = 0$ is a first order line, separating the layered phase and the sublattice phase.

the other cases, the system is in a sublattice phase. The schematic λ_L-λ_c phase diagram for this case, obtained by minimizing the free energy at different sample phase points, is summarized in Fig. 4.11.

4.5 Disordered-Layered Transition

In this section, we describe the phase transition from disordered phase to layered phase. To do so, we first define susceptibility χ_i, and Binder cumulant U_i associated with the order parameter q_i [see Eq. (4.4)–(4.6) for definition] as

$$\chi_i = L^3(\langle q_i^2\rangle - \langle q_i\rangle^2), \tag{4.21}$$

$$U_i = 1 - \frac{c_i\langle q_i^4\rangle}{\langle q_i^2\rangle^2}, \tag{4.22}$$

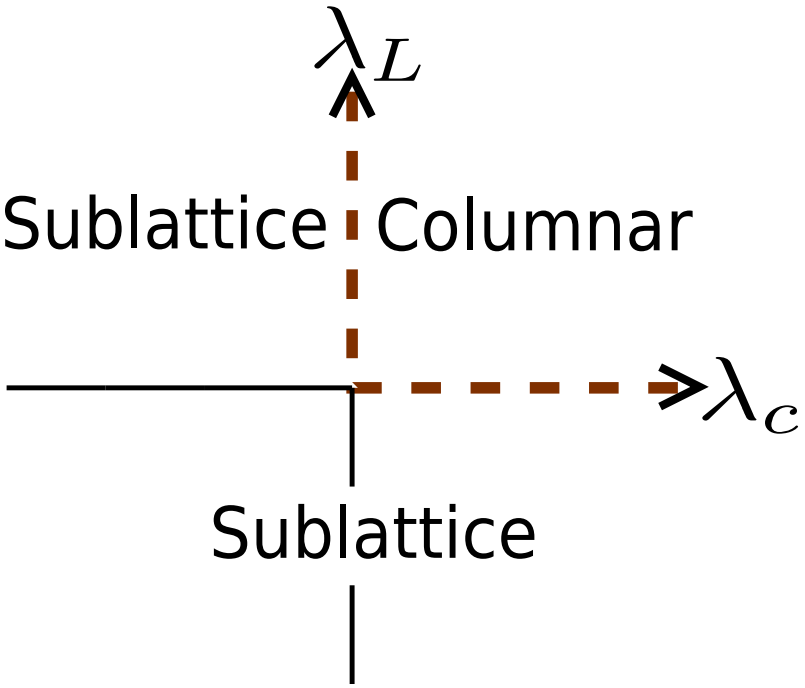

Figure 4.11: The schematic phase diagram in the λ_L-λ_c plane for the Landau free enrgy functional in Eq. (4.19) for the case $a_L < 0$, $a_c < 0$. The other parameters are $b_L = b_c = 8$, $\mu = 2$. The dotted lines which are lines of first order transition, separate the columnar phase and the sublattice phase.

where $c_1 = c_2 = 9/15$ and $c_3 = 1/3$. The values of c_i are chosen so that the Binder cumulant is zero in the disordered phase. We also define the deviation from the critical point as

$$\epsilon = \mu - \mu_c, \tag{4.23}$$

where μ_c is the critical value of the chemical potential.

We find that the disordered-layered transition is continuous. A suitable order parameter to study this transition is q_1 which is zero in the disordered phase and non-zero in layered phase. The critical behaviour may be obtained by studying the non-analytic behaviour of the different physical quantities, which, near the transition, is captured by the finite size

scaling behaviour:

$$q_1(\epsilon, L) \simeq L^{-\beta/\nu} f_q(\epsilon L^{1/\nu}), \tag{4.24}$$

$$\chi_1(\epsilon, L) \simeq L^{\gamma/\nu} f_\chi(\epsilon L^{1/\nu}), \tag{4.25}$$

$$U_1(\epsilon, L) \simeq f_U(\epsilon L^{1/\nu}). \tag{4.26}$$

where f_q, f_χ and f_U are scaling functions, and ν, β, γ and α are the usual critical exponents.

From the Landau theory presented in Sec. 4.4, we expect that the transition belongs to the universality class of three dimensional $O(3)$ model with cubic anisotropy. In $O(N)$ models with cubic anisotropy, the phase transition is in the symmetric $O(N)$ universality class if $N < N_c$ and is in the cubic anisotropic universality class if $N > N_c$. Early work, using perturbative renormalisation group theory [144, 145, 146, 147, 148], high temperature series expansion [149] and non-perturbative RG calculations [150] suggests that $3 < N_c < 4$. Further work using RG calculations upto three loops [151, 152], four loops [153, 154], five loops [155, 156, 157, 158] find $N_c \lesssim 3$, while six loop RG calculations suggest $N_c \approx 2.89$ [159], while recent calculations using six loop ϵ-expansion suggest that $N_c = 3$ [160]. Monte Carlo simulations are consistent with $N_c = 3$ [161]. However, in three dimensions, the exponents for the model with cubic anisotropic critical are very close to the exponents for the Heisenberg model [159]. Therefore, we use the exponents for the three-dimensional Heisenberg model to analyze the data. In the following, we check that the data near the critical point are consistent with these exponents.

The critical point may be determined by the crossing point of the data for Binder cumulant for different system sizes. From this criterion, we find that the critical parameters are $\mu \approx 2.063$ corresponding to $\rho \approx 0.718$ [see Fig. 4.12(a)]. The data for Binder cumulant, susceptibility, and order parameter for different system sizes collapse onto one curve when scaled as in Eqs. (4.24)-(4.26) with the critical exponents for Heisenberg model in three dimensions, as shown in Fig. 4.12. We use the numerical estimates for the critical expo-

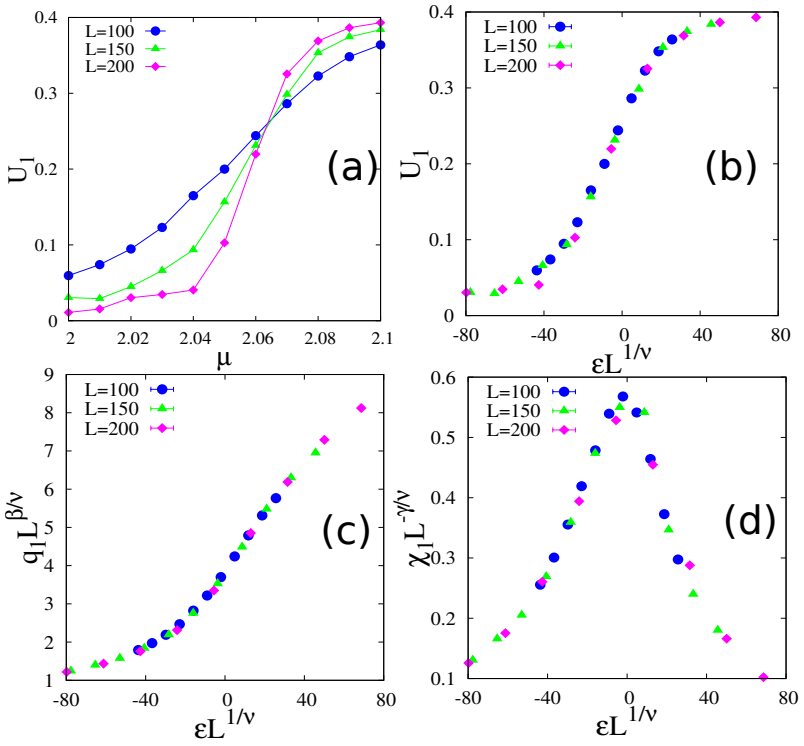

Figure 4.12: (a) The variation of Binder cumulant U_1 with chemical potential μ for different system sizes. The data for (b) Binder cumulant U_1, (c) order parameter q_1 and (d) χ_1 for different system sizes collapse onto a single curve when scaled as in Eqs. (4.24)-(4.26) with the critical exponents of the three dimensional Heisenberg model: $\nu = 0.704$, $\beta = 0.362$, and $\gamma = 1.389$.

nents $\nu = 0.704, \beta = 0.362$ and $\gamma = 1.389$ [162]. We conclude that the disordered-layered transition is consistent with the universality class of the $O(3)$ model.

4.6 Layered-Sublattice Transition

In this section, we study the the nature of the layered-sublattice phase transition. We analyze the transition using the order parameter q_3, defined in Eq. (4.6), which is zero in the layered phase and non-zero in the sublattice phase.

Figures 4.13(a) and (b), show the time evolution of density and q_3 after equilibration. For clarity, we have also superimposed a running average of density, where each point has been averaged over 40 consecutive data points. Both ρ and q_3 exhibit two states, one

in which density is higher and q_3 is non-zero and another where density is lower and q_3 is approximately zero. The system fluctuates in time between these two states. This is characteristic of a first order transition where both the sublattice and layered phases have the same free energy at the transition point.

The probability distribution for density, $P(\rho)$, and q_3, $P(q_3)$ for three different values of μ, close to the transition point, are shown in Figs. 4.13(c) and (d) respectively. Note that we have used the coarse-grained density averaged over a fixed rolling window to obtain the distribution. As the transition point is crossed, it can be seen that the distribution changes from having more area at the lower density to having more area at the higher density. From the value of μ for which $P(\rho)$ has roughly same height, we conclude that the critical chemical potential is $\mu \approx 2.67$. Similar features may be seen for $P(q_3)$. Finally, the effect of system size on the distributions at the critical activity are studied in Figs. 4.13(e) and (f). It can be seen that the peaks become higher and sharper with increasing system size. The jump in density at the transition is ≈ 0.001. These are again characteristic of a first order transition, and we conclude that the layered-sublattice transition is discontinuous.

4.7 Sublattice-Columnar Transition

In this section, we study the the nature of the layered-sublattice phase transition. We analyze the transition using the order parameter q_3, as defined in Eq. (4.6). q_3 is zero in the columnar phase and non-zero in the sublattice phase.

Figures 4.14(a) and (b), show the time evolution of density and q_3 after equilibration. For clarity, we have also superimposed a running average of density, where each point has been averaged over 10 consecutive data points. Both ρ and q_3 exhibit two states, one in which density is higher and q_3 is non-zero and another where density is lower and q_3 is approximately zero. The system fluctuates in time between these two states. This is characteristic of a first order transition or co-existence, where both the sublattice and

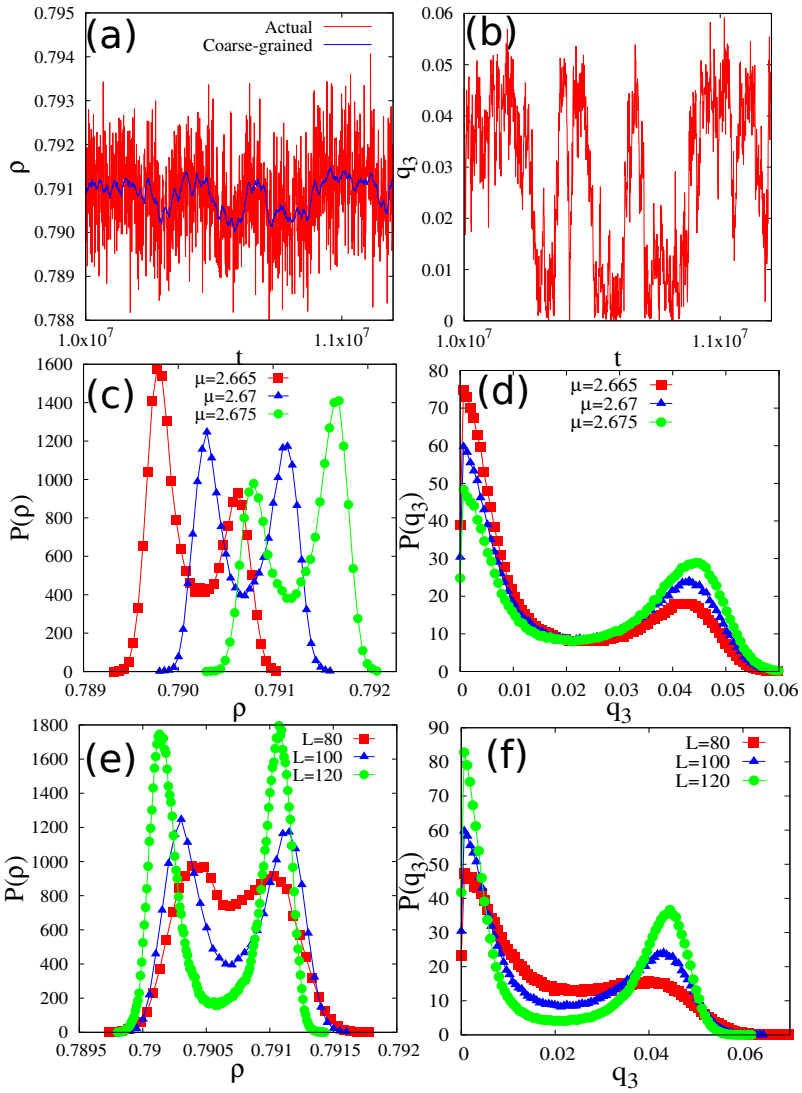

Figure 4.13: The time evolution of (a) density ρ and (b) q_3 when $\mu = 2.67$ and $L = 100$. We have superimposed a running average of density, where each point has been averaged over 40 consecutive data points. The probability density function for (c) ρ and (d) q_3 for different values of μ near the transition point for a system of size $L = 100$. The probability density function for (e) ρ and (f) q_3 for different values of L at the transition point [$\mu = 2.670$ for $L = 80$, and $L = 100$, and $\mu = 2.669$ for $L = 120$].

columnar phases have the same free energy at the transition point. The jump in density across the transition is ≈ 0.0025.

The probability distribution for density, $P(\rho)$, and q_3, $P(q_3)$ for three different values of μ, close to the transition point, are shown in Figs. 4.14(c) and (d) respectively. Note that we have used the smoothened density to obtain the distribution. As the transition point is crossed, it can be seen that the distribution changes from having more area at the lower density to having more area at the higher density. From the value of μ for which $P(\rho)$ has roughly same height, we conclude that the critical chemical potential is $\mu \approx 5.395$ for $L = 60$. Similar features may be seen for $P(q_3)$. Finally, the effect of system size on the distributions at the critical activity are studied in Figs. 4.14(e) and (f). We find that the critical point has a strong finite size dependence. For instance, if the critical density $\rho_c(L)$ is defined as the midpoint between the two peaks in the distribution $P(\rho)$, then we find $\rho_c(50) \approx 0.9522$, $\rho_c(60) \approx 0.9553$, and $\rho_c(70) \approx 0.9572$. Since the difference in $\rho_c(L)$ are of the order of the jump in ρ (approximately 0.0025), we plot the the probability distribution of $\Delta\rho$ where $\Delta\rho = \rho - \rho_c(L)$. From Fig. 4.14(e), we find that, with increasing system size, the peaks become higher and sharper. The same features are seen for $P(q_3)$ [see Fig. 4.14(f)]. These are characteristics of a first order transition, and we conclude that the sublattice-columnar transition is weakly first order.

4.8 Stability of Columnar Phase

In our Monte Carlo simulations, we are unable to equilibrate the system efficiently in the high density phase for densities larger than $\rho \approx 0.96$ for system sizes larger than $L \geq 100$. For these densities, we find that the system often gets stuck in very long-lived metastable states, which consist of layers of size $2 \times L \times L$, each layer having a two dimensional columnar order. However, columnar order in consecutive layers may have different orientations. We illustrate with a typical example that was obtained in

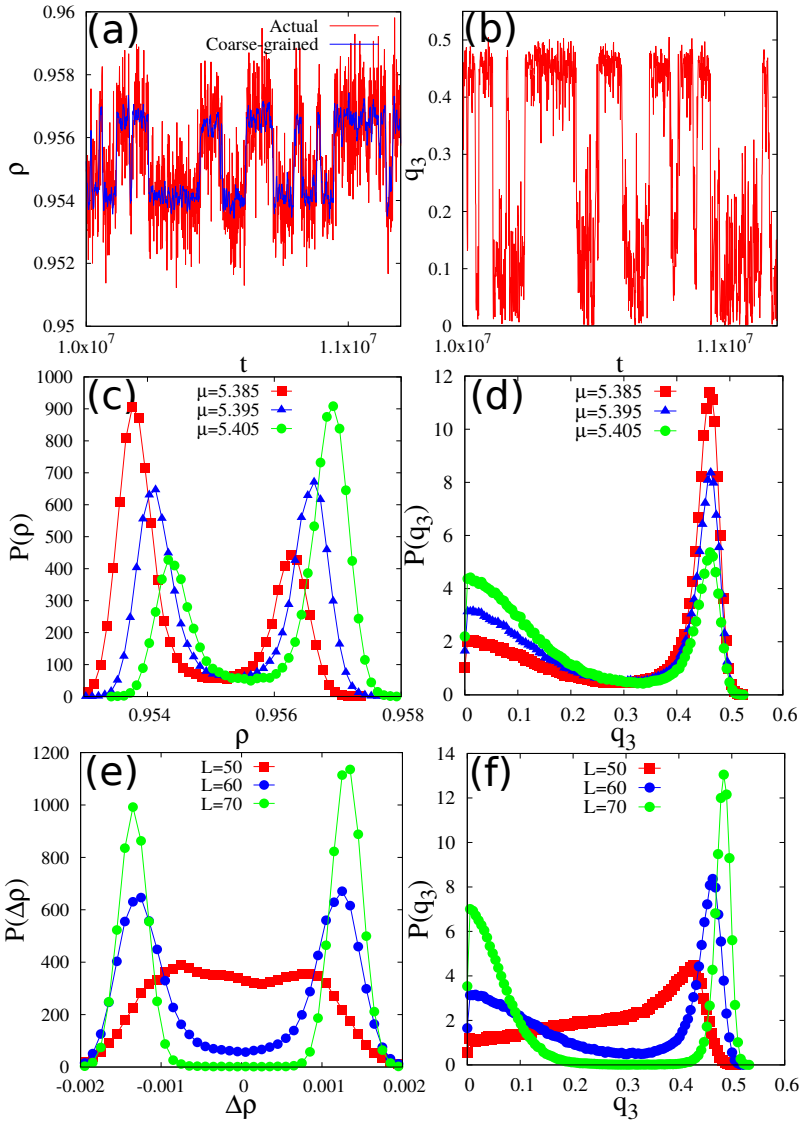

Figure 4.14: The time evolution of (a) density ρ and (b) order parameter q_3 when $\mu = 5.395$ and $L = 60$. We have superimposed a running average of density, where each point has been averaged over 10 consecutive data points. The probability density function for (c) ρ and (d) q_3 for different values of μ near the transition point for a system of size $L = 60$. The probability density function for (e) $\Delta\rho = \rho - \rho_c(L)$, where $\rho_c(L)$ is midpoint between the two peaks in the distribution, and (f) q_3, for different values of L at the transition point [$\mu_c = 5.26, \rho_c \approx 0.9522$ for $L = 50$, $\mu_c = 5.395, \rho_c \approx 0.9553$ for $L = 60$ and $\mu_c = 5.48, \rho_c \approx 0.9572$ for $L = 70$].

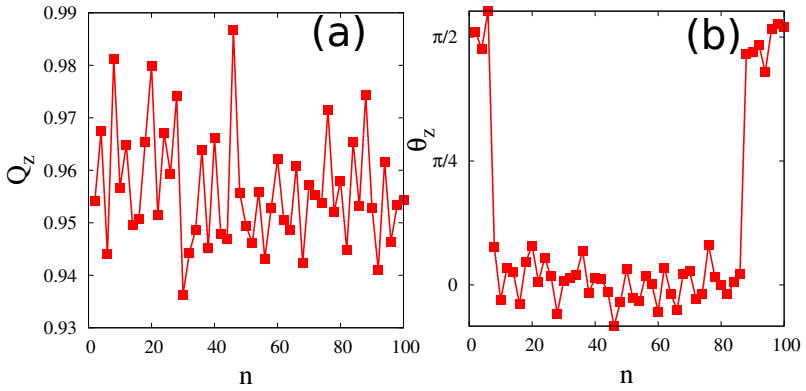

Figure 4.15: Variation of (a) Q_z and (b) θ_z [see Eq. (4.27) for definition] with even z-planes. In the odd planes, there are very few cubes. The data are for $L = 100$ and $\mu = 6.0$ at $t = 10^7$ Monte Carlo steps.

simulations. Consider a system that is layered in the z-direction. We define the columnar order parameter for layer n, $\mathbf{Q}_z(n) = Q_z(n)\mathrm{e}^{i\theta_z(n)}$, as

$$Q_z(n)\,\mathrm{e}^{i\theta_z(n)} = \phi^z_{er}(n) - \phi^z_{or}(n) + i\left[\phi^z_{ec}(n) - \phi^z_{oc}(n)\right], \tag{4.27}$$

where $\phi^z_{er}(n)$ and $\phi^z_{or}(n)$ are the packing fraction of the cubes with heads lying on even and odd rows of the n-th plane respectively, while $\phi^z_{ec}(n)$ and $\phi^z_{oc}(n)$ are the corresponding packing fractions on even and odd columns. For a layer with perfect columnar order, θ_z takes one of four values 0, $\pi/2$, π, $3\pi/2$. Similar definitions hold for $Q_x(n)$ and $Q_y(n)$. In Fig. 4.15, we show the variation of $Q_z(n)$ and $\theta_z(n)$ of a configuration that is layered in the z-direction (even planes are occupied), obtained after equilibrating for 10^7 Monte Carlo steps. It can be see that while the magnitude remains constant across the even layers, $\theta_z(n) = 0$ or $\theta_z(n) = \pi/2$, showing that the columnar order in different planes have different orientations. We find that the system remains stuck in this meta stable phase for upto and beyond 10^7 Monte Carlo steps.

Though such metastable states exist, we will show below that the true equilibrium state is one with the same columnar order in all the layers. The presence of cubes that common to adjacent layers tend to create an aligning interaction. This may be demonstrated though a perturbative calculation. This calculation is similar to the high density expansion

developed for hard squares and rectangles [69, 70, 80, 81, 72].

We start by assuming that the system is layered in the z-direction (even planes), and that z is large enough so that there is perfect columnar order in each layer. We set up a perturbation expansion based on number of cubes with heads in odd planes. To do so, we introduce two activities, z for cubes with heads on even planes and z' for cubes with heads on odd planes. When $z' = 0$, the layers are independent, and the problem reduces to that of 2×2 hard square lattice gas model. We will determine, to first order in perturbation theory, the difference in free energy between a state in which all planes have even-row order and states in which one plane is misaligned with either odd-row order or column-ordered. We will denote these states by S_α, whose partition function $\mathcal{L}^\alpha(z, z')$ and the free-energy $F^\alpha(z, z') = -\ln \mathcal{L}^\alpha(z, z')$, where we have set $k_B T = 1$, can be formally written as

$$\mathcal{L}^\alpha(z, z') = \mathcal{L}_0^\alpha(z) + z' \, \mathcal{L}_1^\alpha(z) + O(z'^2), \tag{4.28}$$

$$F^\alpha(z, z') = F_0^\alpha(z) - z' \, \frac{\mathcal{L}_1^\alpha(z)}{\mathcal{L}_0^\alpha(z)} + O(z'^2). \tag{4.29}$$

For $S_\parallel$, for which all planes have even-row order, the partition function, when there are no defect cubes (cubes with heads on odd planes), is

$$\mathcal{L}_0^\parallel(z) = [\Omega_p(L)^{L/2}]^{L/2}, \tag{4.30}$$

where $\Omega_p(L)$ is the partition function of a periodic column of size $2 \times 2 \times L$. Consider a single defect cube that is placed in any of the $L/2$ odd planes. Within a plane, it can choose any one of L^2 sites. The partition function for $S_\parallel$ in the presence of one defect cube is

$$\mathcal{L}_1^\parallel(z) = \frac{L^3}{4} [\Omega_p(L)]^{\frac{L^2}{4}} \left(\left[\frac{\Omega_o(L-2)}{\Omega_p(L)} \right]^2 + \left[\frac{\Omega_o(L-2)}{\Omega_p(L)} \right]^4 \right), \tag{4.31}$$

where $\Omega_o(L-2)$ is the partition function of an open column of size $2 \times 2 \times (L-2)$. In Eq. (4.31), the first term represents the correction coming when the head of the defect

cube is placed on an even row and second term corresponds to when the head of the defect cube is placed on an odd row.

Consider now a state S_{ro} in which one of the planes (say $z = 0$) is odd-row ordered. Since the partition function with no defect is identical to that for $S_{\parallel}$, the difference in partition function appears only in the first-order correction term:

$$\begin{aligned}\mathcal{L}_1^{ro}(z) = [\Omega_p(L)^{L/2}]^{\frac{L}{2}-2}\Bigg[\left(\frac{L}{2}-2\right)\frac{L^2}{2}\times \\ \left\{[\Omega_o(L-2)\Omega_p(L)^{\frac{L}{2}-1}]^2 + [\Omega_o(L-2)^2\Omega_p(L)^{\frac{L}{2}-2}]^2\right\} \\ + 2L^2\Omega_o(L-2)^3\Omega_p(L)^{L-3}\Bigg].\end{aligned} \tag{4.32}$$

The difference in free-energies, $\Delta F^{\parallel,ro}(z,z')$, may be written as

$$\begin{aligned}\Delta F^{\parallel,ro}(z,z') &= F^{ro}(z,z') - F^{\parallel}(z,z'), \\ &= z'\left(\frac{\mathcal{L}_1^{\parallel}(z) - \mathcal{L}_1^{ro}(z)}{\mathcal{L}_0^{\parallel}(z)}\right).\end{aligned} \tag{4.33}$$

Simplifying Eq. (4.33), we obtain

$$\Delta F^{\parallel,ro}(z,z') = L^2 z'\left(\left[\frac{\Omega_o(L-2)}{\Omega_p(L)}\right]^2 - \left[\frac{\Omega_o(L-2)}{\Omega_p(L)}\right]\right)^2. \tag{4.34}$$

Since the right hand side is a perfect square, $\Delta F^{\parallel,ro}(z,z') > 0$ for any L. Thus, the state with one misaligned row-ordered state has higher free energy, and we conclude that introduction of defect cubes results in an effective aligning interaction that tends to make all the planes have columnar order with the same orientation.

The large z behaviour of $\Delta F^{\parallel,ro}(z,z')$ may be determined by noting that for large L, $\Omega_p(L) = a_p\lambda^L$ and $\Omega_o(L-2) = a_o\lambda^{L-2}$ where λ is the largest root of the equation $x^2 - x - z = 0$. From Ref. [72], we obtain $a_p = 1$, $a_o = \lambda/(2\lambda - 1)$ and $\lambda = (1 + \sqrt{1+4z})/2$.

Setting $z' = z$ and evaluating in the limit of $z \gg 1$, we obtain

$$\Delta F^{\parallel,ro}(z) = \frac{L^2}{4z} + O(z^{-3/2}). \tag{4.35}$$

It is straightforward to generalize this calculation to the state S_{ce} in which one of the planes has column-order. We omit the calculation, but we obtain a similar increase in free energy when a layer is misaligned.

We now ask whether metastable states, as seen in Fig. 4.15, are due to finite size effects or due to the algorithm being unable to equilibrate the system at high densities within available computer time. Though a misaligned plane results in a rise in free energy as Eq. (4.35), there is a gain in entropy $\ln 2$ per column when there are no defect cubes. Thus, we can identify a crossover length L^* at which the free energy gained by alignment of a plane is balanced by the entropy lost due to alignment of such a plane. Equating the two free energies, $\Delta F^{\parallel,ro}(z, z') \sim \ln 2$, we obtain

$$L^* = \sqrt{4z \ln 2}. \tag{4.36}$$

For the metastable state shown in Fig. 4.15, $z = 403.43$ for the state , we obtain $L^* \approx 33$. For system sizes smaller than this length, the misaligned phases are favoured, but are a finite size effect. However, since the system lengths that we have simulated are much larger than L^*, we conclude that the presence of such metastable states are due to an inability of the Monte Carlo algorithm to equilibrate states with misaligned planes for large z, due to large entropic barriers.

4.9 Summary and conclusions

In this chapter we studied the phases and the phase transitions in a system of $2\times2\times2$ hard cubes on a three dimensional cubic lattice. We show the existence of four different phases.

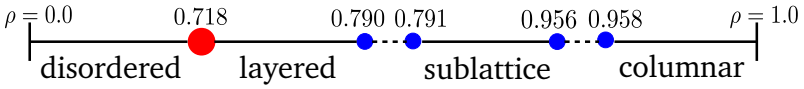

Figure 4.16: Numerically obtained phase diagram for $2 \times 2 \times 2$ hard cubes. The red dot represents a continuous transition and the dotted lines represent regions of coexistence.

In order of increasing density, these are a disordered phase, a layered phase in which the system breaks up into $L/2$ interacting slabs of size $2 \times L \times L$ each having fluid-like order, a solid-like sublattice phase, where the cubes preferentially occupy one sublattice, and a columnar phase in which the system breaks up into $L^2/4$ columns of dimension $2 \times 2 \times L$ with a fluid-like order within a column. The disordered-layered transition is shown to be a continuous transition that is consistent with the universality class of the three dimensional $O(3)$ model with cubic anisotropy. The other two transitions – layered-sublattice and sublattice-columnar – are shown to be discontinuous. The phase diagram is summarized in Fig. 4.16.

We formulated a Landau theory, consistent with the symmetries of the system, that is able to describe all the phases seen in the Monte Carlo simulations. Within the minimal functional, as described in Eq. (4.7), based only on the layering vector $\mathbf{L}$, we find that the columnar phase is unstable for the full range of the parameters, while it predicts the existence and stability of disordered, layered and sublattice phases. It also predicts the disordered-layered and disordered-sublattice transitions to be continuous and belong to the universality class of the three-dimensional $O(3)$ model with cubic anisotropy. The layered-sublattice transition is predicted to be first order. To obtain a stable columnar phase, we extended the free energy functional to explicitly depend on the columnar vector $\mathbf{C}$ [see Eq. (4.19)]. Within this extended functional, it is possible to show the existence and stability of all the different phases observed in simulations.

The results in this paper are not consistent with the theoretical predictions of density functional theory. Density functional theory predicts that $2 \times 2 \times 2$ hard cubes cubes undergo transitions from a disordered phase to layered phase to a columnar phase at high densities [21]. However, it does not predict the sublattice phase, that is seen in our Monte

Carlo simulations. Understanding why the theory fails, and how it should be modified to give the correct predictions is a promising area for future study. For $6 \times 6 \times 6$ cubes, the theory predicts a transition from a disordered to solid to two types of columnar phase [21]. Testing these predictions in simulations would also be of interest.

The results in this paper are also in contradiction to earlier Monte Carlo simulations [20], wherein no phase transitions were found even though the simulations were performed close to full packing (in Ref. [20], the problem of cubes correspond to $\sigma = 2$). This discrepancy could be due to small system sizes that were studied ($L = 18, 24$) in Ref. [20] compared to the systems sizes studied in the current paper (L upto 200).

The existence of a sublattice phase is quite surprising. It would appear that as you introduce vacancies at full packing, the sublattice phase gets destabilised in favour of the columnar phase. However, a larger number of vacancies somehow stabilizes the sublattice phase. This feature is also seen in the system of freely-rotating cubes in the continuum, whereby a large concentration of vacancies stabilise the crystalline phase at anomalously low densities [117, 127]. Also, it implies that the interactions between the different layers in the layered phase are not weak. If they were weak, then we would expect that once the system becomes layered, the problem becomes effectively a problem of hard squares in two dimensions. This lower dimensional system does not exhibit a sublattice phase.

In the continuum, the system of parallel hard cubes undergoes a continuous freezing transition from a disordered fluid phase to a solid phase as density is increased [131, 132], consistent with theoretical predictions using density functional theory [133]. The continuum limit may be reached by determining the phase diagram for $k \times k \times k$ cubes and extrapolating for large k. Preliminary simulations for $3 \times 3 \times 3$ cubes suggest that the sublattice phase does not exist, but the layered and columnar phases exist. Thus, for larger k, the layered-columnar transition would appear to be similar to the disordered-columnar transition in $k \times k$ hard squares. For this model, high density expansions suggest that the critical density tends to an asymptotic value that is less than one for large k [80]. If this

were true, the continuum problem should have two transitions. Re-examining the problem of parallel hard cubes in the continuum is a promising area for future study.

Bibliography

[1] P. N. Pusey and W. van Megen, "Phase behaviour of concentrated suspensions of nearly hard colloidal spheres," *Nature*, vol. 320, no. 16, pp. 340–342, 1986.

[2] D. Frenkel and A. A. Louis, "Phase separation in binary hard-core mixtures: An exact result," *Phys. Rev. Lett.*, vol. 68, pp. 3363–3365, Jun 1992.

[3] A. Patrykiejew, S. Sokołowski, and K. Binder, "Phase transitions in adsorbed layers formed on crystals of square and rectangular surface lattice," *Surf. Sci. Rep.*, vol. 37, no. 6, pp. 207 – 344, 2000.

[4] P. G. de Gennes and J. Prost, *The physics of liquid crystals*, vol. 83. Oxford university press, 1995.

[5] M. F. Islam, A. M. Alsayed, Z. Dogic, J. Zhang, T. C. Lubensky, and A. G. Yodh, "Nematic nanotube gels," *Phys. Rev. Lett.*, vol. 92, p. 088303, Feb 2004.

[6] S. Fraden, G. Maret, D. L. D. Caspar, and R. B. Meyer, "Isotropic-nematic phase transition and angular correlations in isotropic suspensions of tobacco mosaic virus," *Phys. Rev. Lett.*, vol. 63, pp. 2068–2071, Nov 1989.

[7] Z. Dogic and S. Fraden, "Cholesteric phase in virus suspensions," *Langmuir*, vol. 16, no. 20, pp. 7820–7824, 2000.

[8] M. P. B. van Bruggen, F. M. van der Kooij, and H. N. W. Lekkerkerker, "Liquid crystal phase transitions in dispersions of rod-like colloidal particles," *J. Phys.: Condens. Matter*, vol. 8, no. 47, p. 9451, 1996.

[9] A. Kuijk, A. van Blaaderen, and A. Imhof, "Synthesis of monodisperse, rodlike silica colloids with tunable aspect ratio," *J. Am. Chem. Soc.*, vol. 133, no. 8, pp. 2346–2349, 2011.

[10] Y. Maeda, T. Niori, J. Yamamoto, and H. Yokoyama, "Phase behavior of banana-shaped molecules under pressure," *Thermochimica Acta*, vol. 431, no. 1-2, pp. 87 – 93, 2005.

[11] S. H. Kang, S. Shan, A. Košmrlj, W. L. Noorduin, S. Shian, J. C. Weaver, D. R. Clarke, and K. Bertoldi, "Complex ordered patterns in mechanical instability induced geometrically frustrated triangular cellular structures," *Phys. Rev. Lett.*, vol. 112, p. 098701, Mar 2014.

[12] R. Zwanzig, "First-order phase transition in a gas of long thin rods," *J. Chem. Phys.*, vol. 39, no. 7, pp. 1714–1721, 1963.

[13] P. J. Flory, "Statistical thermodynamics of semi-flexible chain molecules," *Proc Math Phys Eng Sci.*, vol. 234, no. 1196, pp. 60–73, 1956.

[14] E. A. DiMarzio, "Statistics of orientation effects in linear polymer molecules," *J. Chem. Phys.*, vol. 35, no. 2, pp. 658–669, 1961.

[15] D. Dhar, R. Rajesh, and J. F. Stilck, "Hard rigid rods on a bethe-like lattice," *Phys. Rev. E*, vol. 84, p. 011140, Jul 2011.

[16] A. Ghosh and D. Dhar, "On the orientational ordering of long rods on a lattice," *Eur. Phys. Lett.*, vol. 78, no. 2, p. 20003, 2007.

[17] J. Kundu, R. Rajesh, D. Dhar, and J. F. Stilck, "A monte carlo algorithm for studying phase transition in systems of hard rigid rods," *AIP Conf. Proc.*, vol. 1447, no. 1, pp. 113–114, 2012.

[18] J. Kundu, R. Rajesh, D. Dhar, and J. F. Stilck, "Nematic-disordered phase transition in systems of long rigid rods on two-dimensional lattices," *Phys. Rev. E*, vol. 87, p. 032103, Mar 2013.

[19] K. Ramola, K. Damle, and D. Dhar, "Columnar order and ashkin-teller criticality in mixtures of hard squares and dimers," *Phys. Rev. Lett.*, vol. 114, p. 190601, May 2015.

[20] A. Z. Panagiotopoulos, "Thermodynamic properties of lattice hard-sphere models," *J. Chem. Phys.*, vol. 123, no. 10, p. 104504, 2005.

[21] L. Lafuente and J. A. Cuesta, "Phase behavior of hard-core lattice gases: A fundamental measure approach," *J. Chem. Phys.*, vol. 119, no. 20, pp. 10832–10843, 2003.

[22] M. Dijkstra and D. Frenkel, "Evidence for entropy-driven demixing in hard-core fluids," *Phys. Rev. Lett.*, vol. 72, pp. 298–300, Jan 1994.

[23] L. Lafuente and J. A. Cuesta, "Elusiveness of fluid-fluid demixing in additive hard-core mixtures," *Phys. Rev. Lett.*, vol. 89, p. 145701, Sep 2002.

[24] L. Landau, "The theory of phase transitions," *Nature*, vol. 138, no. 3498, pp. 840–841, 1936.

[25] A. Giuliani, "Universality and non-universality in the ashkin-teller model," *arXiv:cond-mat/0412176*, 2004.

[26] J. Ashkin and E. Teller, "Statistics of two-dimensional lattices with four components," *Phys. Rev.*, vol. 64, pp. 178–184, Sep 1943.

[27] L. P. Kadanoff, "Connections between the critical behavior of the planar model and that of the eight-vertex model," *Phys. Rev. Lett.*, vol. 39, pp. 903–905, Oct 1977.

[28] C. Fan, "On critical properties of the ashkin-teller model," *Physics Letters A*, vol. 39, no. 2, p. 136, 1972.

[29] L. Onsager, "The effects of shape on the interaction of colloidal particles," *Ann. N. Y. Acad. Sci.*, vol. 51, no. 4, pp. 627–659, 1949.

[30] J. M. Polson and D. Frenkel, "First-order nematic-smectic phase transition for hard spherocylinders in the limit of infinite aspect ratio," *Phys. Rev. E*, vol. 56, pp. R6260–R6263, Dec 1997.

[31] D. Frenkel, H. Lekkerkerker, and A. Stroobants, "Thermodynamic stability of a smectic phase in a system of hard rods," *Nature*, vol. 332, no. 6167, pp. 822–823, 1988.

[32] J. G. Kirkwood, E. K. Maun, and B. J. Alder, "Radial distribution functions and the equation of state of a fluid composed of rigid spherical molecules," *J. Chem. Phys.*, vol. 18, no. 8, pp. 1040–1047, 1950.

[33] B. J. Alder and T. E. Wainwright, "Phase transition for a hard sphere system," *J. Chem. Phys.*, vol. 27, no. 5, pp. 1208–1209, 1957.

[34] W. W. Wood and J. D. Jacobson, "Preliminary results from a recalculation of the monte carlo equation of state of hard spheres," *J. Chem. Phys.*, vol. 27, no. 5, pp. 1207–1208, 1957.

[35] D. E. Taylor, E. D. Williams, R. L. Park, N. C. Bartelt, and T. L. Einstein, "Two-dimensional ordering of chlorine on ag(100)," *Phys. Rev. B*, vol. 32, pp. 4653–4659, Oct 1985.

[36] P. Bak, P. Kleban, W. N. Unertl, J. Ochab, G. Akinci, N. C. Bartelt, and T. L. Einstein, "Phase diagram of selenium adsorbed on the ni(100) surface: A physical

realization of the ashkin-teller model," *Phys. Rev. Lett.*, vol. 54, pp. 1539–1542, Apr 1985.

[37] B. Dünweg, A. Milchev, and P. A. Rikvold, "A model for adsorption of o on mo(110): Phase transitions with nonuniversal behavior," *J. Chem. Phys.*, vol. 94, no. 5, pp. 3958–3973, 1991.

[38] Y. Zhang, V. Blum, and K. Reuter, "Accuracy of first-principles lateral interactions: Oxygen at pd(100)," *Phys. Rev. B*, vol. 75, p. 235406, Jun 2007.

[39] M. T. Koper, "A lattice-gas model for halide adsorption on single-crystal electrodes," *J Electroanal Chem*, vol. 450, no. 2, pp. 189 – 201, 1998.

[40] K. Zhao, R. Bruinsma, and T. G. Mason, "Entropic crystal–crystal transitions of brownian squares," *Proc. Natl. Acad. Sci. U.S.A.*, vol. 108, no. 7, pp. 2684–2687, 2011.

[41] A. Donev, J. Burton, F. H. Stillinger, and S. Torquato, "Tetratic order in the phase behavior of a hard-rectangle system," *Phys. Rev. B*, vol. 73, p. 054109, Feb 2006.

[42] E. Frezza, A. Ferrarini, H. B. Kolli, A. Giacometti, and G. Cinacchi, "The isotropic-to-nematic phase transition in hard helices: Theory and simulation," *J. Chem. Phys.*, vol. 138, no. 16, p. 164906, 2013.

[43] T. Schilling, S. Pronk, B. Mulder, and D. Frenkel, "Monte carlo study of hard pentagons," *Phys. Rev. E*, vol. 71, p. 036138, Mar 2005.

[44] M. P. Allen, G. T. Evans, D. Frenkel, and B. Mulder, "Hard convex body fluids," *Adv. Chem. Phys.*, vol. 86, pp. 1–166, 1993.

[45] M. Marechal and M. Dijkstra, "Stability of orientationally disordered crystal structures of colloidal hard dumbbells," *Phys. Rev. E*, vol. 77, p. 061405, Jun 2008.

[46] M. Marechal and M. Dijkstra, "Colloidal hard dumbbells under gravity: structure and crystallization," *Soft Matter*, vol. 7, pp. 1397–1408, 2011.

[47] R. Tavarone, P. Charbonneau, and H. Stark, "Phase ordering of zig-zag and bow-shaped hard needles in two dimensions," *J. Chem. Phys.*, vol. 143, no. 11, p. 114505, 2015.

[48] J. A. C. Veerman and D. Frenkel, "Phase behavior of disklike hard-core mesogens," *Phys. Rev. A*, vol. 45, pp. 5632–5648, Apr 1992.

[49] N. Pakalidou, D. L. Cheung, A. J. Masters, and C. Avendaño, "Macroscopic chiral symmetry breaking in monolayers of achiral nonconvex platelets," *Soft Matter*, vol. 13, pp. 8618–8624, 2017.

[50] D. Dhar, "Exact solution of a directed-site animals-enumeration problem in three dimensions," *Phys. Rev. Lett.*, vol. 51, pp. 853–856, Sep 1983.

[51] M. V. Tamm, S. K. Nechaev, and I. Y. Erukhimovich, "Statistics of ideal randomly branched polymers in a semi-space," *Eur. Phys. J E Soft Matter*, vol. 17, pp. 209–219, Jun 2005.

[52] G. Parisi and N. Sourlas, "Critical behavior of branched polymers and the lee-yang edge singularity," *Phys. Rev. Lett.*, vol. 46, pp. 871–874, Apr 1981.

[53] M. E. Zhitomirsky and H. Tsunetsugu, "Lattice gas description of pyrochlore and checkerboard antiferromagnets in a strong magnetic field," *Phys. Rev. B*, vol. 75, p. 224416, Jun 2007.

[54] O. Derzhko and J. Richter, "Finite low-temperature entropy of some strongly frustrated quantum spin lattices in the vicinity of the saturation field," *Phys. Rev. B*, vol. 70, p. 104415, Sep 2004.

[55] A. J. Ramirez-Pastor, T. P. Eggarter, V. D. Pereyra, and J. L. Riccardo, "Statistical thermodynamics and transport of linear adsorbates," *Phys. Rev. B*, vol. 59, pp. 11027–11036, Apr 1999.

[56] A. Coniglio and M. Nicodemi, "The jamming transition of granular media," *J. Phys.: Condens. Matter*, vol. 12, pp. 6601–6610, jul 2000.

[57] C. Domb, "Some theoretical aspects of melting," *Il Nuovo Cimento (1955-1965)*, vol. 9, pp. 9–26, Mar 1958.

[58] O. J. Heilmann and E. H. Lieb, "Theory of monomer-dimer systems," *Commun. Math. Phys.*, vol. 25, no. 3, pp. 190–232, 1972.

[59] P. Kasteleyn, "The statistics of dimers on a lattice: I. the number of dimer arrangements on a quadratic lattice," *Physica*, vol. 27, no. 12, pp. 1209 – 1225, 1961.

[60] H. N. V. Temperley and M. E. Fisher, "Dimer problem in statistical mechanics-an exact result," *Philosophical Magazine*, vol. 6, no. 68, pp. 1061–1063, 1961.

[61] M. E. Fisher and J. Stephenson, "Statistical mechanics of dimers on a plane lattice. ii. dimer correlations and monomers," *Phys. Rev.*, vol. 132, pp. 1411–1431, Nov 1963.

[62] D. A. Huse, W. Krauth, R. Moessner, and S. L. Sondhi, "Coulomb and liquid dimer models in three dimensions," *Phys. Rev. Lett.*, vol. 91, p. 167004, Oct 2003.

[63] R. J. Baxter, "Hard hexagons: exact solution," *J. Phys. A*, vol. 13, no. 3, p. L61, 1980.

[64] A. Verberkmoes and B. Nienhuis, "Triangular trimers on the triangular lattice: An exact solution," *Phys. Rev. Lett.*, vol. 83, pp. 3986–3989, Nov 1999.

[65] M. Disertori and A. Giuliani, "The nematic phase of a system of long hard rods," *Commun. Math. Phys.*, vol. 323, no. 1, pp. 143–175, 2013.

[66] M. Disertori, A. Giuliani, and I. Jauslin, "Plate-nematic phase in three dimensions," *arXiv:1805.05700*, 2018.

[67] A. Ghosh, D. Dhar, and J. L. Jacobsen, "Random trimer tilings," *Phys. Rev. E*, vol. 75, p. 011115, Jan 2007.

[68] A. Bellemans and R. K. Nigam, "Phase transitions in the hard-square lattice gas," *Phys. Rev. Lett.*, vol. 16, pp. 1038–1039, Jun 1966.

[69] A. Bellemans and R. K. Nigam, "Phase transitions in two-dimensional lattice gases of hard-square molecules," *J. Chem. Phys.*, vol. 46, no. 8, pp. 2922–2935, 1967.

[70] K. Ramola and D. Dhar, "High-activity perturbation expansion for the hard square lattice gas," *Phys. Rev. E*, vol. 86, p. 031135, Sep 2012.

[71] F. H. Ree and D. A. Chesnut, "Phase transition of a hard - core lattice gas. the square lattice with nearest - neighbor exclusion," *J. Chem. Phys.*, vol. 45, no. 11, pp. 3983–4003, 1966.

[72] T. Nath, D. Dhar, and R. Rajesh, "Stability of columnar order in assemblies of hard rectangles or squares," *Eur. Phys. Lett.*, vol. 114, no. 1, p. 10003, 2016.

[73] D. Mandal, T. Nath, and R. Rajesh, "Estimating the critical parameters of the hard square lattice gas model," *J. Stat. Mech.*, vol. 2017, no. 4, p. 043201, 2017.

[74] D. A. Matoz-Fernandez, D. H. Linares, and A. J. Ramirez-Pastor, "Determination of the critical exponents for the isotropic-nematic phase transition in a system of long rods on two-dimensional lattices: Universality of the transition," *Eur. Phys. Lett.*, vol. 82, no. 5, p. 50007, 2008.

[75] E. Eisenberg and A. Baram, "Random closest packing in a 2d lattice model," *J. Phys. A*, vol. 33, no. 9, p. 1729, 2000.

[76] B. C. Barnes, D. W. Siderius, and L. D. Gelb, "Structure, thermodynamics, and solubility in tetromino fluids," *Langmuir*, vol. 25, no. 12, pp. 6702–6716, 2009.

[77] J. Kundu and R. Rajesh, "Phase transitions in a system of hard rectangles on the square lattice," *Phys. Rev. E*, vol. 89, p. 052124, May 2014.

[78] J. Kundu and R. Rajesh, "Phase transitions in systems of hard rectangles with non-integer aspect ratio," *Eur. Phys. J. B*, vol. 88, no. 5, p. 133, 2015.

[79] J. Kundu and R. Rajesh, "Asymptotic behavior of the isotropic-nematic and nematic-columnar phase boundaries for the system of hard rectangles on a square lattice," *Phys. Rev. E*, vol. 91, p. 012105, Jan 2015.

[80] T. Nath, J. Kundu, and R. Rajesh, "High-activity expansion for the columnar phase of the hard rectangle gas," *J. Stat. Phys.*, vol. 160, no. 5, pp. 1173–1197, 2015.

[81] T. Nath and R. Rajesh, "Multiple phase transitions in extended hard-core lattice gas models in two dimensions," *Phys. Rev. E*, vol. 90, p. 012120, Jul 2014.

[82] T. Nath and R. Rajesh, "The high density phase of the k -nn hard core lattice gas model," *J. Stat. Mech.*, vol. 2016, no. 7, p. 073203, 2016.

[83] D. Mandal, T. Nath, and R. Rajesh, "Phase transitions in a system of hard y-shaped particles on the triangular lattice," *Phys. Rev. E*, vol. 97, p. 032131, Mar 2018.

[84] J. Kundu, J. F. Stilck, and R. Rajesh, "Phase diagram of a bidispersed hard-rod lattice gas in two dimensions," *Eur. Phys. Lett.*, vol. 112, no. 6, p. 66002, 2016.

[85] J. F. Stilck and R. Rajesh, "Polydispersed rods on the square lattice," *Phys. Rev. E*, vol. 91, p. 012106, Jan 2015.

[86] D. Mandal and R. Rajesh, "Columnar-disorder phase boundary in a mixture of hard squares and dimers," *Phys. Rev. E*, vol. 96, p. 012140, Jul 2017.

[87] U. Agarwal and F. A. Escobedo, "Mesophase behaviour of polyhedral particles," *Nature Materials*, vol. 10, no. 3, p. 230, 2011.

[88] P. F. Damasceno, M. Engel, and S. C. Glotzer, "Predictive self-assembly of polyhedra into complex structures," *Science*, vol. 337, no. 6093, pp. 453–457, 2012.

[89] T. Fischer and R. L. C. Vink, "Restricted orientation "liquid crystal" in two dimensions: Isotropic-nematic transition or liquid-gas one(?)," *Eur. Phys. Lett.*, vol. 85, no. 5, p. 56003, 2009.

[90] N. D. Mermin and H. Wagner, "Absence of ferromagnetism or antiferromagnetism in one- or two-dimensional isotropic heisenberg models," *Phys. Rev. Lett.*, vol. 17, pp. 1133–1136, Nov 1966.

[91] J. P. Straley, "Liquid crystals in two dimensions," *Phys. Rev. A*, vol. 4, pp. 675–681, Aug 1971.

[92] M. D. Khandkar and M. Barma, "Orientational correlations and the effect of spatial gradients in the equilibrium steady state of hard rods in two dimensions: A study using deposition-evaporation kinetics," *Phys. Rev. E*, vol. 72, p. 051717, Nov 2005.

[93] D. Frenkel and R. Eppenga, "Evidence for algebraic orientational order in a two-dimensional hard-core nematic," *Phys. Rev. A*, vol. 31, pp. 1776–1787, Mar 1985.

[94] R. L. Vink, "The isotropic-to-nematic transition in a two-dimensional fluid of hard-needles: a finite-size scaling study," *Eur. Phys. J. B*, vol. 72, no. 2, pp. 225–231, 2009.

[95] C. Gruber and H. Kunz, "General properties of polymer systems," *Commun. Math. Phys.*, vol. 22, no. 2, pp. 133–161, 1971.

[96] H. Kunz, "Location of the zeros of the partition function for some classical lattice systems," *Phys. Lett. A*, vol. 32, no. 5, pp. 311 – 312, 1970.

[97] R. Dickman, "Discontinuous phase transition in a dimer lattice gas," *J. Chem. Phys.*, vol. 136, no. 17, p. 174105, 2012.

[98] F. Alet, J. L. Jacobsen, G. Misguich, V. Pasquier, F. Mila, and M. Troyer, "Interacting classical dimers on the square lattice," *Phys. Rev. Lett.*, vol. 94, p. 235702, Jun 2005.

[99] S. Papanikolaou, D. Charrier, and E. Fradkin, "Ising nematic fluid phase of hard-core dimers on the square lattice," *Phys. Rev. B*, vol. 89, p. 035128, Jan 2014.

[100] I. Jauslin and E. H. Lieb, "Nematic liquid crystal phase in a system of interacting dimers and monomers," *Commun. Math. Phys.*, vol. 363, pp. 955–1002, Nov 2018.

[101] M. E. Fisher and J. Stephenson, "Statistical mechanics of dimers on a plane lattice. ii. dimer correlations and monomers," *Phys. Rev.*, vol. 132, pp. 1411–1431, Nov 1963.

[102] A. Giuliani, V. Mastropietro, and F. Toninelli, "Height fluctuations in non-integrable classical dimers," *Europhys. Lett.*, vol. 109, p. 60004, mar 2015.

[103] R. Kenyon, "Dominos and the gaussian free field," *Ann. Probab.*, vol. 29, pp. 1128–1137, 07 2001.

[104] M. Zahradnik, "A Short Course On The Pirogov Sinai Theory," Tech. Rep. MP-ARC-96-300, Jun 1996.

[105] J. Kundu and R. Rajesh, "Reentrant disordered phase in a system of repulsive rods on a bethe-like lattice," *Phys. Rev. E*, vol. 88, p. 012134, Jul 2013.

[106] D. A. Matoz-Fernandez, D. H. Linares, and A. J. Ramirez-Pastor, "Critical behavior of long straight rigid rods on two-dimensional lattices: Theory and monte carlo simulations," *J. Chem. Phys.*, vol. 128, no. 21, p. 214902, 2008.

[107] D. Matoz-Fernandez, D. Linares, and A. Ramirez-Pastor, "Critical behavior of long linear k-mers on honeycomb lattices," *Physica A: Statistical Mechanics and its Applications*, vol. 387, no. 26, pp. 6513 – 6525, 2008.

[108] D. H. Linares, F. Romá, and A. J. Ramirez-Pastor, "Entropy-driven phase transition in a system of long rods on a square lattice," *J. Stat. Mech.*, vol. 2008, no. 03, p. P03013, 2008.

[109] H. C. M. Fernandes, J. J. Arenzon, and Y. Levin, "Monte carlo simulations of two-dimensional hard core lattice gases," *J. Chem. Phys.*, vol. 126, no. 11, p. 114508, 2007.

[110] P. Bolhuis and D. Frenkel, "Tracing the phase boundaries of hard spherocylinders," *J. Chem. Phys.*, vol. 106, no. 2, pp. 666–687, 1997.

[111] G. J. Vroege and H. N. W. Lekkerkerker, "Phase transitions in lyotropic colloidal and polymer liquid crystals," *Rep. Prog. Phys.*, vol. 55, no. 8, p. 1241, 1992.

[112] A. Gschwind, M. Klopotek, Y. Ai, and M. Oettel, "Isotropic-nematic transition for hard rods on a three-dimensional cubic lattice," *Phys. Rev. E*, vol. 96, p. 012104, Jul 2017.

[113] D. Dhar and S. Chandra, "Exact entropy of dimer coverings for a class of lattices in three or more dimensions," *Phys. Rev. Lett.*, vol. 100, p. 120602, Mar 2008.

[114] M. Oettel, M. Klopotek, M. Dixit, E. Empting, T. Schilling, and H. Hansen-Goos, "Monolayers of hard rods on planar substrates. i. equilibrium," *J. Chem. Phys.*, vol. 145, no. 7, p. 074902, 2016.

[115] Z. Pu, M. Cao, J. Yang, K. Huang, and C. Hu, "Controlled synthesis and growth mechanism of hematite nanorhombohedra, nanorods and nanocubes," *Nanotechnology*, vol. 17, no. 3, p. 799, 2006.

[116] A. P. Gantapara, J. de Graaf, R. van Roij, and M. Dijkstra, "Phase diagram and structural diversity of a family of truncated cubes: Degenerate close-packed structures and vacancy-rich states," *Phys. Rev. Lett.*, vol. 111, p. 015501, Jul 2013.

[117] M. Marechal, U. Zimmermann, and H. Löwen, "Freezing of parallel hard cubes with rounded edges," *J. Chem. Phys.*, vol. 136, no. 14, p. 144506, 2012.

[118] R. D. Batten, F. H. Stillinger, and S. Torquato, "Phase behavior of colloidal superballs: Shape interpolation from spheres to cubes," *Phys. Rev. E*, vol. 81, p. 061105, Jun 2010.

[119] S. Sun, C. B. Murray, D. Weller, L. Folks, and A. Moser, "Monodisperse fept nanoparticles and ferromagnetic fept nanocrystal superlattices," *Science*, vol. 287, no. 5460, pp. 1989–1992, 2000.

[120] S. Torquato and Y. Jiao, "Dense packings of polyhedra: Platonic and archimedean solids," *Phys. Rev. E*, vol. 80, p. 041104, Oct 2009.

[121] T. Hanrath, J. J. Choi, and D.-M. Smilgies, "Structure/processing relationships of highly ordered lead salt nanocrystal superlattices," *ACS Nano*, vol. 3, no. 10, pp. 2975–2988, 2009.

[122] J. A. Champion, Y. K. Katare, and S. Mitragotri, "Particle shape: A new design parameter for micro- and nanoscale drug delivery carriers," *J. Control Release*, vol. 121, no. 1, pp. 3 – 9, 2007.

[123] J. Li, R. Rajagopalan, and J. Jiang, "Polymer-induced phase separation and crystallization in immunoglobulin g solutions," *J. Chem. Phys.*, vol. 128, no. 20, p. 205105, 2008.

[124] W. H. Soe, C. Manzano, N. Renaud, P. de Mendoza, A. De Sarkar, F. Ample, M. Hliwa, A. M. Echavarren, N. Chandrasekhar, and C. Joachim, "Manipulating molecular quantum states with classical metal atom inputs: Demonstration of a single molecule nor logic gate," *ACS Nano*, vol. 5, no. 2, pp. 1436–1440, 2011.

[125] W.-H. Soe, C. Manzano, A. De Sarkar, F. Ample, N. Chandrasekhar, N. Renaud, P. de Mendoza, A. M. Echavarren, M. Hliwa, and C. Joachim, "Demonstration of a nor logic gate using a single molecule and two surface gold atoms to encode the logical input," *Phys. Rev. B*, vol. 83, p. 155443, Apr 2011.

[126] S. Godlewski, M. Kolmer, H. Kawai, B. Such, R. Zuzak, M. Saeys, P. de Mendoza, A. M. Echavarren, C. Joachim, and M. Szymonski, "Contacting a conjugated molecule with a surface dangling bond dimer on a hydrogenated ge(001) surface allows imaging of the hidden ground electronic state," *ACS Nano*, vol. 7, no. 11, pp. 10105–10111, 2013.

[127] F. Smallenburg, L. Filion, M. Marechal, and M. Dijkstra, "Vacancy-stabilized crystalline order in hard cubes," *Proc. Nat. Acad. Scs.*, vol. 109, no. 44, pp. 17886–17890, 2012.

[128] W. G. Hoover, "High-density equation of state for hard parallel squares and cubes," *J. Chem. Phys.*, vol. 40, no. 4, pp. 937–938, 1964.

[129] R. W. Zwanzig, "Virial coefficients of "parallel square" and "parallel cube" gases," *J. Chem. Phys.*, vol. 24, no. 4, pp. 855–856, 1956.

[130] W. G. Hoover and A. G. D. Rocco, "Sixth and seventh virial coefficients for the parallel hard-cube model," *J. Chem. Phys.*, vol. 36, no. 12, pp. 3141–3162, 1962.

[131] E. A. Jagla, "Melting of hard cubes," *Phys. Rev. E*, vol. 58, pp. 4701–4705, Oct 1998.

[132] B. Groh and B. Mulder, "A closer look at crystallization of parallel hard cubes," *J. Chem. Phys.*, vol. 114, no. 8, pp. 3653–3658, 2001.

[133] S. Belli, M. Dijkstra, and R. van Roij, "Free minimization of the fundamental measure theory functional: Freezing of parallel hard squares and cubes," *J. Chem. Phys.*, vol. 137, no. 12, p. 124506, 2012.

[134] R. H. Swendsen and J.-S. Wang, "Nonuniversal critical dynamics in monte carlo simulations," *Phys. Rev. Lett.*, vol. 58, pp. 86–88, Jan 1987.

[135] P. W. Kasteleyn and C. M. Fortuin, "Phase Transitions in Lattice Systems with Random Local Properties," *JPS Conf. Proc.*, vol. 26, p. 11, 1969.

[136] U. Wolff, "Collective monte carlo updating for spin systems," *Phys. Rev. Lett.*, vol. 62, pp. 361–364, Jan 1989.

[137] C. Dress and W. Krauth, "Cluster algorithm for hard spheres and related systems," *J .Phys. A Math Gen.*, vol. 28, pp. L597–L601, dec 1995.

[138] W. Krauth and R. Moessner, "Pocket monte carlo algorithm for classical doped dimer models," *Phys. Rev. B*, vol. 67, p. 064503, Feb 2003.

[139] N. Vigneshwar, D. Dhar, and R. Rajesh, "Different phases of a system of hard rods on three dimensional cubic lattice," *J. Stat. Mech.*, vol. 2017, no. 11, p. 113304, 2017.

[140] K. Binder, "Finite size scaling analysis of ising model block distribution functions," *Z. Phys., B, Condens. Matt.*, vol. 43, pp. 119–140, Jun 1981.

[141] K. Vollmayr, J. D. Reger, M. Scheucher, and K. Binder, "Finite size effects at thermally-driven first order phase transitions: A phenomenological theory of the order parameter distribution," *Zeitschrift für Physik B Condensed Matter*, vol. 91, pp. 113–125, Mar 1993.

[142] N. Vigneshwar, D. Mandal, K. Damle, D. Dhar, and R. Rajesh, "Phase diagram of a system of hard cubes on the cubic lattice," *Phys. Rev. E*, vol. 99, p. 052129, May 2019.

[143] A. Aharony and A. D. Bruce, "Polycritical points and floplike displacive transitions in perovskites," *Phys. Rev. Lett.*, vol. 33, pp. 427–430, Aug 1974.

[144] I. J. Ketley and D. J. Wallace, "A modified epsilon expansion for a hamiltonian with cubic point-group symmetry," *J. Phys. A*, vol. 6, no. 11, p. 1667, 1973.

[145] D. J. Wallace, "Critical behaviour of anisotropic cubic systems," *J. Phys. C*, vol. 6, no. 8, p. 1390, 1973.

[146] A. Aharony, "Critical behavior of anisotropic cubic systems," *Phys. Rev. B*, vol. 8, pp. 4270–4273, Nov 1973.

[147] D. R. Nelson, J. M. Kosterlitz, and M. E. Fisher, "Renormalization-group analysis of bicritical and tetracritical points," *Phys. Rev. Lett.*, vol. 33, pp. 813–817, Sep 1974.

[148] E. Brézin, J. C. Le Guillou, and J. Zinn-Justin, "Discussion of critical phenomena for general *n*-vector models," *Phys. Rev. B*, vol. 10, pp. 892–900, Aug 1974.

[149] M. Ferer, J. P. Van Dyke, and W. J. Camp, "Effect of a cubic crystal field on the critical behavior of a 3d model with heisenberg exchange coupling: A high-temperature series investigation," *Phys. Rev. B*, vol. 23, pp. 2367–2373, Mar 1981.

[150] M. Tissier, D. Mouhanna, J. Vidal, and B. Delamotte, "Randomly dilute ising model: A nonperturbative approach," *Phys. Rev. B*, vol. 65, p. 140402, Mar 2002.

[151] I. O. Maier and A. I. Sokolov, "Is a cubic crystal "isotropic" in the critical point?," *Ferroelectrics Lett.*, vol. 9, no. 4, pp. 95–98, 1988.

[152] N. Shpot, "Critical behavior of the mn-component field model in three dimensions ii. three-loop results," *Phys. Lett. A*, vol. 142, no. 8, pp. 474 – 478, 1989.

[153] I. O. Mayer, A. I. Sokolov, and B. N. Shalayev, "Critical exponents for cubic and impure uniaxial crystals: most accurate (?) theoretical values," *Ferroelectrics*, vol. 95, no. 1, pp. 93–96, 1989.

[154] K. B. Varnashev, "Stability of a cubic fixed point in three dimensions: Critical exponents for generic n," *Phys. Rev. B*, vol. 61, pp. 14660–14674, Jun 2000.

[155] D. V. Pakhnin and A. I. Sokolov, "Five-loop renormalization-group expansions for the three-dimensional n-vector cubic model and critical exponents for impure ising systems," *Phys. Rev. B*, vol. 61, pp. 15130–15135, Jun 2000.

[156] H. Kleinert, S. Thoms, and V. Schulte-Frohlinde, "Stability of a three-dimensional cubic fixed point in the two-coupling-constant φ^4 theory," *Phys. Rev. B*, vol. 56, pp. 14428–14434, Dec 1997.

[157] H. Kleinert and V. Schulte-Frohlinde, "Exact five-loop renormalization group functions of φ^4-theory with $o(n)$-symmetric and cubic interactions. critical exponents up to ϵ^5," *Phys. Lett. B*, vol. 342, no. 1, pp. 284 – 296, 1995.

[158] H. Kleinert and S. Thoms, "Large-order behavior of a two-coupling-constant φ^4 theory with cubic anisotropy," *Phys. Rev. D*, vol. 52, pp. 5926–5943, Nov 1995.

[159] J. Manuel Carmona, A. Pelissetto, and E. Vicari, "n-component ginzburg-landau hamiltonian with cubic anisotropy: A six-loop study," *Phys. Rev. B*, vol. 61, pp. 15136–15151, Jun 2000.

[160] L. T. Adzhemyan, E. V. Ivanova, M. V. Kompaniets, A. Kudlis, and A. I. Sokolov, "Six-loop ϵ expansion study of three-dimensional n-vector model with cubic anisotropy," *Nucl. Phys. B*, vol. 940, pp. 332 – 350, 2019.

[161] M. Caselle and M. Hasenbusch, "The stability of the $o(n)$ invariant fixed point in three dimensions," *J. Phys. A*, vol. 31, no. 20, p. 4603, 1998.

[162] C. Holm and W. Janke, "Critical exponents of the classical three-dimensional heisenberg model: A single-cluster monte carlo study," *Phys. Rev. B*, vol. 48, pp. 936–950, Jul 1993.

Thesis Highlight

Name: N Vigneshwar
Name of CI/OCC: IMSc, Chennai **Enrollment No.:** PHYS10201404002
Thesis Title: Entropy driven phase transition in hard core lattice gas models in three dimensions
Discipline: Physical Sciences **Sub-area of discipline:** Physics (Statistical Mechanics)
Date of viva-voce: 03/07/2020

There is a class of phase transitions where the transition to the ordered state is driven by a gain in entropy. These transitions are manifested in experimental systems like freezing in hard-spheres of PMMA colloids, nematic transitions in liquid crystals, etc. The minimal models for studying these transitions are volume exclusion models, in which the constituent particles are not allowed to intersect. When placed on lattices, these models are called hard-core lattice gas models(HCLGs). These models serve as nice abstractions for actual experimental systems and understanding their phase diagram on lattice is helpful in general understanding of entropy-driven phase transitions.

In three-dimensions, it is more complicated to study them because of the lack of efficient algorithms to simulate such systems. Traditional evaporation-deposition algorithms fail to equilibrate at high densities or for large exclusion volumes. So, an adapted version of grand canonical Monte Carlo algorithm with cluster moves thas been implemented with certain optimisations to study such systems. This algorithm has been useful in equilibrating systems at densities close to full-packing or at full-packing. The algorithm can also be easily parallelised.

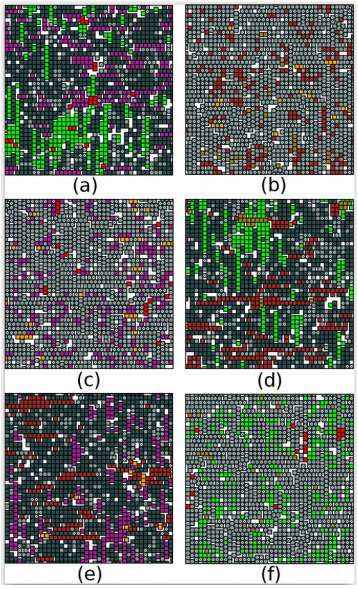

Fig 1 : Snapshot of a sublattice phase seen in a system of hard cubes of size $2 \times 2 \times 2$

Here we study two problems on a cubic lattice: (1) hard rods of length k and (2) hard cubes of size $2 \times 2 \times 2$. We obtain the detailed phase diagram and characterize the nature of the phase transitions for both these models.

For hard cubes of size $2 \times 2 \times 2$ on a cubic lattice, the phases are: disordered, layered, sublattice and columnar in the increasing order of density. In the layered phase, the system breaks up into two dimensional slabs in which the density of the cubes are periodic with period 2 along the direction perpendicular to the slabs. The disordered-layered transition is continuous and was found to be consistent with Heisenberg universality class with cubic anisotropy. The next phase is the sublattice phase, in which the density of cubes is periodic in all the three perpendicular directions with a period 2. And the high density phase is the columnar phase in which the system breaks up into a set of columns and the density of cubes is periodic along the two mutually perpendicular directions with a period 2. Both the layered-sublattice and the sublattice-columnar transitions are first order.